AD-A124 001 MEASUREMENTS OF HIGH FREQUENCY HIGH WAVENUMBER PROCESSES IN THE UPPER OCE..(U) NAVAL OCEAN RESEARCH AND DEVELOPMENT ACTIVITY NSTL STATION MS.. 1/1

UNCLASSIFIED K D SAUNDERS ET AL. AUG 82 F/G 8/10 NL

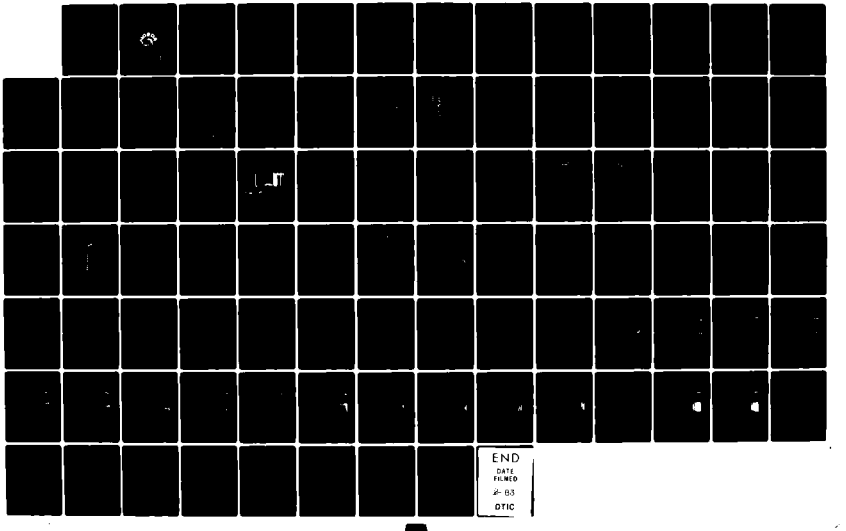

END
DATE FILMED
4-83
DTIC

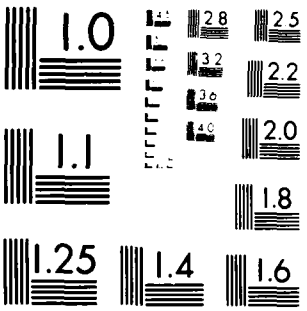

(12)

NORDA Technical Note 129

AD A 12 1 0 1

Naval Ocean Research and
Development Activity
NSTL Station, Mississippi 39529

Measurements of High Frequency, High Wavenumber Processes in the Upper Ocean: The Acoustically Tracked Oceanographic Mooring Experiment (ATOM '79) Final Report, Part I

DTIC
ELECTE
JAN 3 1 1983
S E D

DTIC FILE COPY

K.D. Saunders
A.W. Green

Oceanography Division
Ocean Science and Technology Laboratory

August 1982

ABSTRACT

The ATOM '79 (Acoustically Tracked Ocean Mooring) experiment was designed to study the natural background of high frequency, high wavenumber processes in the upper ocean and to determine the magnitude and effects of mooring motion on the measurements of velocity and temperature. The mooring was deployed for about one month in the central Gulf of Mexico from December 1979 through January 1980.

It was determined that translational mooring motion is not a significant source of error and that torsional motions coupled with the imperfect current meter directional response are a more significant source of error. Observations of the background currents showed no strong correlation between low frequency inertial period activity and high frequency activity, little, if any, effect of the proximity of the peak in the Brunt-Väisälä frequency profile on the high frequency activity, and some significant relation of wind forcing to sub-mixed layer inertial currents.

ACKNOWLEDGEMENTS

This work was sponsored by the NORDA, Code 500 Ocean Measurements Program, Dr. Rudy Hollman, Program Manager.

CONTENTS

ILLUSTRATIONS

TABLES

MEASUREMENTS OF HIGH FREQUENCY, HIGH WAVENUMBER PROCESSES IN THE UPPER OCEAN: THE ACOUSTICALLY TRACKED OCEANOGRAPHIC MOORING EXPERIMENT (ATOM '79) FINAL REPORT, PART I

INTRODUCTION

During the past several years an urgent need has arisen to determine the climatology of the natural variability of the upper ocean (that is, from 0 to 600 m) on time and space scales that correspond to high frequency and high wavenumber internal waves and turbulence. Because the physical environment of the upper ocean is harsh, past experimental programs were faced with technological problems that severely limited the accuracy and duration of the experiments. Quoting Halpern (1978):

> For many years before the 1972 SCOR (Scientific Committee on Oceanic Research) Working Group 21, Third intercomparison test, current measurements were made beneath surface buoys with the realization that the data contained spurious currents produced by vertical motions of the instrument high frequency wave motions and cable vibrations (e.g., Webster, 1967). Results from the 1972 SCOR test (SCOR Working Group 21, 1975; Gould and Sambuco, 1975; Gould et al., 1974) indicated that current measurements made at intermediate depths beneath surface buoys moored in deep water were undoubtedly contaminated by mooring motion. Soon afterwards, it was widely conjectured that erroneous current measurements would be obtained at all depths beneath the surface following buoy. Evidence contrary to this view has since been provided by Zenk et al. 1978, Saunders, P.M. (1976), Halpern et al. (1974), and Pollard (1974).

To date, probably as a result of this widely held view, there have been only two major experiments directly assessing high frequency, high wavenumber upper ocean phenomena between the surface and several hundred meters depth. These two experiments are the MILE experiment (MIxed Layer Experiment) and JASIN (Joint Air Sea Interaction Experiment). The lack of credible data has inhibited progress in deriving a "climatology" of upper ocean variability comparable to the Garrett and Munk model for deep ocean internal waves. Indeed, we should anticipate that future upper ocean measurements would yield results that fundamentally differ from the deep ocean. From the knowledge of the conditions near the ocean surface, we assume that the high frequency and high wavenumber fluctuations are not horizontally isotropic, homogeneous or "stationary." Absence of these conditions is due to the proximity of the air-sea boundary, which is the primary zone of thermal and kinetic energy fluxes between the ocean and the atmosphere. Weather events, which are important external sources of short-term variability, are not generally distributed homogeneously, nor do they propagate isotropically with space time stationarity. Consequently, the simplifying assumptions applicable to the deep ocean fluctuations cannot be applied to the upper ocean.

Another complicating factor is the intensity of the vertical shear, which generally has maxima in the upper hundreds of meters. The upper ocean mean vertical shear distribution is assumed to be continually modulated in space and time by surface weather, inertial waves, internal tides, and the motions resulting from low "mode" internal waves. Theoretical results (Landahl and Criminali, 1977; Chimonas, 1978; and Thorpe, 1978) indicate that the modulation of the high frequency and high wavenumber internal waves by low frequency motions may lead to strong nonlinear coupling of disparate scales of motion or to the breakdown of the high frequency and wavenumber waves. Experimental evidence of the high frequency instabilities and sporadic distributions has been provided by Ericksen (1978) and Korotayev and Panteleyev (1977a, 1977b). Ericksen's results were derived from observations in the

main thermocline, but Korotayev and Panteleyev extracted their results from experiments in the seasonal thermocline. Both experiments had technical problems that created a wide range of valid but different interpretations. This was particularly true of the work of Korotayev and Panteleyev, which presented serious inconsistencies.

The MILE and JASIN experiments were directed toward clarification of upper ocean dynamics and air-sea exchanges. Although both involved good internal wave band measurements, neither was designed to analyze the variability of fluctuations at the maximum of the Brunt-Väisälä frequency and higher. Indeed, this is borne out by the intercomparison tests between different types of current meters on different types of moorings in both of these experiments (Halpern, Weller, Briscoe, Davis, and McCullough, 1981). However, some valuable insights about the qualitative features of the high frequency variability may be available. Resolutions of internal waves imbedded in a finestructure background require a high degree of spatial and temporal resolution that was unattainable by standard instrumentation and mooring techniques.

The Acoustically Tracked Oceanographic Mooring experiment of 1979 (ATOM '79) is the first phase of a comprehensive design process to obtain accurate measurements of the high frequency, high wavenumber processes occurring in the upper ocean. By high frequency, we mean processes which have periods between one hour and the minimum Brunt-Väisälä period. We define high wavenumber processes as those which have wave lengths less than about 30 m and greater than about 1 m in the vertical and less than 1 km in the horizontal directions. The specific region of interest (in depth) is near the peak in the Brunt-Väisälä frequency profile. This typically occurs near the base of the mixed layer which, depending on geographical location and season, may range from the surface of the ocean down to 100 m or more. This region is particularly difficult to study with existing current meters. It is too near the wave zone for the use of subsurface floats in general, and at other times the depth of the mixed layer places it in the zone where measurements from surface-moored floats are inappropriate. For the purposes of the particular experiment described in this report and to minimize the problems involved with the use of a surface mooring, we chose to employ a subsurface mooring in conjunction with a deep, winter mixed layer.

DESIGN PHILOSOPHY

NORDA has been tasked with developing methods for measuring high frequency, high wavenumber variability in the upper ocean that can be transferred to other branches of the Navy for use in routine surveys for obtaining climatology of this variability on a geographical and seasonal basis. The primary purpose of the ATOM mooring, therefore, is to provide input to the design procedure that will result in the development of such standard observational methods. In one sense then, the ATOM project may be thought of as being an engineering test of a specific mix of observational instrumentation. On the other hand, because the processes in the upper ocean are so poorly known, it has a very strong scientific component that is required to obtain information on the structure of the motions in this region of the ocean.

OBJECTIVES

There are five major objectives to the present study; three are primarily scientific in nature and two are primarily technical. These objectives are:

Scientific

1. determine the degree to which high frequency variability in the upper range of the internal gravity wave frequency spectrum is strongly dependent on the proximity of the peak in the buoyancy profile and on the effect of modulation by low frequency processes;

2. determine the degree to which low frequency processes are governed by local surface meteorology;

3. measure the vertical coherence of the high frequency current and temperature fields;

Technical

1. investigate the contamination of the current and temperature data induced by mooring motion;

2. determine whether it is possible to remove a significant amount of the mooring motion contamination.

DATA REQUIREMENTS

To meet the objectives current and temperature data were required at a rapid sampling rate, about one sample per minute. The spatial sampling had to be on the order of about 5 to 10 m in the vertical and cover a distance of around 100 m near the maximum of the Brunt-Väisälä frequency profile. To determine the local buoyancy profile and to provide information on the vertical wavenumber structure of the current and salinity fields as functions of depth, profiles of temperature and salinity were required during the deployment and recovery of the current meter mooring. Simultaneous current profiles made with the use of expendable current profilers (XCP) were also made at the time of deployment to obtain information on the vertical wavenumber structure of the current shear field. Expendable bathythermograph and air-deployed expendable bathythermograph surveys were required to assess the mesoscale features of the oceanic circulation in the vicinity of the mooring at the time of deployment. Meteorological data and wave data from nearby weather data buoys were also required for determining the degree to which the local meteorology affects the low frequency and, ultimately, the high frequency processes occurring in the upper layers of the ocean.

Determining the effects of mooring motion on the current and temperature data was a major factor in the design of the mooring; this requirement made it necessary to track the positions of the mooring elements as they changed with time. Strictly speaking, it is impossible to precisely characterize the time-varying state of a single point mooring, which by definition has an infinite number of degrees of freedom. The best that can be done with a limited number of instruments is to record the time-position history of various parts of the mooring. For this experiment, we chose to measure the position of two points on the mooring (one point being above the dense array of current meters and one below that array) using acoustic pulse and Doppler navigation techniques; these techniques are complementary to each other. The depth of the mooring at four positions on the cable was determined by four temperature/pressure (T/P) recorders. The direction of the mooring and tension at various points on the mooring was to have been measured by three force-vector recorders (FVRs) supplied by the C.S. Draper Lab at M.I.T. Torsional effects of the mooring were estimated from the case orientations of the various current meters. The case

orientation of the vector averaging current meters may be obtained every averaging cycle (these sample periods were 15/16ths and 15/8ths of a minute). The case orientation of the acoustic current meters were sampled once every 8 minutes.

Moorings such as these are expensive due to the bulk of subsequent data processing and the cost of the instruments. It is therefore desirable to exercise dynamical models of the mooring to simulate motion under realistic current conditions prior to implantation. One objective of this study was to obtain current data at a number of points along the mooring which could be used as input numerical mooring motion models. The validity of these models could then be tested against the observed parameters of the ATOM mooring configuration. At present, only one dynamic mooring motion model is known to have been qualitatively compared with actual mooring motion data. This model was developed at the Draper Lab, by Chhabra (1977). This model did not appear to accurately simulate mooring motions at the very high frequencies that were important in this experiment.

The site for the ATOM '79 mooring experiment was in the center of the Gulf of Mexico at approximately 26°N 90°W. This location was considered favorable due to the historical absence of large currents, the presence of a meteorological data buoy, and the presence of a relatively flat bottom, which should not be expected to act as a generator for internal waves. It was also located far from the continental shelf break, and thus was not expected to be near a source of internal tidal generation. Nevertheless, this mooring was high risk.

The risk to the mooring was predicated on the large number of instruments used in the mooring and on the physical risks to that instrumentation. A further risk involved the use of relatively new current meter instrumentation that had been only marginally tested. The majority of the current meters used in this mooring were Neil Brown acoustic current meters. These were chosen on the basis of linearity in speed, small digital sampling noise, and because of relatively good horizontal response (obtained through the manufacturer specifications). Although prototypes of this type current meter had been tested rather extensively by McCullough and others (McCullough, 1978; Appell, 1978), the lot used by NORDA consisted of the first production batch. Due to the short preparation time for the mooring experiment, it was not possible to extensively subject these current meters to severe environmental tests and burn them in electronically. Thus, it was not known what the data return or data quality would be. In order to circumvent the possibility of a very poor data return, a number of vector averaging current meters were used in the vicinity of the densely instrumented part of the mooring.

The environment in which the current meters were to be implanted also presented a number of serious risk considerations. The first consideration was the maximum expected current. The central area of the Gulf of Mexico, while having a generally low background current, is known to occasionally be subject to very strong current and shear fields due to either Loop Current extensions or eddies shed from the Loop Current. It is now known that currents as high as several knots may be present.

The second consideration involved ship time. The mooring was designed to be implanted in mid-winter. This was favorable from the point of view of having a deep mixed layer, but the incidence of relatively intense cold-weather fronts over the central Gulf of Mexico left a very small time frame in which to implant the meters. In fact, there was a period of only two days wherein the mooring could have safely been implanted. Fortunately the clear calm weather persisted long enough for deployment. The third major environmental risk factor to be considered was human

interference. (The NOAA Data Buoy Office has lost several data buoys due to fishermen "accidentally" cutting the mooring lines.)

About six months prior to deployment of the mooring, a workshop was held at NORDA to assess the risk factors involved. A number of academic and institutional contractors were invited to comment on our mooring design. Comments were made and responses were presented. In general, the information given NORDA Code 331 by workshop participants turned out to be of questionable value, since the experiment instrumentation and scientific objectives did not match well with the participants' experiences, which had been based on somewhat different requirements.

DATA PROCESSING

SHIPBOARD DATA

Three types of shipboard survey data were taken: expendable bathythermograph (XBT), expendable current profiler data (XCP), and conductivity-temperature-depth (CTD). A semi-automatic XBT logging data system developed by NORDA Code 350 (R. Holland, 1980) and modified by Mark Bergin of NORDA Code 331 recorded the expendable bathythermograph data. The only data processing included in this system was the transformation of the fall time of the XBT into depth and the application of the appropriate resistance to temperature formula to obtain the temperature as a function of depth. The data from the Neil Brown CTDs were recorded on audio tape for later shore-based processing. At the same time the raw CTD data were plotted and monitored with a Hewlett-Packard 9825A-based system. The expendable shear probe data were simply recorded at sea for later shore-based processing.

CTD DATA PROCESSING

The CTD data were transcribed from audio to a nine-track 800 bpi computer compatible tape. The data were then subsequently processed on the NAVOCEANO UNIVAC 1108 computer system. The basic processing consisted of translating the data into engineering units, editing and filtering the data to reduce the temperature and conductivity time response mismatch, and final incorporation of the temperature, conductivity, salinity, and pressure data to 1 decibar pressure intervals.

XBT DATA PROCESSING

The shore-based processing of the XBT data consisted primarily of producing waterfall plots, first differences, and high-pass filtered profiles. No further processing has been accomplished to date. The plots of the XBT data are to be found in Saunders, Green, and Bergin (1980).

EXPENDABLE CURRENT PROFILER (XCP) DATA PROCESSING

The XCP data were taken by the Johns Hopkins Applied Physics Laboratory. The data were then transmitted to Dr. Tom Sanford of the University of Washington, Applied Physics Laboratory, for processing in the manner described in Sanford, et al. (1978). The processed data were transmitted to NORDA on a 1600 bpi nine-track EBCDIC card image format. These records consisted of the vertical coordinate (in decibars) calculated from the drop time, the temperature (in degrees Celsius), the east and north velocity components plus five auxiliary variables (for engineering purposes). Forty-five XCP drops were made. Of these, 25 were made concurrently with a CTD profile. The availability of temperature records in both the CTD and with the XCP provided a means for correcting the fall times of the XCPs using the temperature as a

fiducial variable. The details of the analysis for correcting the fall rates of the expendable shear profilers are summarized in Green and Saunders (1981) which appears as Appendix A in this report.

RICHARDSON NUMBER CALCULATIONS

The 25 simultaneous CTD and XCP casts provided both density and velocity information required for the calculation of Richardson number profiles. The expendable shear profiler data were corrected for fall rate and interpolated to 1 dbar pressure intervals. The CTD and XCP records were then low-pass filtered with a cut-off of about 8 m. The Richardson number profiles were then computed from the low-passed 1 m XCP and CTD records. Listings of all the programs used in the shipboard and onshore reduction of the shipboard data will be presented in future reports.

MOORED INSTRUMENT DATA

Acoustic Tracking Data

The initial processing of the acoustic tracking data, both the pulse and Doppler data for the upper and lower positions of the receiving equipment, was by Dr. Robert Spindel of Woods Hole Oceanographic Institution. The lower unit at 200 m nominal depth ran from the time of deployment until the transponders failed on January 8, 1980, at about 1845Z. The upper unit also ran; but as it did not stop at the end of tape mark, it overwrote the first part of the data. Thus, the data on the upper unit started at 1730Z on December 28, 1979, and ended at January 8, 1980, at 1845Z. The sampling rate for the pulse data was once every half hour. The lower unit interrogated the transponders at 15 and 45 minutes after the hour while the upper unit interrogated the transponders on the hour and half-hour. The initial position data were computed by Spindel and transmitted to NORDA on a standard ASCII tape.

During the initial processing it was found that where considerable numbers of gaps where the data were missing entirely. These gaps were not noticed initially and led to the appearance of a number of very large spurious speeds, which made the spectrum appear to be much flatter than it actually was. We also learned that the algorithm used to process the data included an assumption that the depth of the acoustic receiver transmitters was constant at 100 and 200 m, respectively, for the upper and lower receiver transmitter units. We subsequently obtained the raw travel time information between each of the transponders and receiver transmitters on the mooring line. The depth of the mooring was estimated using the temperature/pressure recorder data. These data were then used with the travel time data to calculate the horizontal and vertical positions of the acoustic receiver transmitters on the mooring line. The gaps in the time series were eliminated through linear interpolation between pairs of "good" points.

The Doppler data were also processed by Spindel at Woods Hole. They were received and used without any further processing to attempt to correct errors in the data.

TEMPERATURE PRESSURE RECORDER DATA

At the termination of the ATOM recovery cruise the temperature/pressure recorders were shipped to the Charles Stark Draper Laboratory in Cambridge, Massachusetts. The data were then translated into engineering units, recorded on magnetic tape and mailed to NORDA. Initial plots of the raw data were also produced at the Draper Laboratory and sent under separate cover to NORDA. The depth and temperature limits of

the temperature/pressure recorders were preset prior to deployment so that maximum resolution could be obtained. There were several periods during the mooring when the temperature pressure recorder dropped below the upper pressure limit and below the lower temperature limit on the recorder; thus, there were no direct pressure measurements at the maximum depths to which the mooring was depressed.

The initial temperature versus time and pressure versus time plots appeared at first look to be very similar. A plot of temperature versus pressure confirmed this conjecture and a calculation of the correlation coefficient yielded a value of -0.97.

This result implied that it should be possible to estimate the pressure/time history of the mooring from the temperature record in the gaps where the pressure sensor was out of range. A linear least squares fit of temperature to pressure was used for the extrapolation formula.

CURRENT-TEMPERATURE DATA

The basic data processing for ACMs and VACMs is the same. The data were transcribed from the cassette tapes of each current meter on to a nine-track (ACM) or seven-track (VACM) tape for further processing on NAVOCEANO's UNIVAC 1108 computer. Next, the data were translated into engineering units and placed in standard FEB (Fast and Easy Binary) files (Hallock, 1980). The current and temperature data were screened and edited, corrections were made in situations where there were obviously erroneous data points attributable to electronic system noise. The corrections were applied by linear interpolation between pairs of "good" data points. After the data were edited; the basic plots of the current and temperature data were produced. Temperature and current autospectra were computed using the standard NAVOCEANO spectral processing program. (Cross-spectra were not computed at this stage due to inappropriate frequency band averaging in the NAVOCEANO program.) The basic current statistics were also computed and are plotted in Saunders, Green, and Bergin (1980). The cross-spectral analyses presented in this report were computed using a quasi-ensemble averaging technique. Each data record was broken up into non-overlapping segments 512 points long. A Hanning window (Nuttall, 1981) was applied in the time domain to each segment and were Fourier transformed. The raw spectral estimates were computed by multiplying one transform by the complex conjugate of the other; these were then averaged across the quasi-ensemble of estimates to produce a smoothed estimate of the cross-specta and the auto-spectra for each signal pair. The coherence and phase were then computed in the usual manner from the auto and cross spectra. Other than the application of the Hanning window to reduce long distance frequency leakage by f^{-6} (Nuttall, 1981), no frequency band averaging was applied.

Estimates of the vertical velocity of the water were made from the temperature observations between pairs of ACMs. The vertical velocity was estimated by the equation (the deviation of which is given in Appendix B)

$$w \cong - \frac{\partial T}{\partial t} \Big/ \frac{\partial T}{\partial z} - \frac{1}{\bar{\rho} g} \frac{dp}{dt}$$

This raw estimate was then corrected by subtracting the observed vertical velocity of the mooring as obtained from the temperature pressure records.

An attempt was made to estimate the vertical component of the eddy viscosity. This was done by the following method (derived in Appendix B):

$$\nu_{E_u} = \frac{\overline{w'u'}}{\bar{u}_z} \quad ; \quad \nu_{E_v} = \frac{\overline{w'v'}}{\bar{v}_z}$$

The calculations gave widely scattered results with $\nu_{E_{u,v}}$, varying from between $+10^3$ cm^2/s to -10^3 cm^2/s.

The calculations of ν_{E_u} and ν_{E_v} proved to be inconsistent with respect to the length of the averaging interval and the position of the current meter. We surmise that either the assumptions on which the estimate for the ν_E's were derived were wrong or, more than likely, the current meter spacing was too large to allow for good estimates of u_z and U' W' (the error is probably in the U' component). This second possibility is deduced from the low vertical coherences of u and v discussed later.

RESULTS

MOORING MOTION CHARACTERIZATION EXPERIMENT

One of the major goals of the ATOM experiment was to obtain information characterizing the motion of the mooring. The primary purpose of this effort was to determine the extent to which the mooring motion introduces "error" in the current (and temperature) measurements. The secondary purpose was to obtain information on the currents that cause the mooring to move, as well as the motion of selected points on the mooring that could be used to test the validity of numerical mooring motion models. The tertiary purpose was to obtain information on the stresses in the mooring, as well as the high frequency accelerations that could be used for improved engineering design. The experiment succeeded in the first two purposes and was unsuccessful in the third due to failure of the force-vector recorders.

Mooring motion can affect current measurements by translational additive effects and interaction with the instrument response characteristics.

ACOUSTIC TRACKING/PRESSURE MEASUREMENTS

An integral part of the ATOM design was the capability to determine the position of two points on the mooring using acoustic tracking methods. A combination of a time-travel/pulsed system and a Doppler tracking system was used. The operation of the Doppler system is described in Porter, et al. (1973) and Spindel, et al. (1978). The combined system is described in Spindel, et al. (1976). One pair of pulse and Doppler tracking recorders was located just above the dense current meter array, the second was below (Fig. 1). Three acoustic transponders with CW beacons were implanted on the sea floor after the mooring was deployed. The positions of these beacons were then determined by a ship survey. The survey positions are shown in Figure 2 (R. C. Spindel, personal communication, 15 May 1980). Dr. Spindel was responsible for preparing the instruments prior to deployment, conducting the ship-board beacon survey, and translating the collected data into a format usable by NORDA.

FINAL CONFIGURATION FOR ATOM '79

(Acoustically Tracked Oceanographic Mooring)

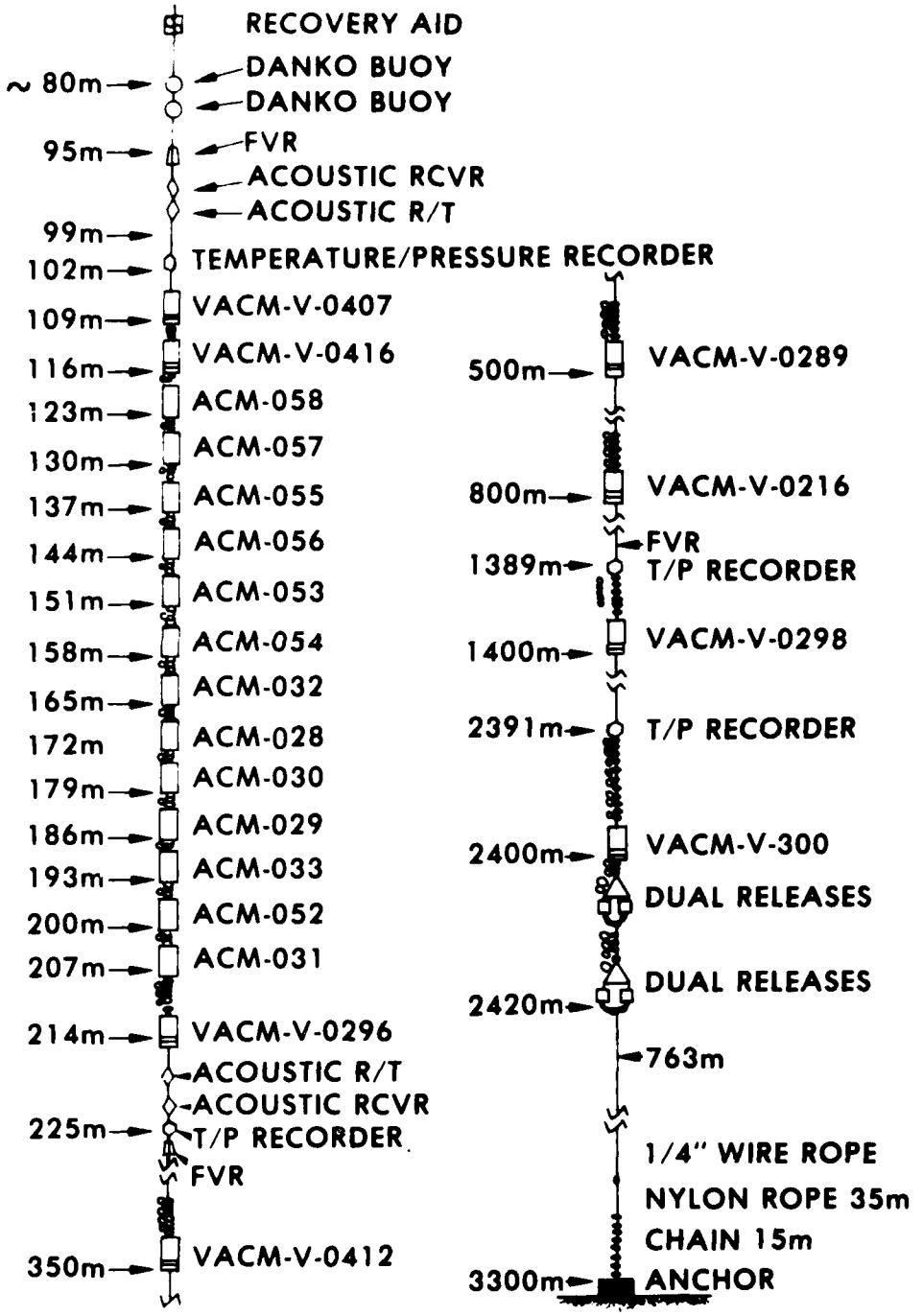

Figure 1. Schematic diagram of ATOM '79 mooring

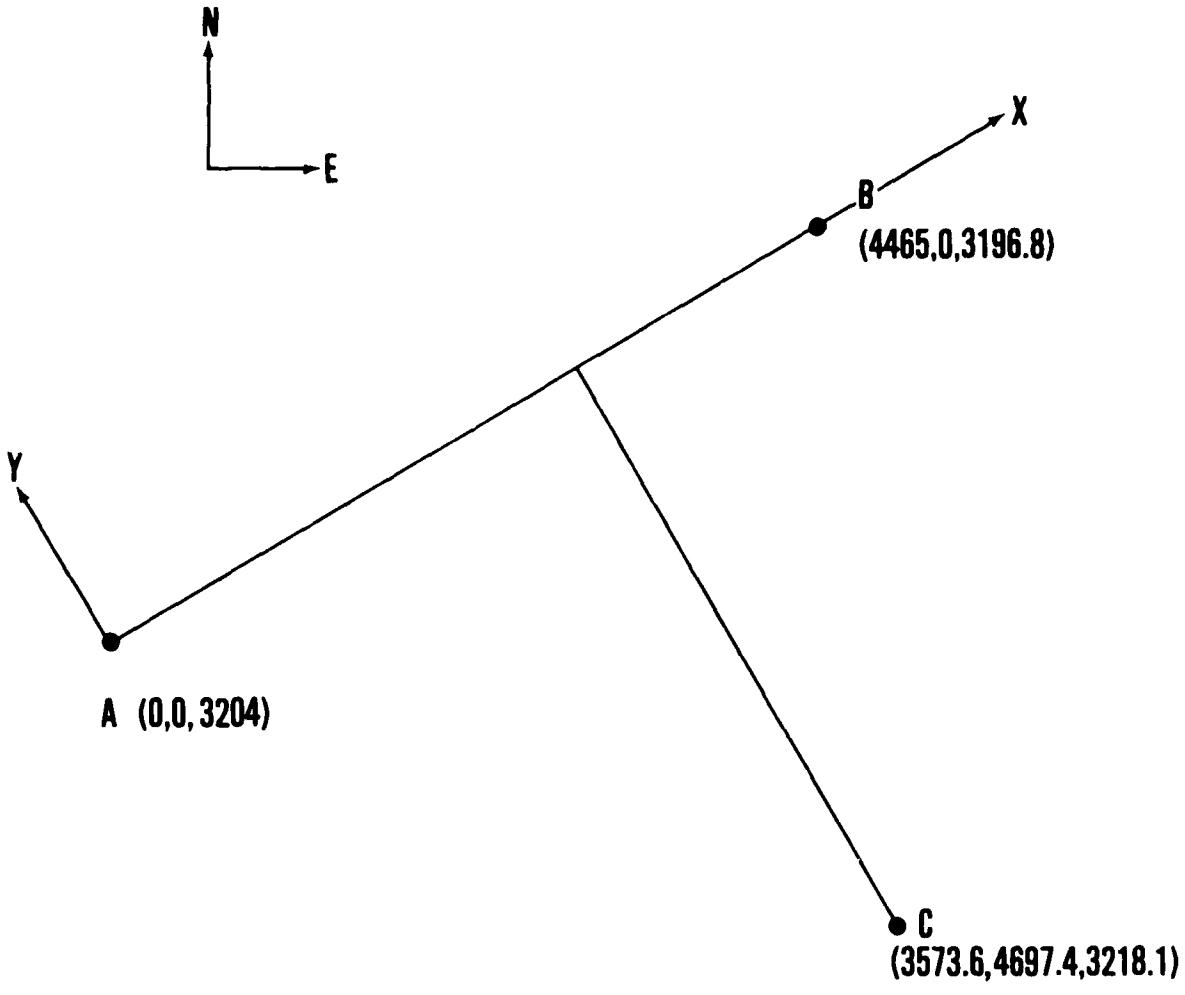

Figure 2. Location of bottom acoustic beacons

DATA QUALITY

The acoustic positioning system proved somewhat less than totally reliable. The transponders (at least two out of three) failed on 8 January 1980 at 1845Z. Prior to this failure, the lower transponder unit (S/N 003) ran from deployment, while a mechanical problem in the upper unit (S/N 004) caused an overwriting of the beginning of the tape, leaving data from the period of 28 December 1979, 1730Z, to 8 January 1980, 1845Z. The pulse data were sampled at a rate of two samples per hour, while the Doppler data were sampled at 120 samples per hour. At any one time there were usually only two working (i.e., with acceptable data returns) transponders for the pulse system. It was not unusual to find instances where no good pulse data were returned. Because we did not, in general, have three ranges from the transponders to the recording units, a third measurement was required to determine the position of the unit.

TEMPERATURE/PRESSURE (DEPTH) MEASUREMENTS

This third parameter was the depth of the instrument. Temperature/pressure (T/P) recorders of C.S. Draper Laboratory design were located at four points on the mooring. A T/P recorder was located near each of the acoustic recording units (Fig. 1). As a result it was a simple matter to determine the depth of the acoustic units as a function of time as long as the depth of the T/P recorder was less than that corresponding to the maximum pressure setting. To estimate depths when pressure exceeded the dynamic ranges of the instrument, we used the tight correlation between the temperature and pressure. As previously noted, the correlation coefficient was -0.97. (A scatter plot of pressure temperature is shown in Fig. 3.) A linear least square regression equation was obtained between pressure and temperature at the nearest acoustic current meter over the period when the pressure recorder was in range. The estimates of the pressure when the recorder over-ranged were made by applying this equation to the upper ACM temperature.

POSITION DATA PROCESSING

Using the pressure records and extrapolated values, the depth of the acoustic units were computed in the usual manner by integrating

$$dp = -\bar{\rho}\, g\, dz.$$

The horizontal positions of the acoustic units were calculated using simple geometry (e.g., Spindel, personal communication, 15 May 1980). The significant gaps in the position data were filled by linear interpolation from the nearest "good" points. The position data were then edited to remove spikes. The position data were time differenced to obtain an estimate of the mooring's horizontal velocity. Figure 4 presents the time history of the mooring velocity, while the position history is shown in Figure 5. From this latter figure, we see that the mooring moved about 0.8 km in the north-south direction and about 0.45 km in the east-west direction. A stereo plot of the position of the acoustic receiver/transponder (R/T) is shown in Figure 6. The pulse data velocity statistics are summarized in Figures 7 and 8. Figure 7 is a joint speed/direction histogram. The pertinent statistics are:

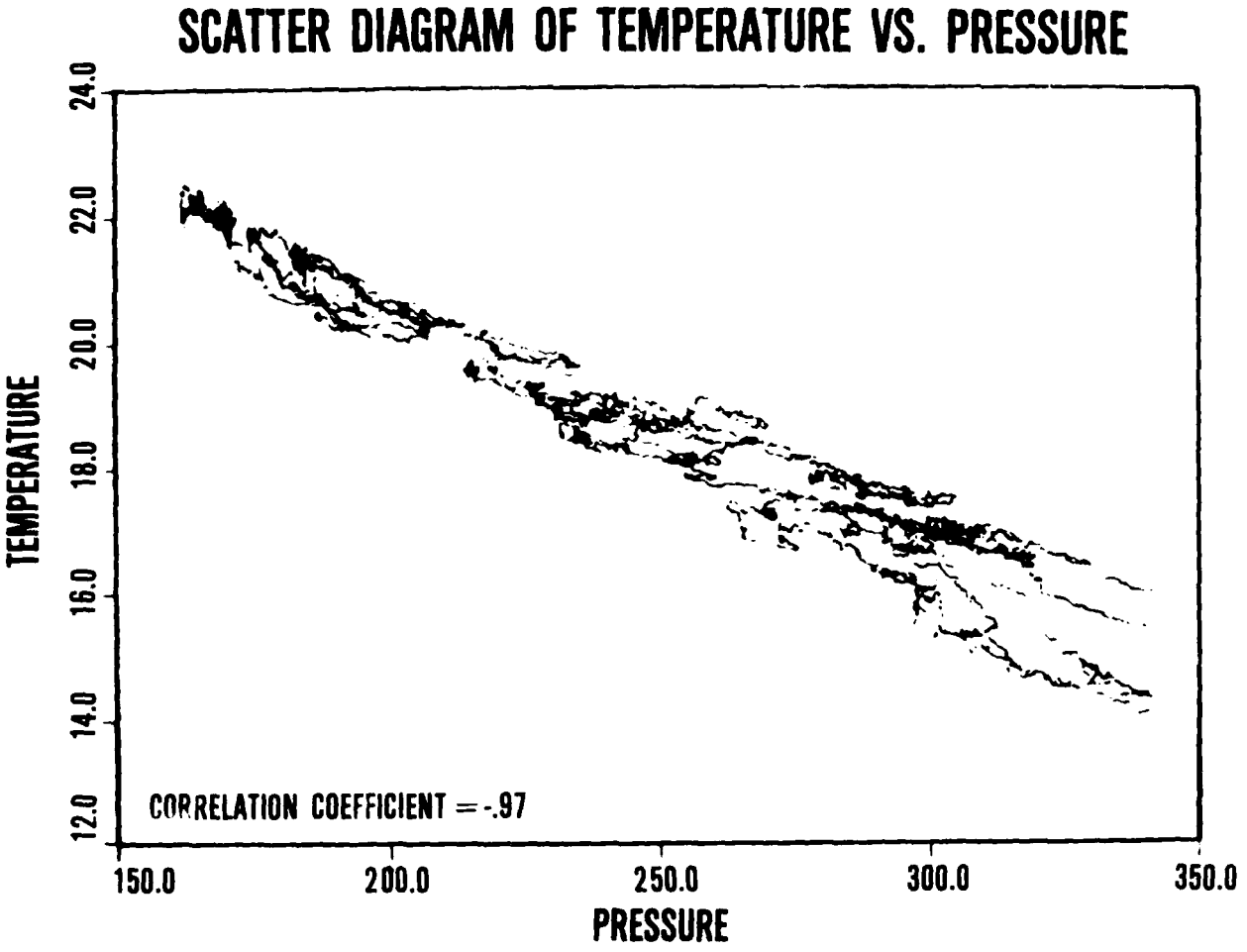

Figure 3. Scatter diagram of temperature vs. pressure on upper temperature/ pressure recorder

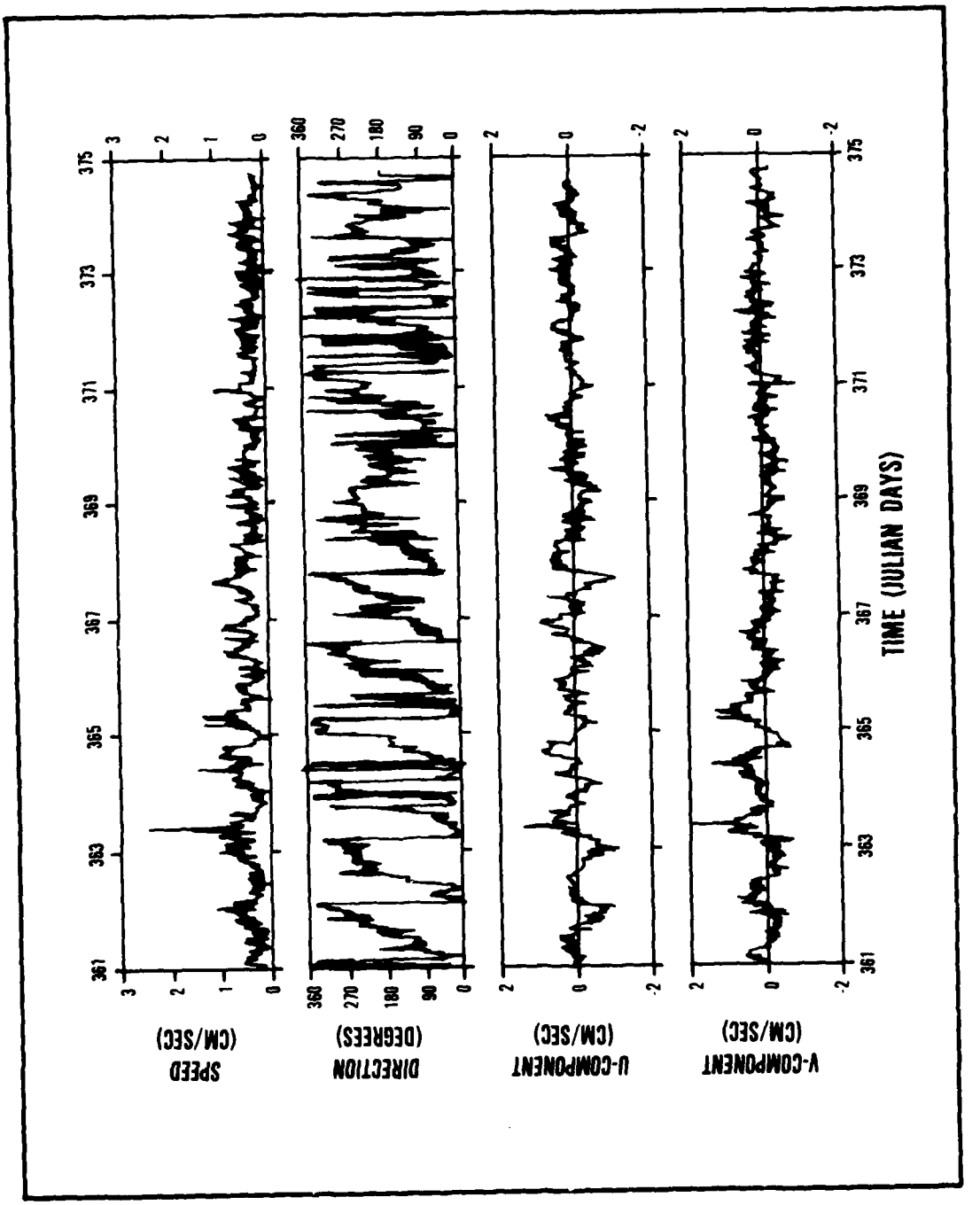

Figure 4. Observed mooring velocities at upper acoustic tracking unit

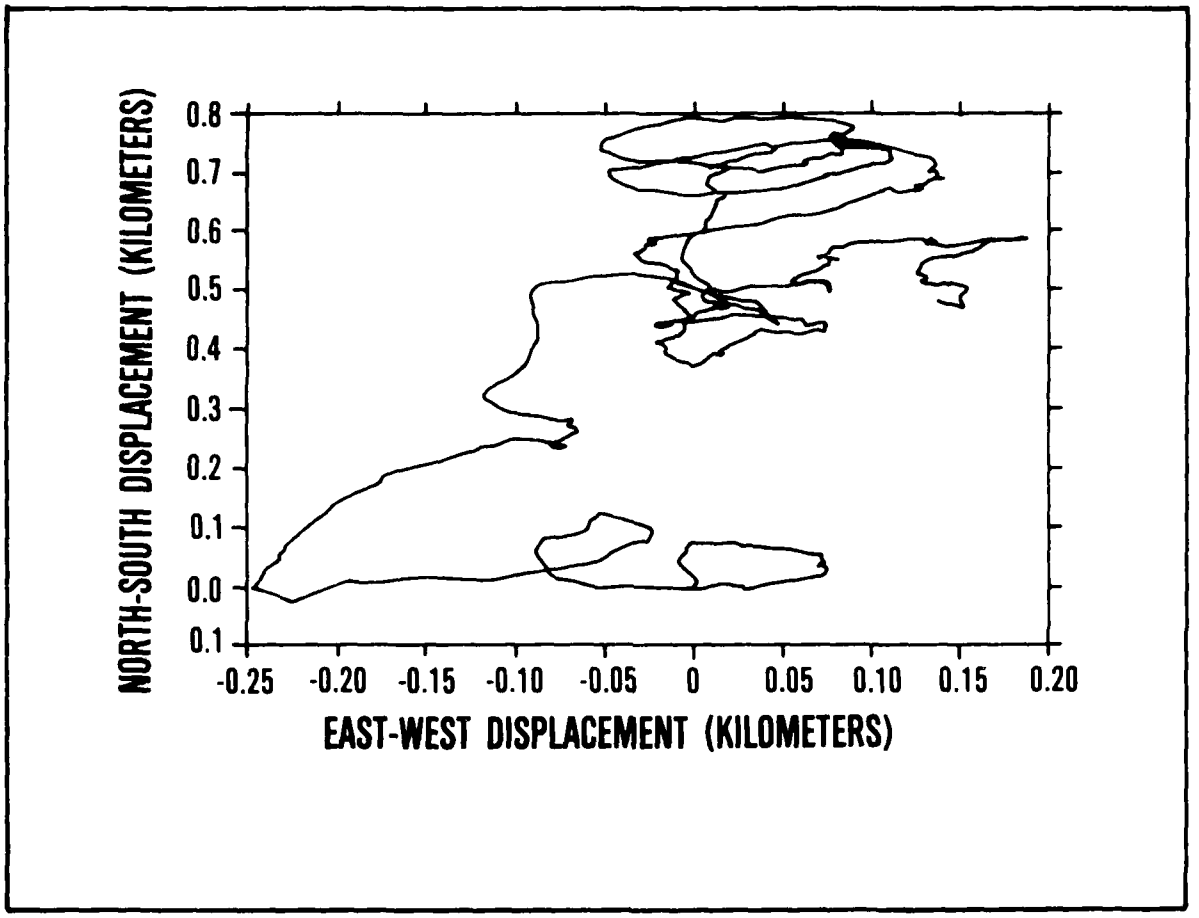

Figure 5. Observed horizontal position of the ATOM mooring at the upper acoustic tracking unit

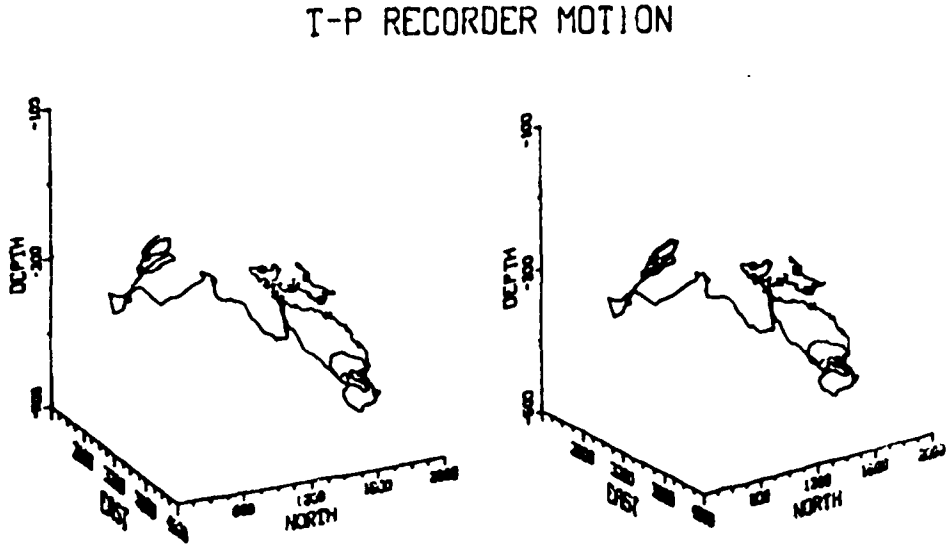

Figure 6. Stereo pair representation of the three-dimensional track of the upper acoustic tracking unit

FILE TRK
METER 01
DEPTH 100

ARRAY: [illegible]
START: 27 DEC 1981
END: 09 JAN 1982

LATITUDE: .000000
LONGITUDE: .000000

0- 10	1	4	4	1	3	1	4		1				2									21	3.[illegible]
10- 20		7	8	5	9	7	2	2			2											42	6.4
20- 30		1	1	5		1		2	1											1		1[illegible]	[illegible]
30- 40		4	[illegible]	6	4	2			1		2											[illegible]	[illegible]
40- 50		2	9	2	4	3	1		5													[illegible]	[illegible]
50- 60	[illegible]	4	3	3	2	4	2															[illegible]	[illegible]
60- 70		1	5	4	5	6	2															23	[illegible]
70- 80		3	5	4	1	3	1		1	1												19	2.9
80- 90	1	1	3	1	8	2		1	1													18	2.7
90-100		5	3	8	3		1	1		1												22	3.3
100-110	1	6	5	1	6	2	1		1													[illegible]	3.5
110-120	[illegible]	5	1	1	2	2	1															[illegible]	[illegible]
120-130	2	[illegible]	10	1	1	3				1												[illegible]	3.8
130-140	[illegible]	[illegible]	4	1	4	1			3													[illegible]	[illegible]
140-150		2	1	1	1																	5	[illegible]
150-160		9	3		1																	13	[illegible]
160-170	[illegible]	4	1	8	3			1														[illegible]	[illegible]
170-180	4	5	6	1	2																	[illegible]	[illegible]
180-190		1	4	4	5		1															[illegible]	[illegible]
190-200	2	3	2		3		1															11	1.[illegible]
200-210		1	6	4		4	2															17	[illegible]
210-220		4	2	3	3	2		1		1												16	2.4
220-230	2	6	12	8	3	4	2	1	3													41	6.[illegible]
230-240	1	2	8	3	3	3																20	3.0
240-250	1	3	2	5	5	1	6	4	1													[illegible]	4.[illegible]
250-260	1		3	2	1	1	1			1												10	[illegible]
260-270					3	3	1			1	1											[illegible]	[illegible]
270-280	1	1	2		2	1					2											[illegible]	[illegible]
280-290		3	3		1	1	2		1	1												[illegible]	[illegible]
290-300	3	[illegible]	1	3	1	1	1		1													[illegible]	[illegible]
300-310	2	1	3	3	1	3					1											14	[illegible]
310-320	3	[illegible]	7	1		2	3	1														[illegible]	[illegible]
320-330		4	1	3	5	1																14	[illegible]
330-340		4	10		3	2																19	[illegible]
340-350		3	3		2	2	1	3														14	[illegible]
350-360		1	1	1	3	3	1	1	1				1									13	2.[illegible]
SPEED	.0	.1	.2	.3	.4	.5	.6	.7	.8	.9	1.0	1.1	1.2	1.3	1.4	1.5	1.6	1.7	1.8	1.9	2.0		
NUM	34	116	147	94	100	70	40	19	21	7	8	0	1	2	0	0	0	0	0	1	[illegible]	66[illegible]	
PER CT.	5.[illegible]	17.6	22.3	14.2	15.2	10.6	6.1	2.9	3.2	1.1	1.2	0	.2	.3	.0	.0	.0	.0	.0	[illegible]	[illegible]		

NUMBER OF ZERO SPEEDS	0		PERCENTAGE ZERO SPEEDS	.0		
NUMBER OF OBS.	660		NUMBER MISSING OBS	0		
AVERAGE SCALAR SPEED	.38	CM/SEC	MAXIMUM/MINIMUM U	1.38 CM/SEC	-1.06	CM/SEC
STANDARD DEVIATION	.26	CM/SEC	MAXIMUM/MINIMUM V	3.40 CM/SEC	-.83	CM/SEC
VECTOR MEAN SPEED	.04	CM/SEC	MAXIMUM SPEED	3.67 CM/SEC		
VECTOR MEAN DIRECTION	18.01	DEGREES	DIRECTION OF MAX SPD	22.15 DEGREES		

55[illegible]

Figure 7. Histogram of mooring speeds and directions with associated statistics

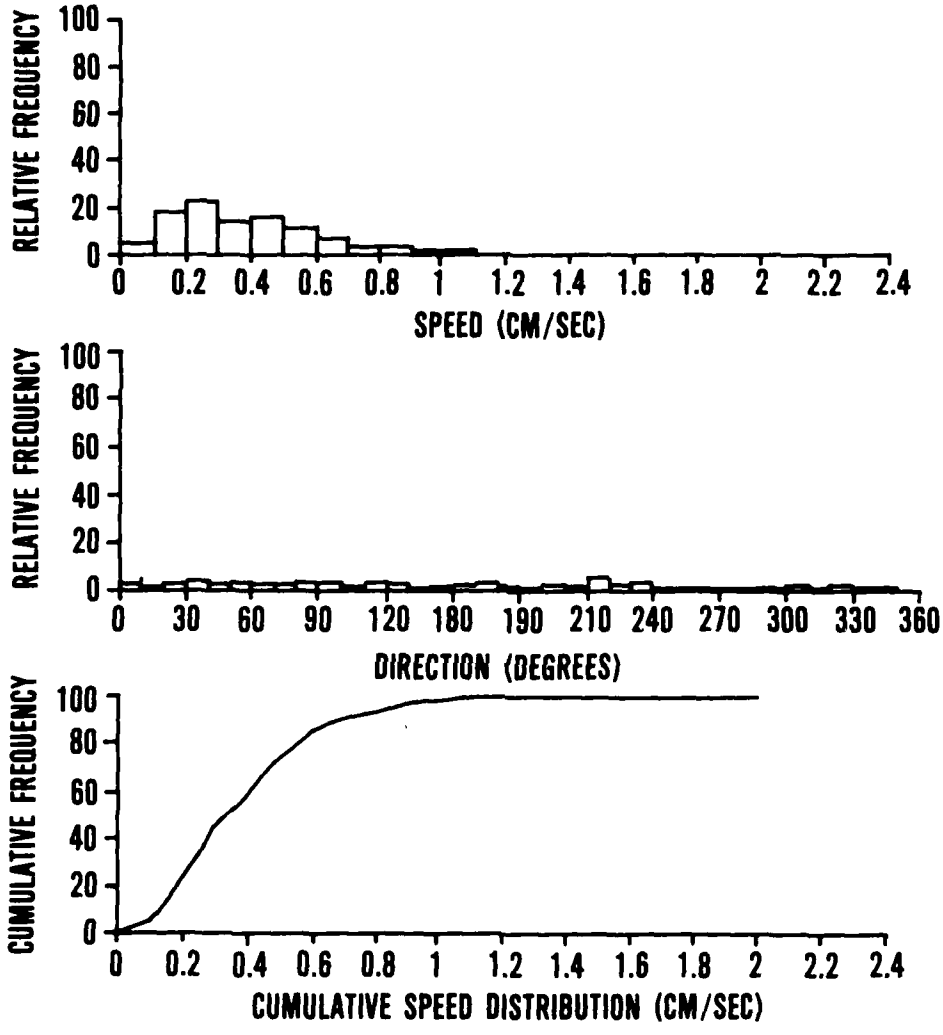

Figure 8. Summary histogram plots of mooring speeds and directions

1. Average speed: 0.38 cm/sec
2. Standard deviation: 0.26 cm/sec
3. Maximum speed: 3.67 cm/sec*
4. Vector record speed: 0.04 cm/sec

The graphs of the speed and direction histograms and the cumulative distribution function for speed are shown in Figure 8.

Velocity variance spectra were also computed for both the pulse and Doppler data. The combined spectra are plotted along with a typical ACM current spectrum in Figure 9. The Doppler spectra appear to agree quite well with the pulse spectra in the overlap region. The spectral level of the mooring velocities is about a factor of 20 below the current spectral level until a frequency of about 3-4 cph. The Doppler spectrum then becomes quite flat.

FLATTENING OF THE DOPPLER SPECTRUM

In order to understand the cause of this flattening, we will consider the effect of least significant bit error in the Doppler system. According to Spindel et al. (1976), the change in a range position over a single estimate is given by

$$\Delta R_j = \frac{Ki\ \bar{c}}{4f_j}$$

where Ki is the count from the quadrant detector, $\bar{c}$ is the average sound speed and f_j is the beacon frequency. For the ATOM experiment

$$\bar{c} = 1503.6 \text{ m/s}$$
$$f_j = 13 \text{ kHz}$$

Thus, the least significant bit error, Δ, is given by

$$\Delta = \frac{\bar{c}}{4f_j} = 2.89 \text{ cm}$$

Spindel et al. (1976) states: "the cycle counter makes an independent phase measurement every 0.1 second." Thus, the total displacement during a time T is given by

$$\delta(T) = \sum_{j=1}^{10T} \delta_j + \sum_{j=1}^{10T} \Delta_j$$

*There was only one such observation. The next higher speed was about 1.3 cm/sec This was probably an erroneous spike that was missed in the editing process.

where δi is the true displacement over each 0.1 sec, T is the time in seconds, and Δi is a random variable, uniformly distributed over $-\Delta/2$ to $\Delta/2$. The variance of Δ is then

$$\sigma_\delta^2 = \frac{10T\Delta^2}{12}$$

The corresponding velocity variance is given by

$$\sigma_v^2 = \frac{\sigma_\delta^2}{T^2} = \frac{10\Delta^2}{12T}$$

If we consider that this variance will appear in the spectrum as white noise, evenly distributed over the frequency range [o, fn] (fn = Nyquist frequency = 1/2T), then the spectral level of the Least Significant Bit (LSB) noise is given by

$$S_{LSB}(f) = \frac{\sigma_v^2}{f_N} = \frac{10\Delta^2}{6} = 1.66\Delta^2$$

The units are in $cm^2/s^2/Hz$. To transform to the more usual units of $cm^2/s^2/cph$, we must divide by 3600 giving:

$$S_{LSB}(f) = 4.611 \times 10^{-4}\Delta^2$$
$$= 3.85 \times 10\Delta^{-3}\ cm^2/s^2/cph$$

This value is plotted as a horizontal line, labeled LSB, in Figure 9. It is clear that this lies very close to the flat portion of the Doppler spectrum and is probably the cause of this flattening. (There is no evidence to support or reject the hypothesis that the mooring motion is significantly below the currents in the frequency band 3-30 cph.)

ORIENTATION EFFECTS

No current meter has a perfectly linear response under all conditions of flow. This correct statement, but unfortunate fact, affects all attempts to measure and interpret current. The interaction between the current meter's response to the flow and the mooring motion produce signals that differ from the true ocean currents. For lack of a better term, we will call the difference between the signal and the local relative current "response error."

The response error may arise from a number of different sources, among which are:

1. nonlinear response of the flow sensors (inertial effects, bearing friction, etc.),

2. horizontal and vertical variations caused by instrument geometry and near-field flow patterns (tie rod interference),

3. mismatch of speed and direction sensors (vanes/rotors). For the acoustic current meters, the primary response errors are due to rotation of the current meter along its axis due to torsional motion of the mooring line (horizontal response error) and to the tilt of the current meter from a vertical position (vertical response error).

Three force vector recorders (FVRs) were supplied by the C.S. Draper Laboratory, Cambridge, Massachusetts (to measure the tilt and torsional effects of the mooring). These FVRs were to have recorded acceleration, magnetic field, pressure, and tension information at three points on the mooring. The lower two units failed to yield useful data, and the upper unit appeared to produce data of doubtful quality soon after deployment.

Information relating to the tilt of the mooring from a vertical position was deduced from the upper two T/P recorders. Torsional motions could be estimated from the case direction measurements of the current meters. The VACMs returned a case direction every sampling interval (either 15/16 or 15/8 min), and the acoustic current meters returned a case direction every 3 minutes.

VERTICAL RESPONSE ERRORS

The vertical tilt was estimated by computing

$$\theta = \text{arcosine } (\Delta D/L)$$

where ΔD is the difference in the depth of the upper two T/P recorders computed from the observed pressures, and L is the distance between the T/P recorders (123 m). The angles computed in this manner are less than 10° for the periods in which the pressure sensors were in range. The error caused by this 10° tilt is about 2% (McCullough, 1978), see Figure 10; thus, the error is expected to be less than this. Furthermore, this error is subject to very low frequency modulation and would not be expected to significantly contaminate the high frequency region of the spectrum.

HORIZONTAL RESPONSE ERRORS

Saunders (1980) studied the horizontal response function of the ACM. Figure 11 consists of plots of typical horizontal speed and response functions for the ACM. It may be seen that the observed speed may vary between about +8% and -6% of the true speed, depending on the orientation of the current meter case to the mean flow. The apparent direction may also vary between ±5° of the mean current direction. The angle between the case of an ACM and the observed current is plotted as a function of time for a typical case in Figure 12. Long periods of little case/current angle variation may be seen interspersed with abrupt large changes in angles. These changes introduce the possibility of contamination of the records by as much as 6-8% of the mean speed. This, of course, is a worst case situation, though one which might be expected to produce apparent high frequency contamination of the current data with spectral slopes of f^{-2} (step response). As the existing data have this type of slope, it would be difficult to detect this type of contamination through spectral processing; however, it would be expected to appear in the records as jump

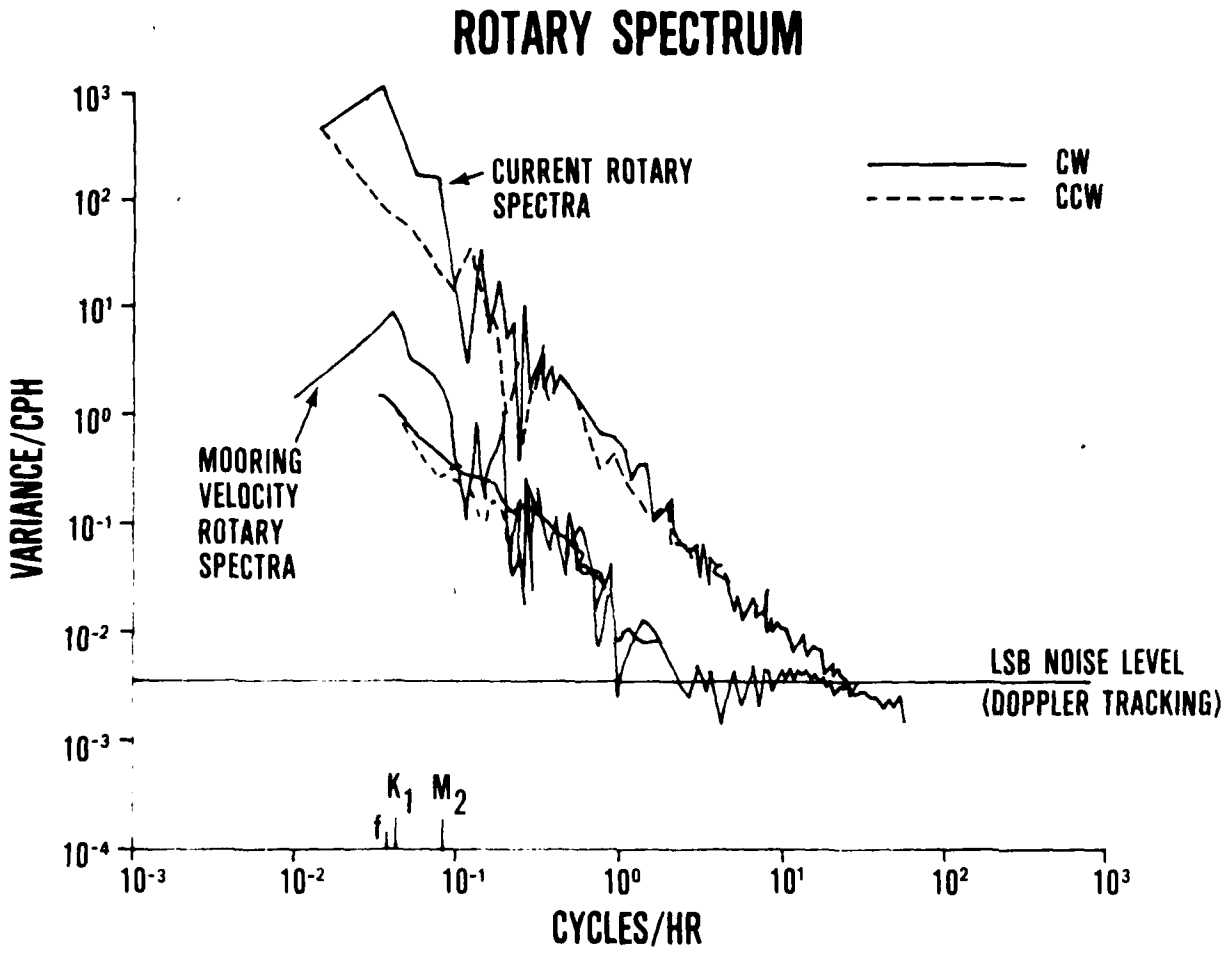

Figure 9. Rotary spectra of currents and mooring velocities

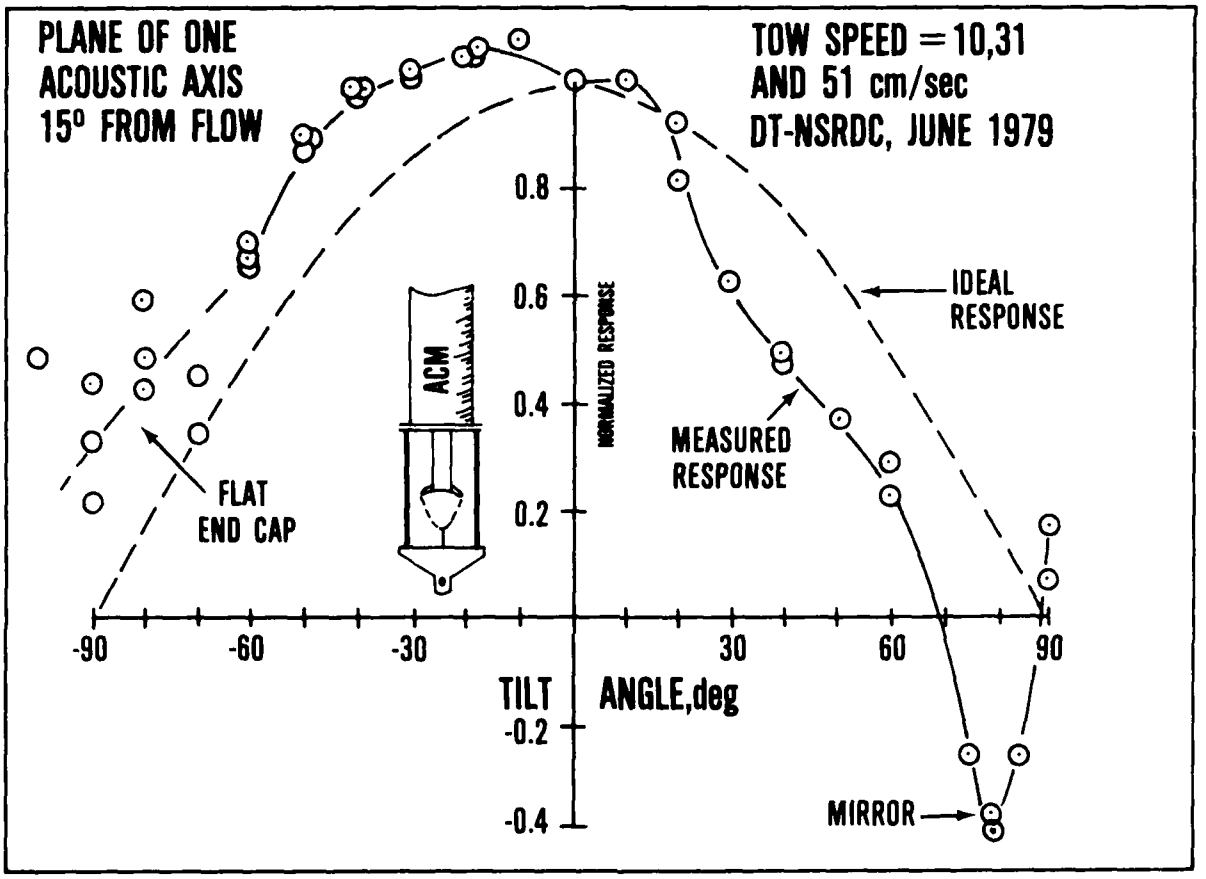

Figure 10. Vertical response of the Neil Brown acoustic current meter

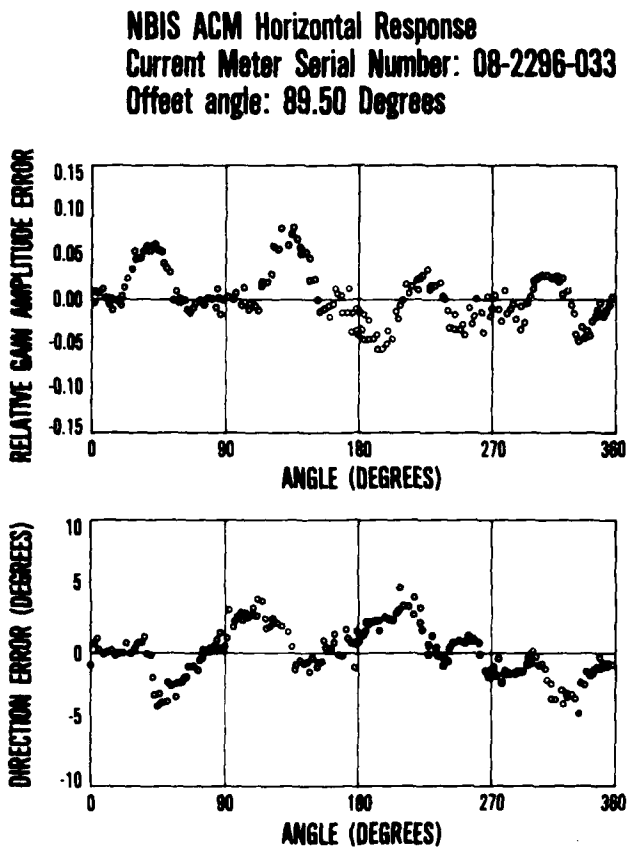

Figure 11. Observed horizontal response of Neil Brown acoustic current meter

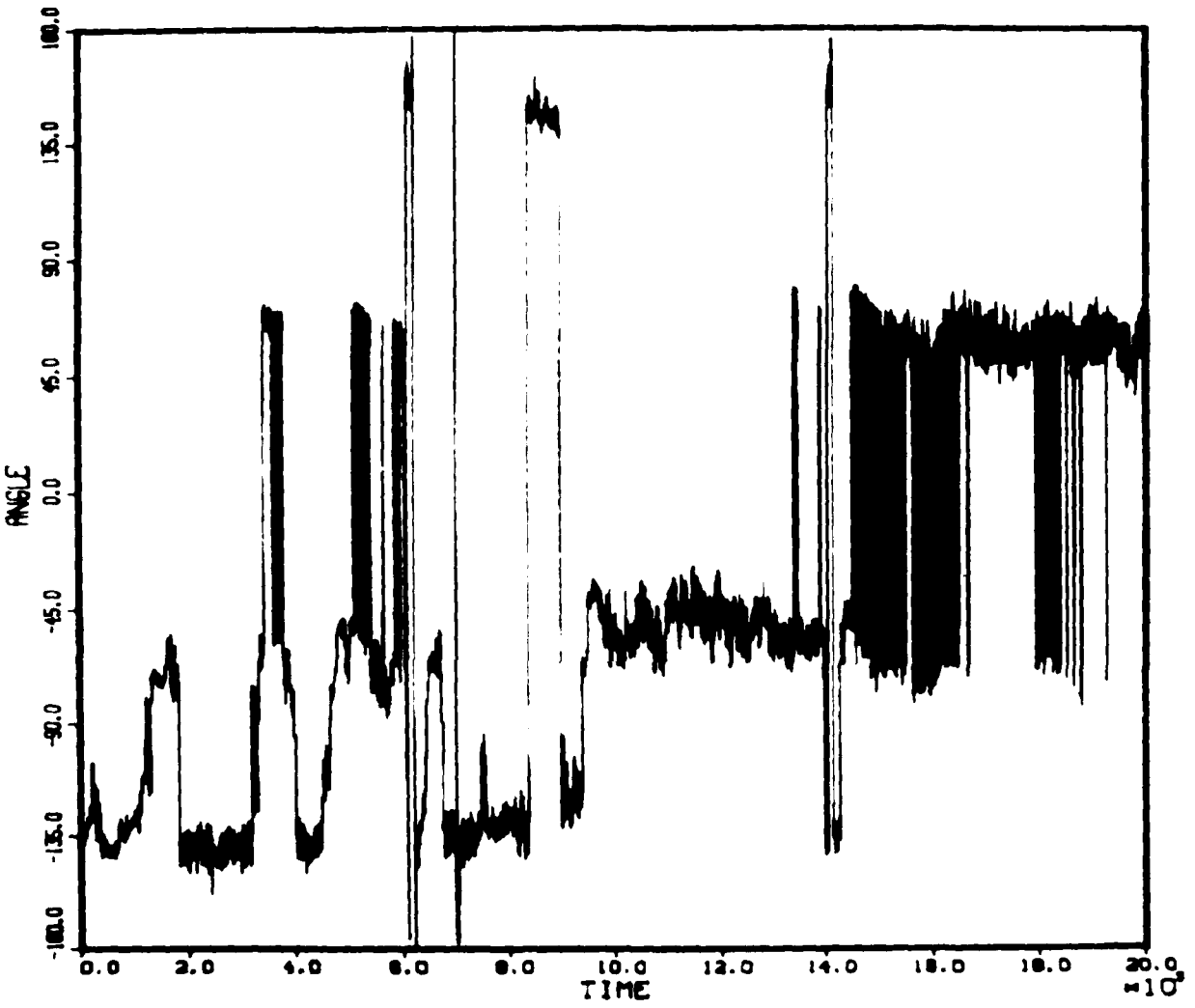

Figure 12. Time history of current meter case-current angle

discontinuities in the velocity components. Some discontinuities do appear, but it is not known at this time whether they are attributable to the case response/mooring motion interation.

To estimate the magnitude of the case orientation error, the response function of Figure 11 was applied to obtain estimates of the error term, based on the observed currents at the upper acoustic current meter. The statistics for these errors are summarized in Figure 13, which also depicts a "speed-direction" histogram of the torsional error components. The RMS error is 1.16 cm/sec with a standard deviation of 0.58 cm/sec. This is about three times as large as the errors due to translational motions. The magnitude and direction histograms are plotted in Figure 14. Figures 15-17 are spectral plots of the observed currents at the upper current meter compared with the spectra of the angular response error. From these plots, we can see that the torsional errors fall off with about the same spectral slope as do the current components.

Because of the FVRs failures, no useful data that could be used to obtain high frequency accelerations of the mooring or tension records to be used in future mooring design and modeling were returned.

ENVIRONMENTAL MEASUREMENTS

The background measurements collected during the ATOM 1979 experiment fall into two broad categories: shipboard and moored measurements. The data collected from the ship provided information on the vertical structure of the oceanic temperatures, salinity and horizontal component of velocity fields during the deployment, and recovery phases of the experiment. The moored instruments provided a moderately long time series of temperature and horizontal velocity over the period between deployment and recovery (approximately 26 days at a sampling rate of 1/min). The ship survey data will be discussed first, and is followed by a discussion of the moored time series data.

SHIPBOARD SURVEYS

The primary purpose of the data collected from the ship during deployment and recovery was to provide information on the vertical structure of density and currents near the mooring site, and to provide a relationship between temperature and density that could be used in future analysis of the current/temperature data.

The primary instrument used for temperature and salinity determination was the Neil Brown CTD. The instrument was calibrated prior to the deployment cruise, both statically and dynamically. CTD, serial number 4017 was used. The average static errors for temperature, conductivity, and salinity were -0.0014°C, -0.00052 mmho/cm and -0.00014°/oo, respectively. The time constants, obtained from dynamic drop tests were approximately 243 ms (temperature) and 59 ms (conductivity). The large mismatch between the temperature and conductivity time responses required matched low-pass filtering to avoid spiking in the computed salinity profiles. The drop rates were typically about 1 m/sec, thus, the data were low-pass filtered to give a 1 m resolution (actually 1 dbar resolution was used) and the edited and filtered CTD data were interpolated and recorded at 1 dbar intervals. From these standard files were computed secondary quantities: depth, salinity, σ_T, σ_θ, Brunt-Väisälä frequency and sound speed.

The vertical structure of the horizontal currents were obtained from expendable shear probe drops. The horizontal components of current are obtained by inference

FILE: ACM
METER: 790100
DEPTH: 000123

ARRAY: [illegible]OM79
START: 19 DEC 1900
END: 11 JAN 1901

LATITUDE: 25.805555
LONGITUDE: -89.744165

0- 10	24	64	126	114	124	119	144	129	125	134	224	270	114	21							1732	5.[illegible]
10- 20	36	50	96	71	79	86	98	95	101	126	165	205	87	15	4						1319	4.[illegible]
20- 30	47	53	63	49	41	47	65	39	42	56	86	41	60	18							707	2.[illegible]
30- 40	55	80	56	38	16	7	8	6	4	3	1										274	[illegible]
40- 50	14	107	41	12	1																180	.5
50- 60	11	37	26	2																	76	.2
60- 70	10	37	27																		74	[illegible]
70- 80	10	75	55																		140	.4
80- 90	6	132	40	2																	180	.5
90-100	15	40	95	23	7																230	.7
100-110	35	47	119	65	24	12	5	1													308	.9
110-120	37	74	124	128	97	54	35	59	19												627	1.[illegible]
120-130	34	89	105	139	200	191	258	225	78	2											1321	4.0
130-140	43	105	128	208	292	358	536	474	121	6											2271	6.9
140-150	35	102	164	239	415	623	663	603	157	2											3003	9.1
150-160	39	88	161	241	492	624	674	506	133	4											2962	8.9
160-170	33	81	161	267	469	554	473	390	60												2488	7.5
170-180	44	74	158	229	315	244	127	107	38												1336	4.0
180-190	25	76	157	161	135	73	18	2	1												648	[illegible]
190-200	17	96	141	59	66	28	3														[illegible]	[illegible]
200-210	12	115	66	29	44	18	5														[illegible]	[illegible]
210-220	5	77	54	13	4																[illegible]	[illegible]
220-230	6	35	26	2																	69	[illegible]
230-240	6	60	23																		89	[illegible]
240-250	14	121	27																		[illegible]	[illegible]
250-260	40	61	13																		114	[illegible]
260-270	50	23	52	5																	[illegible]	.4
270-280	37	41	47	33	2																160	.5
280-290	32	74	56	43	32	17		2													[illegible]	[illegible]
290-300	2[illegible]	41	63	55	46	46	21	16	19	15	3	14		1							40[illegible]	[illegible]
300-310	33	54	77	68	75	62	73	75	53	66	60	73	3[illegible]	7							[illegible]	[illegible]
310-320	[illegible]	63	106	110	102	134	133	143	115	110	99	100	47	6							1286	3.[illegible]
320-330	19	87	106	109	111	195	277	297	236	225	113	60	25								[illegible]	[illegible]
330-340	[illegible]	61	108	153	168	270	377	391	340	389	112	74	24	3	1						[illegible]	[illegible]
340-350	24	82	107	175	205	259	290	264	280	311	133	162	52	5	3						2352	[illegible]
350-360	25	85	85	160	167	250	264	227	242	207	170	224	66	12	4						2208	6.[illegible]
SPEED	.0	.2	.4	.6	.8	1.0	1.2	1.4	1.6	1.8	2.0	2.2	2.4	2.6	2.8	3.0	3.2	3.4	3.6	3.8	4.0	
N	941	2684	3061	3002	3729	4271	4547	4051	2164	1656	1166	1223	525	91	12	0	0	0	0	0	0	33120
PERCENT	2.8	8.1	9.2	9.1	11.3	12.9	13.7	12.2	6.5	5.0	3.5	3.7	1.6	.3	.0	.0	.0	.0	.0	.0	.0	

NUMBER OF ZERO SPEEDS 0 — PERCENTAGE ZERO SPEEDS
TOTAL NUMBER OF OBS. 33120
AVERAGE SCALAR SPEED 1.16 CM/SEC — MAXIMUM/MINIMUM V 1.54 CM/SEC -2.36 CM/SEC
STANDARD DEVIATION .58 CM/SEC — MAXIMUM/MINIMUM 2.89 CM/SEC -1.72 CM/SEC
VECTOR MEAN SPEED .20 CM/SEC — MAXIMUM SPEED 2.93 CM/SEC
VECTOR MEAN DIRECTION 19.23 DEGREES — DIRECTION OF MAX SPD 337.52 DEGREES

Figure 13. Histogram and statistics of velocity errors due to horizontal current meter response

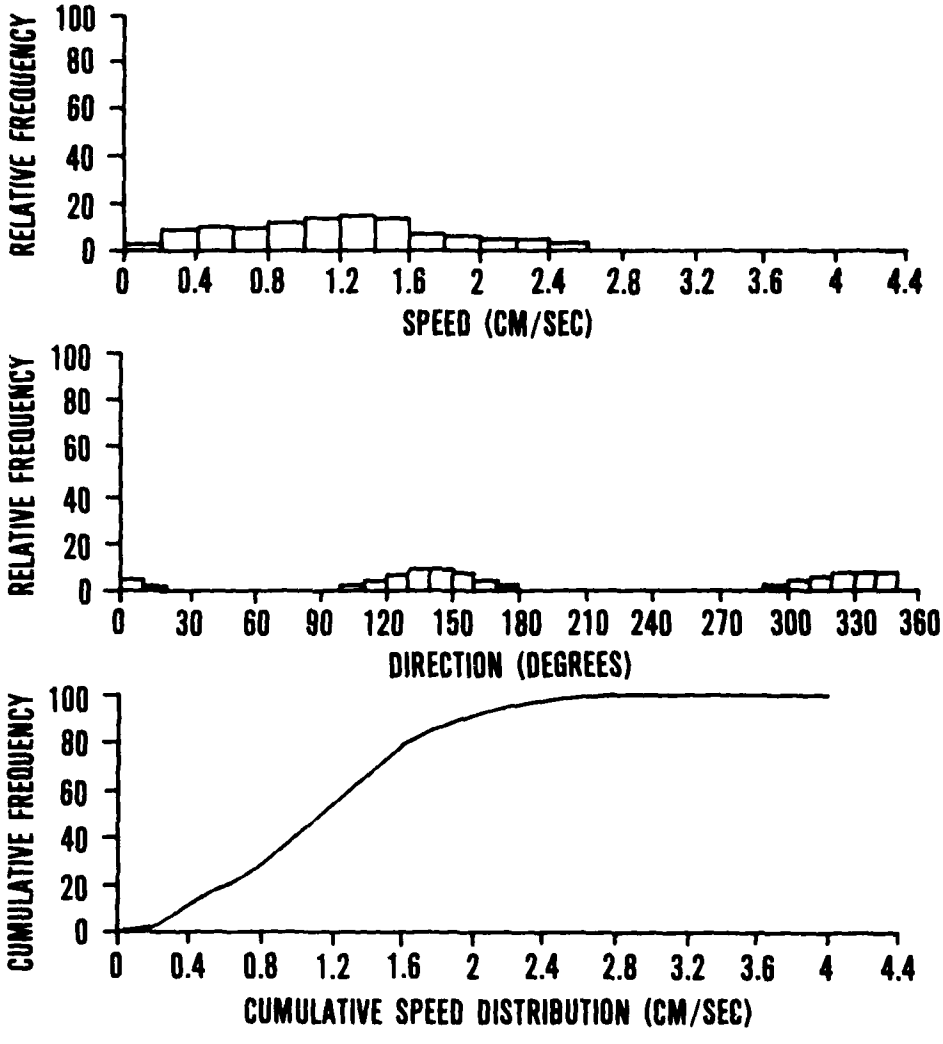

Figure 14. Histogram plots of velocity errors due to horizontal current meter response

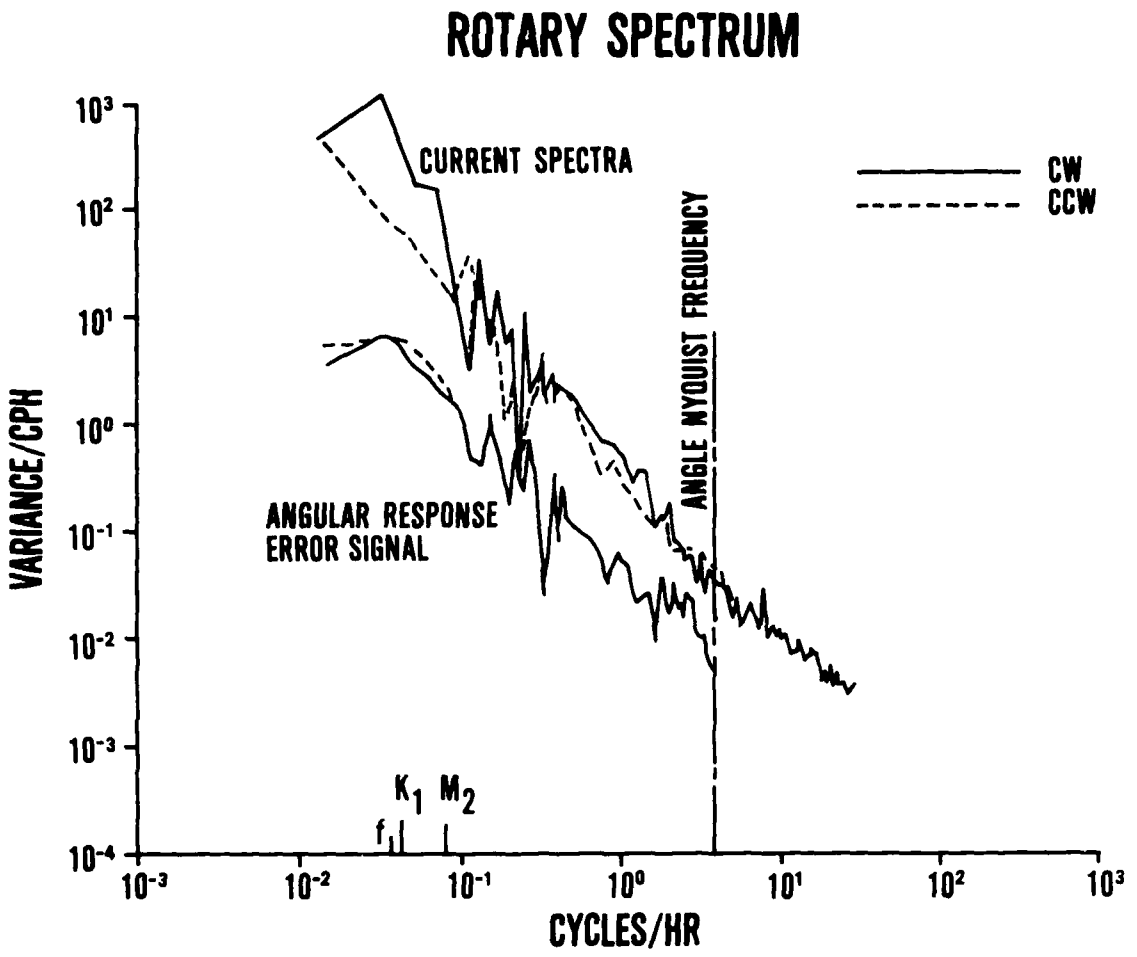

Figure 15. Rotary spectra of current and angular response errors

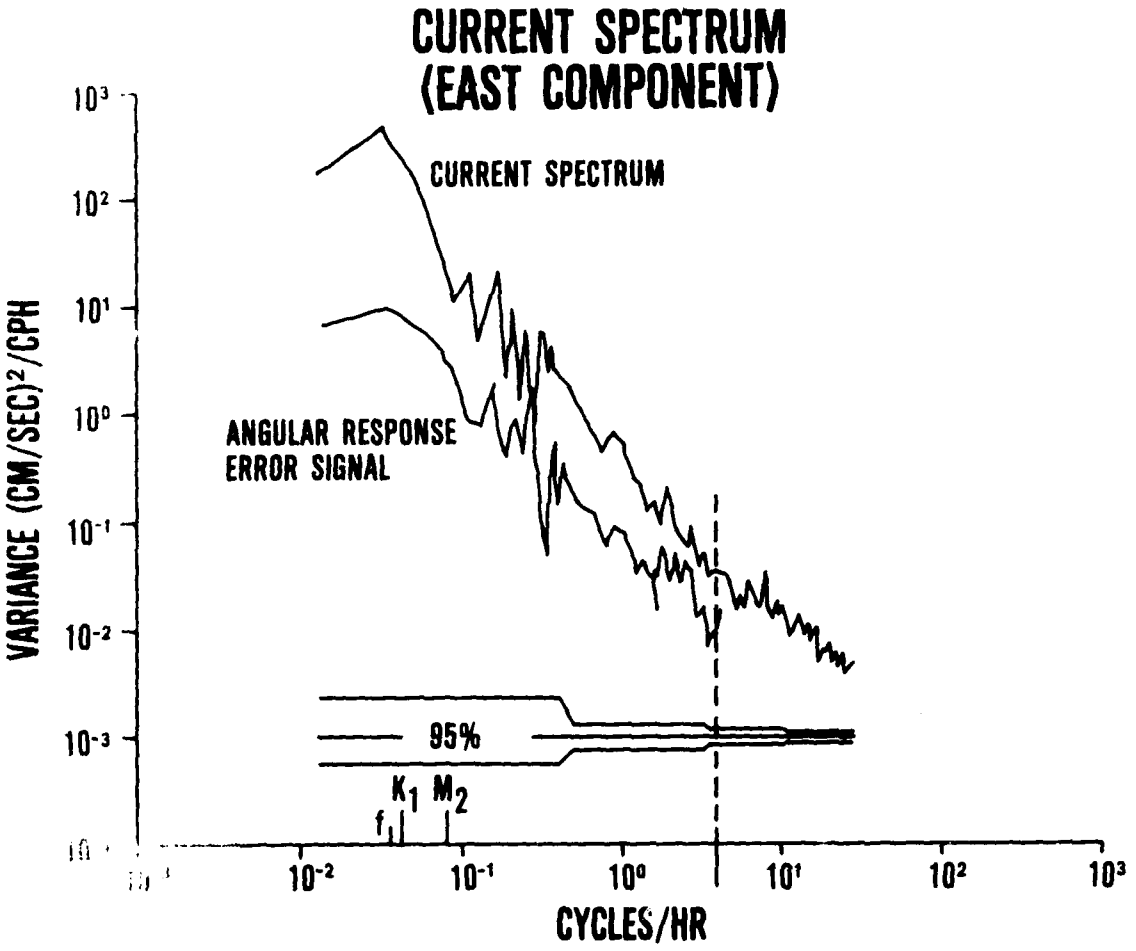

Figure 16. Spectrum of U components of current and angular response errors

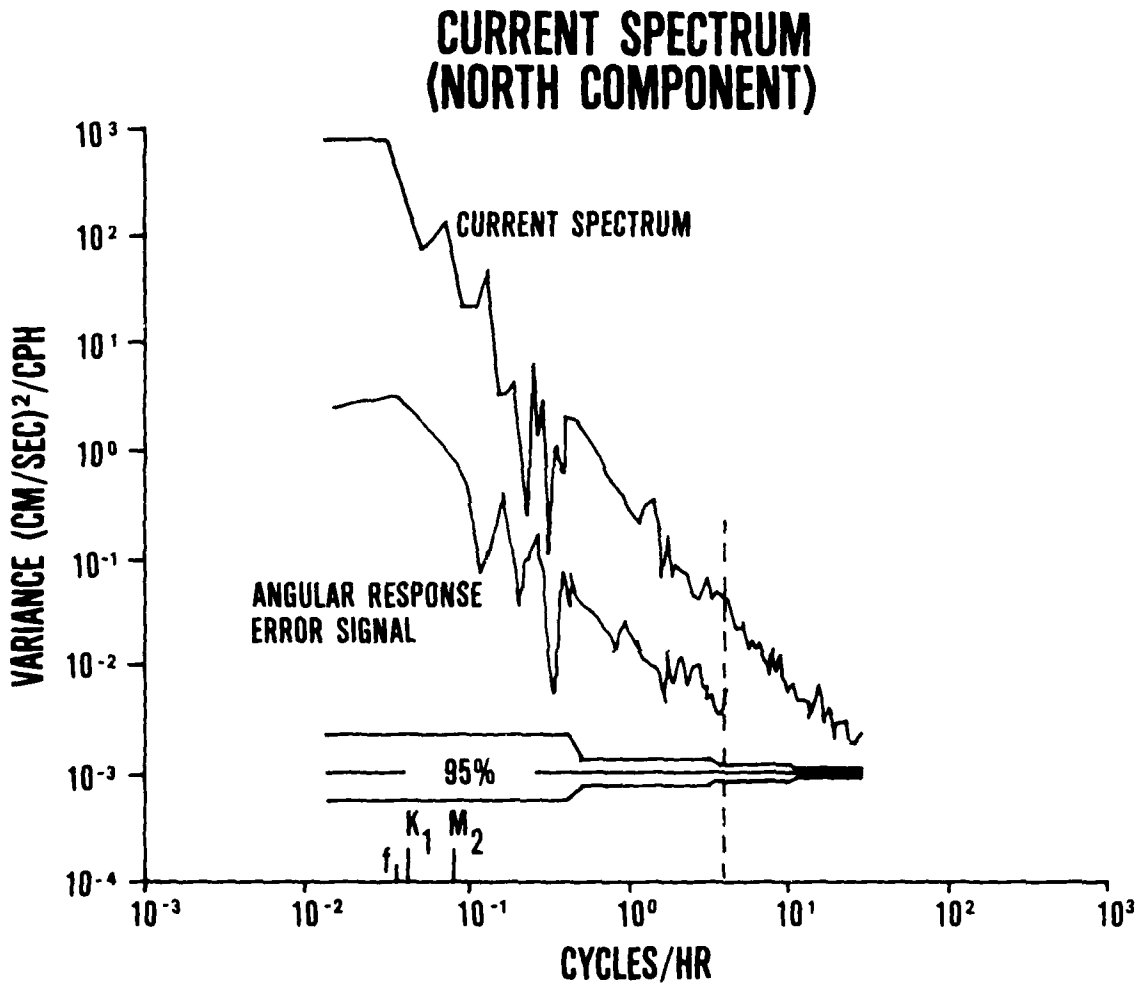

Figure 17. Spectrum of V components of current and angular response errors

[illegible] measured EMF gradient. This gradient arises from the passage of the ocean [illegible] through the earth's magnetic field. The principle of operation has been documented [illegible] Sanford et al. (1974).

[illegible] depth of the XCP is determined by an empirical formula relating the depth [illegible] fall time. Twenty-five concurrent CTD casts and XCP drops were made to test [illegible] of this method. Of these, twenty-one had acceptable shear data (Table [illegible] results are reported in Appendix A. It was found that the standard equation [illegible] accurate enough for use in calculations of Richardson number (Ri). (The reason for this lies in the flatness of the velocity wave number spectrum down to scales of 0.1 cpm--if the depth accuracy of the XCP is not considerably better than 10 m then the velocities being uncorrelated over scales larger than 10 m will lead to unacceptably large errors in the estimation of Ri.)

To improve the depth resolution of the XCPs, the initially computed depths were corrected in each case where a concurrent CTD cast was available. The XCP data were then interpolated to 1 dbar intervals.

For calculations of Richardson number both the XCP velocity data and the CTD [illegible] data were low-pass filtered with an 8 dbar cutoff wave length. The [illegible] numbers were computed from these filtered data. Typical profiles of [illegible] frequency, du/dz, dv/dz, and log (1/Ri) are shown in Figures 18 and [illegible].

[illegible] structure functions for the profiles of the Richardson number and [illegible]) were computed, and a typical example is plotted in Figure 20. The (unnormalized) structure function for a variable, (x), is defined as

$$S\phi(\xi;x) = \langle [\phi(x) - \phi(x + \xi)]^2 \rangle$$

[illegible] the ensemble average of X)

[illegible] related to the covariance (when it exists) by:

$$S\phi(\xi;x) = \langle \phi(x)^2 \rangle + \langle \phi^2(x+\xi) \rangle - 2 \langle \phi(x)\phi(x+\xi) \rangle$$

[illegible] of the structure function over the covariance function is that it may [illegible] the variance and covariance function do not. (For example, just consider [illegible] $\phi(x) = x$).

[illegible] uniformity in plotting, we have normalized $S\phi(\xi;x)$ by

$$4\langle [\phi(x) - \langle \phi(x) \rangle]^2 \rangle$$

[illegible] the averages by the average over all depths. Thus, the structure functions [illegible] interpreted as follows: for $S_\phi(\xi) = 0$, the process is correlated perfectly at lag ξ; for $S_\phi(\xi) = 1/2$, the process is uncorrelated at lag ξ; and $S\phi(\xi) = -1$

means a perfect negative correlation. The structure function is used in preference to the correlation function, primarily due to its greater inherent stability in such nonstationary fields as the thermal and salinity fields in the upper ocean.

Due to low-pass filtering with an 8 m cutoff, the structure function with lags less than 8 m are not well defined. For lags greater than 8 m, it may be seen that the structure function for both Ri and $\log(1/Ri)$ are essentially 0.5, meaning that Richardson numbers with spacings larger than 8 m are essentially uncorrelated.

Wave-number spectra for N, U_z, V_z, Ri and $\log(1/Ri)$ have also been computed. Segment averaging was used over all records which had a depth range greater than 512 m in which the shear profile was not contaminated by the presence of the CTD. These spectra are plotted in Figures 21 through 25. We can see that for wavelengths greater than the low-pass cutoff, the spectra are essentially flat. This observation is in agreement with the results of Gargett et al. (1980). The implication is that the shear field is too uncorrelated in the vertical (in the environment encountered in ATOM) for either moored sensor measurements with separations of 8 m (or so) or XCP probes used in conjunction with CTD profiles to determine the background Richardson number field.

TIME SERIES DATA

Another major facet of the ATOM '79 experiment was the requirement to collect current and temperature time series from a densely spaced moored vertical array. The purposes of these measurements were

1. to determine the relation, if any, between the high frequency variability and inertial frequency motions,
2. to determine the relation, if any, between the meteorological forcing and the inertial frequency motions,
3. to determine the degree to which current components in different frequency bands and vertical separations are correlated (particularly for the higher frequency bands),
4. to determine the effect of proximity to the Brunt-Väisälä frequency maximum on the level of high frequency variability.

THE DATA SET

In order to test the hypotheses, a subset of the total current and temperature data was selected. This data set consisted of 20,000 minutes (approximately 14 days) of ACM data from each of the 13 acoustic current meters, starting at 0000Z, 20 December 1979 (Day 35[illegible].0000). Both components of current and one temperature channel were used. The full length of data from the mooring was not used because one current meter failed (documented in Saunders and Green, 1980). The VACM data were not used due to the differing sampling interval and the different horizontal response. A 5000 minute record from the full data set is plotted in Figures 26-30. The eastward velocity components are plotted in Figure 26, the northward velocity components in Figure 27, the speeds in Figure 28, the temperatures in Figure 29, and the temperature differences in Figure 30.

RELATION BETWEEN HIGH FREQUENCY ACTIVITY AND INERTIAL MOTION

One of the hypotheses of the ATOM experiment was that inertial period motions in the upper ocean would produce a shear field that would modulate the high frequency internal wave intensity. The mechanism for stimulating such activity would be

TABLE 1

XCP & CTD Correspondence

XCP #	CTD #	Temp Corr.	Temp Corr. + good error	
1 (bad)	5	x		
2	-	x		
3 (bad)	-	x		
4	6	✓	✓	
5 (bad)	7	x		
6	7 (up)	x		
7	-	x		
8	8	✓	✓	
9	9	✓	✓	
10 (bad)	-	x		
11	10	✓	✓	
12	11	✓	✓	? anomaly
13	12	✓	✓	
14	13	✓	✓	
15	14	✓	✓	
16	15	✓	✓	
17	16	✓	✓	
18	17	✓	✓	
19 (bad)	18	x		
20	18	✓	✓	
21	19	✓	✓	
22	20	✓	✓	
23	21	✓	✓	
24 (bad)	--	x		
25	22			
26	23	✓	✓	
27 (?)	24	x		
28 (?)	25	x		
29	26	✓		
30 (bad)	27	x		
31	27	✓	✓	
32	28	✓	✓	
33	--	x	✓	
34	30	✓	✓	
35	31	✓	✓	
36	32	✓	✓	
37	33	✓	✓	
38	34	✓	✓	
39	35	x		
40	--	x		

25 good comparisons.

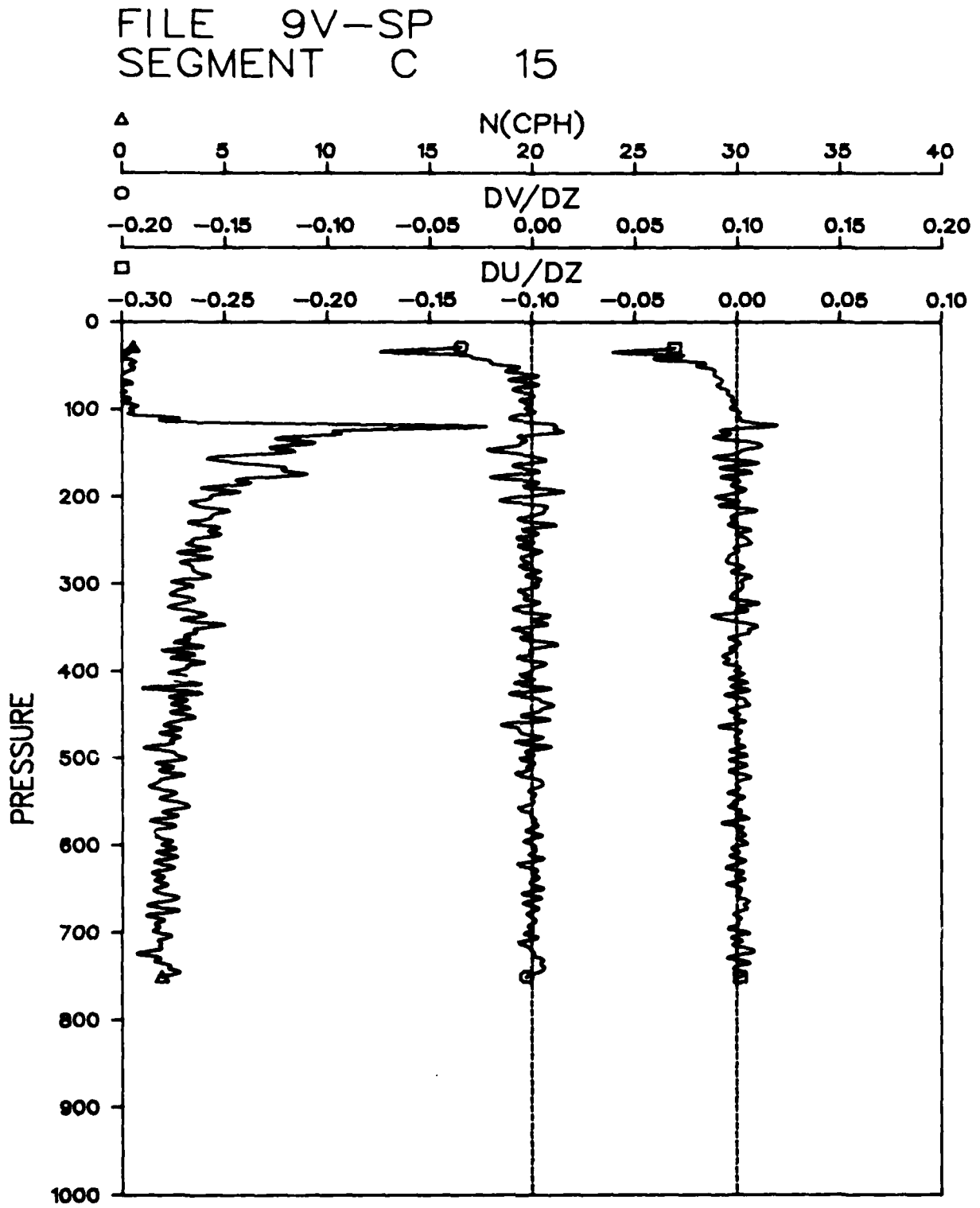

Figure 18. Typical profiles of Brunt-Väisälä frequency, U and V shears

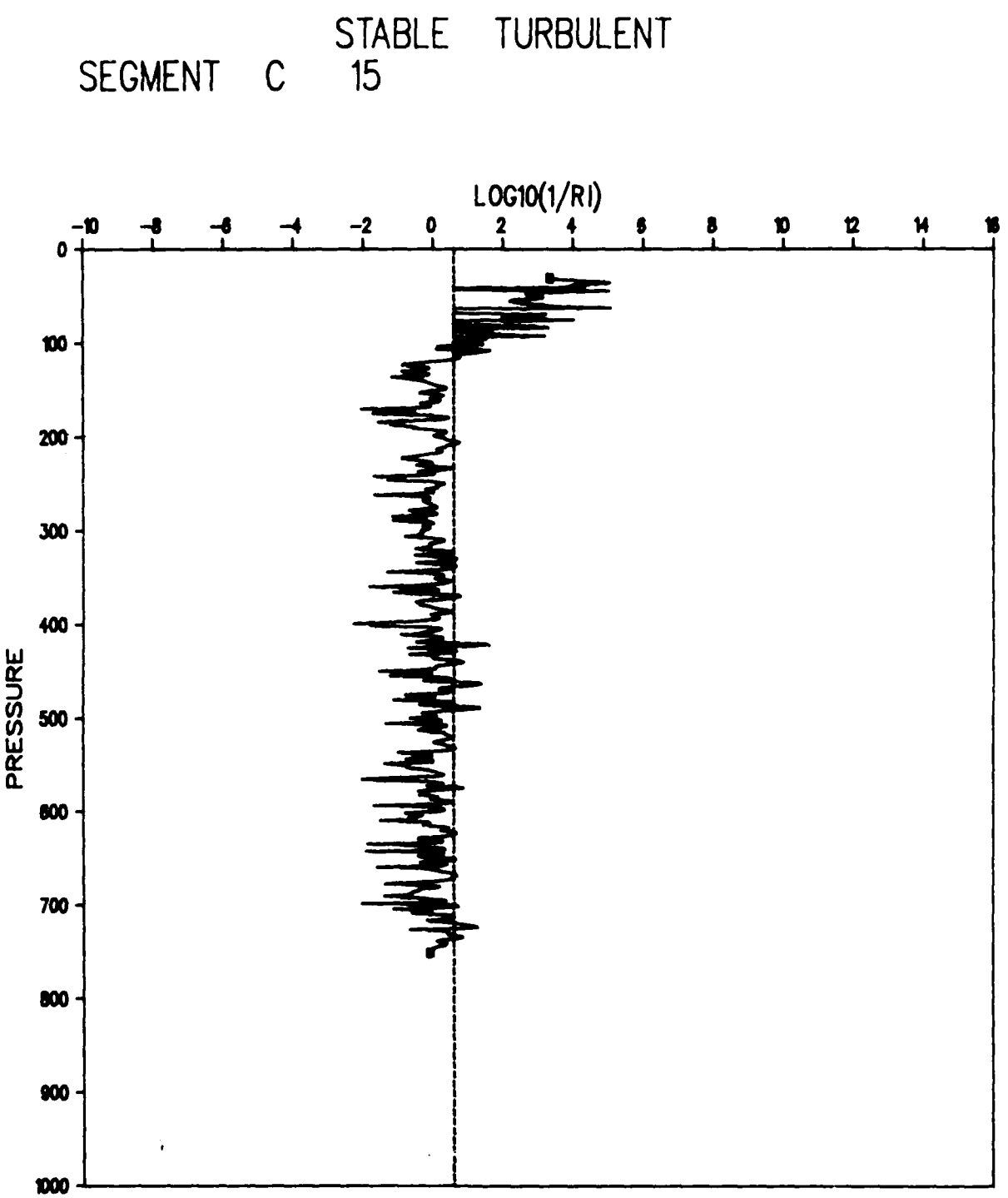

Figure 19. Typical profile of $-\text{Log}_{10}$ (Richardson number)

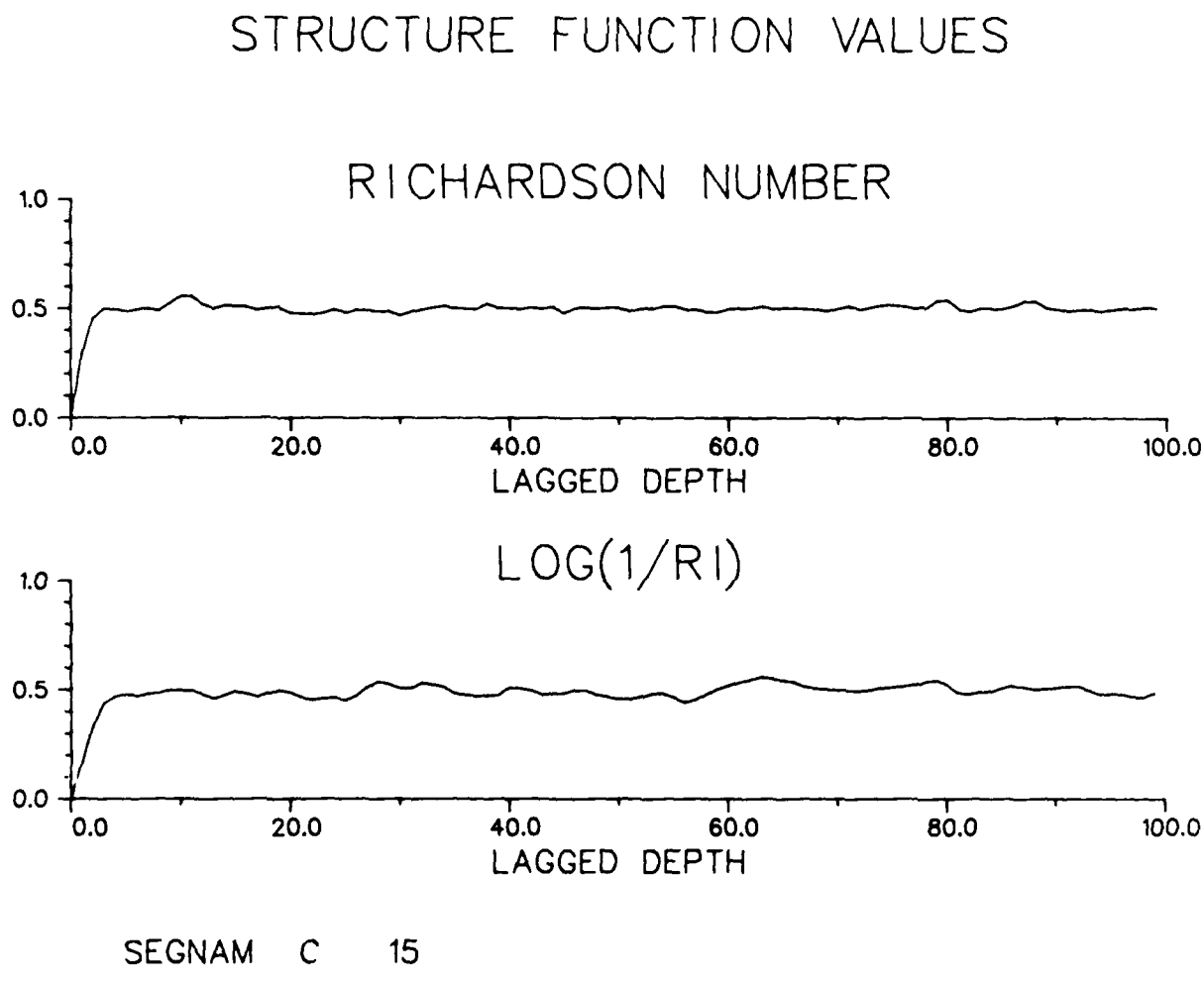

Figure 20. Typical Richardson number structure functions

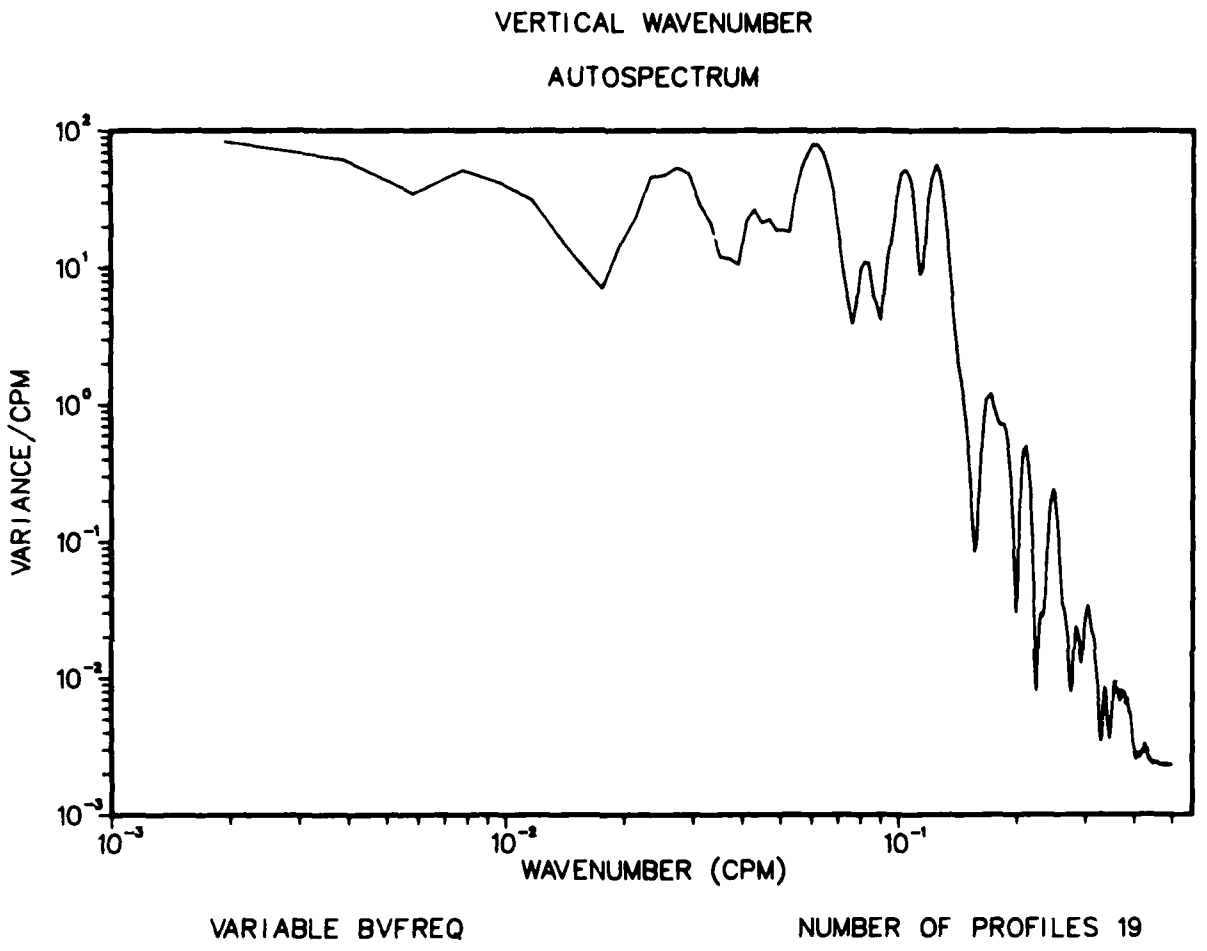

Figure 21. Vertical wavenumber spectrum of Brunt-Väisälä frequency

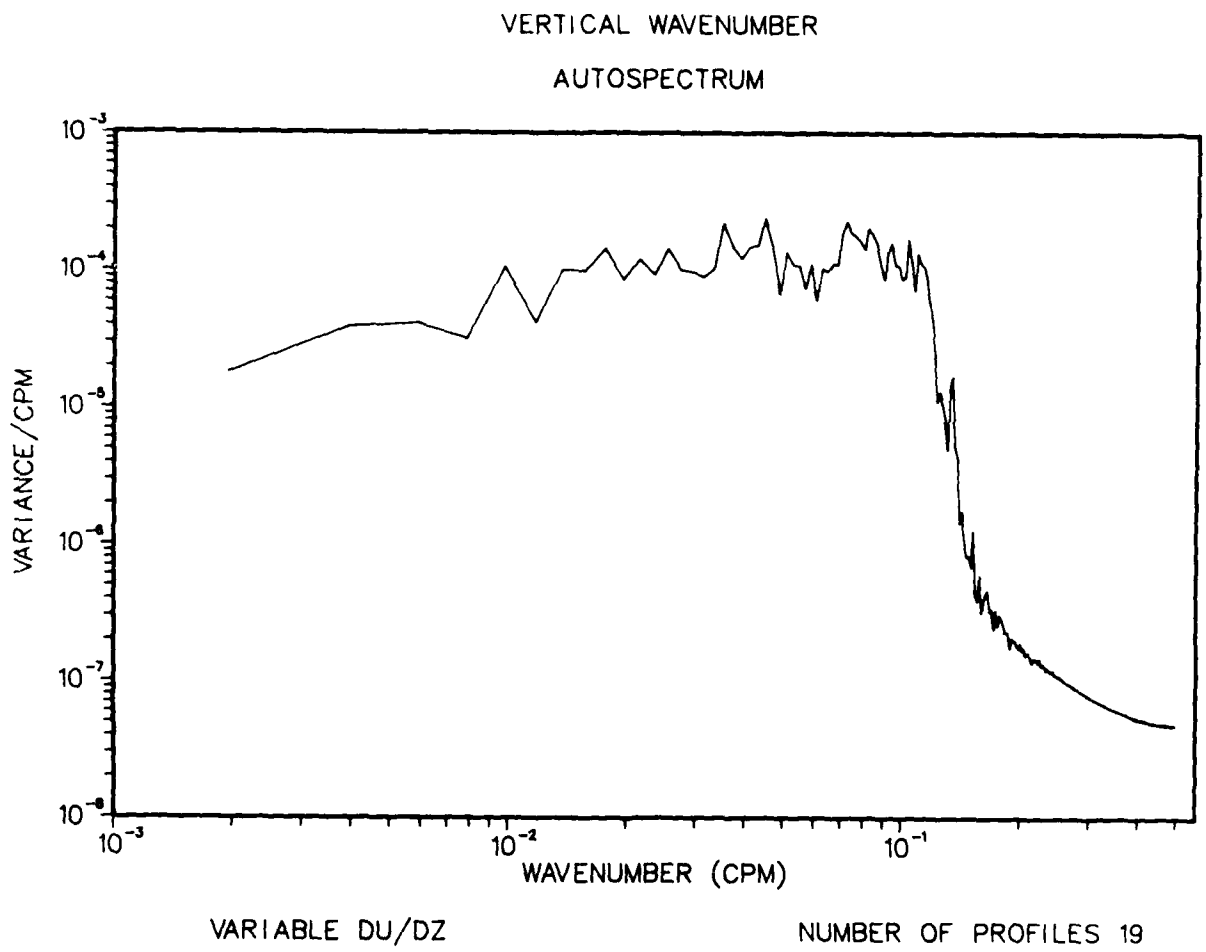

Figure 22. Vertical wavenumber spectrum of U shear

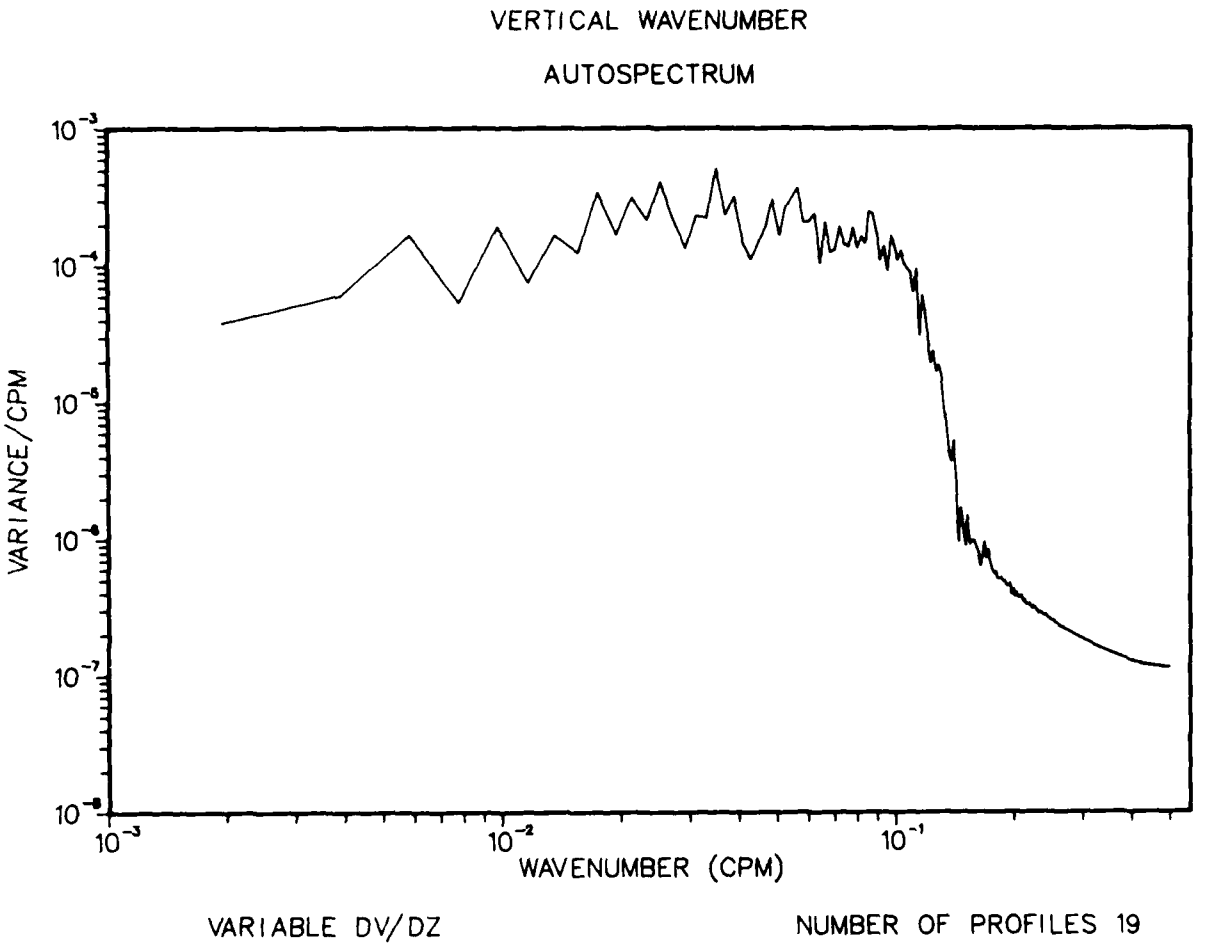

Figure 23. Vertical wavenumber spectrum of V shear

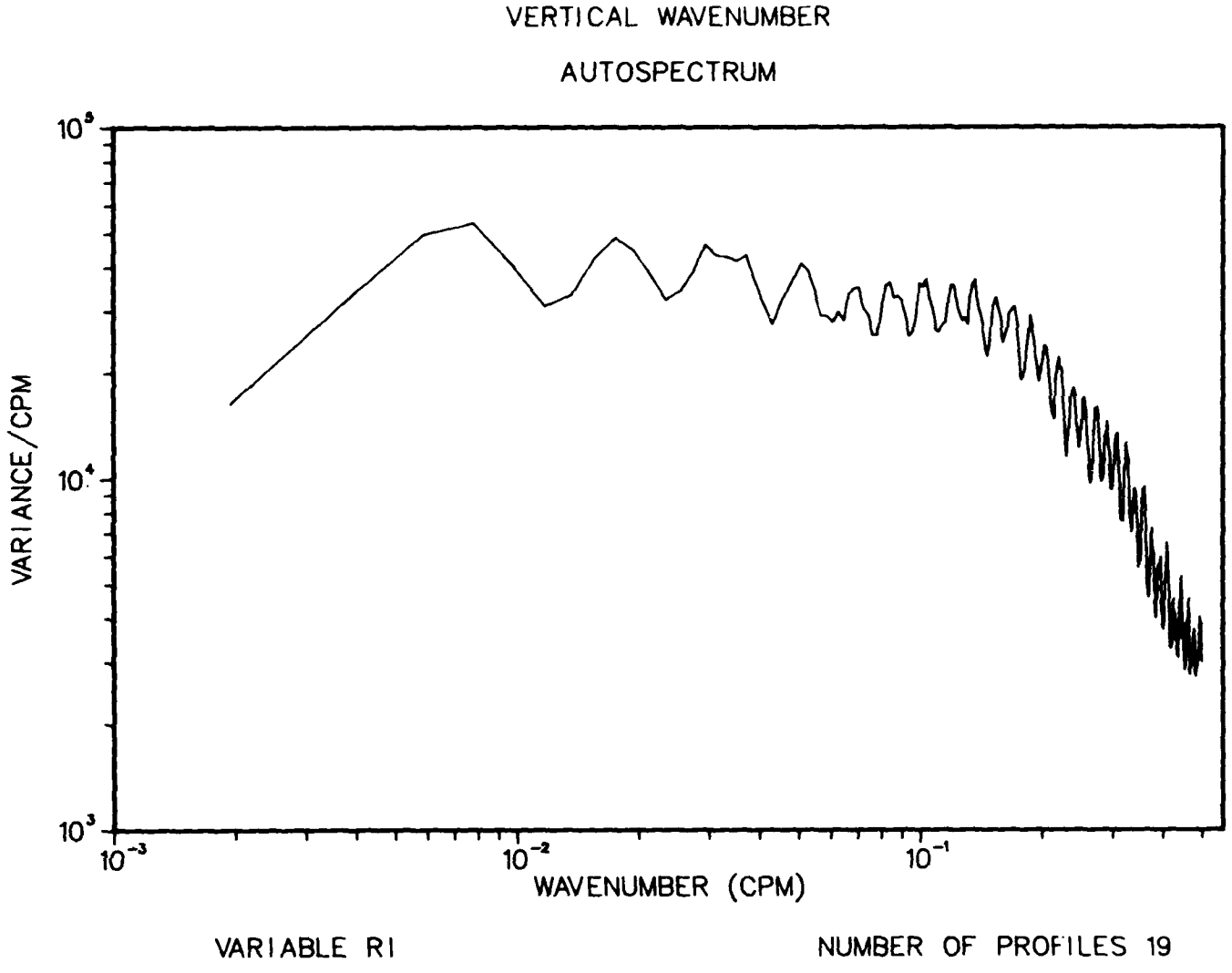

Figure 24. Vertical wavenumber spectrum of Richardson number

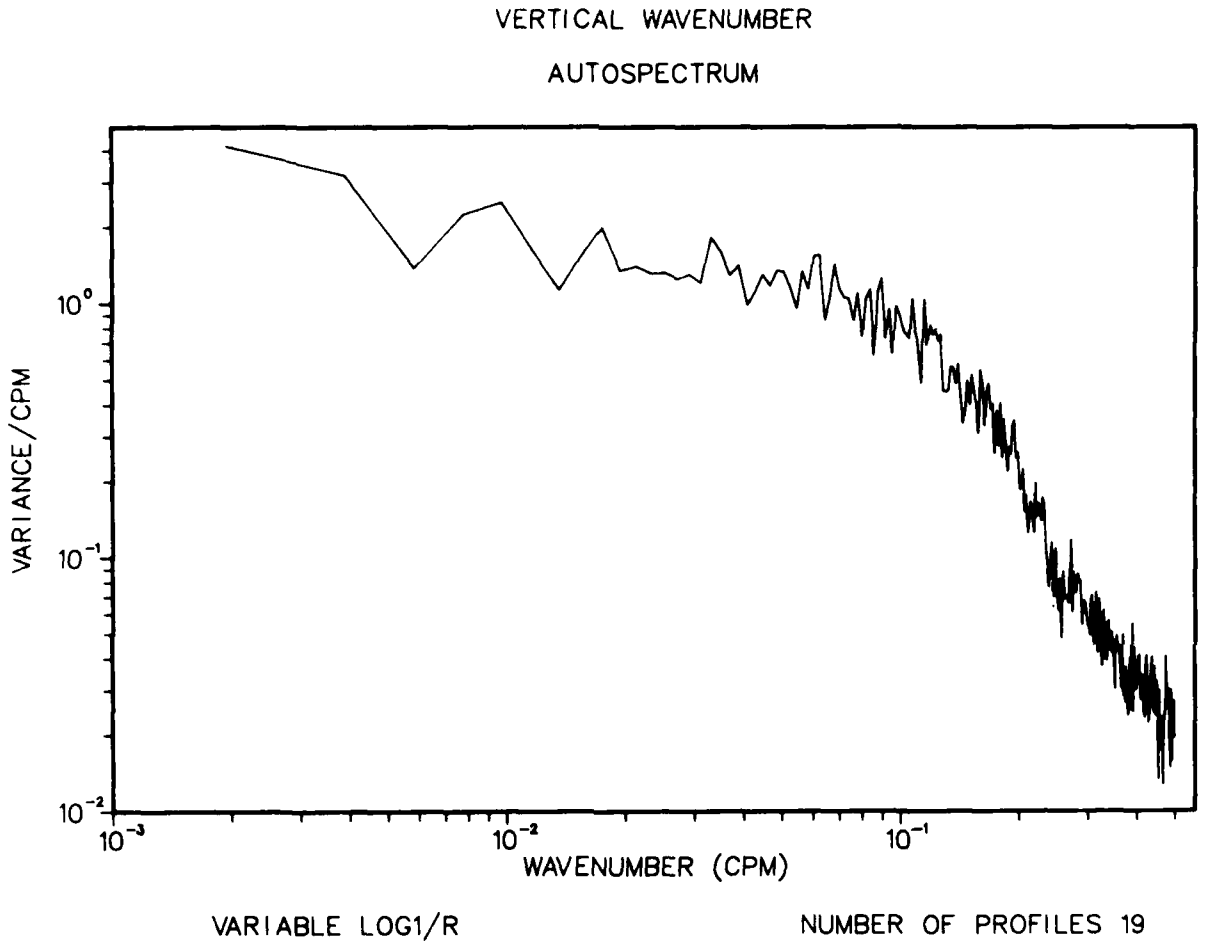

Figure 25. Vertical wavenumber spectrum of $-\text{Log}_{10}$ (Ri)

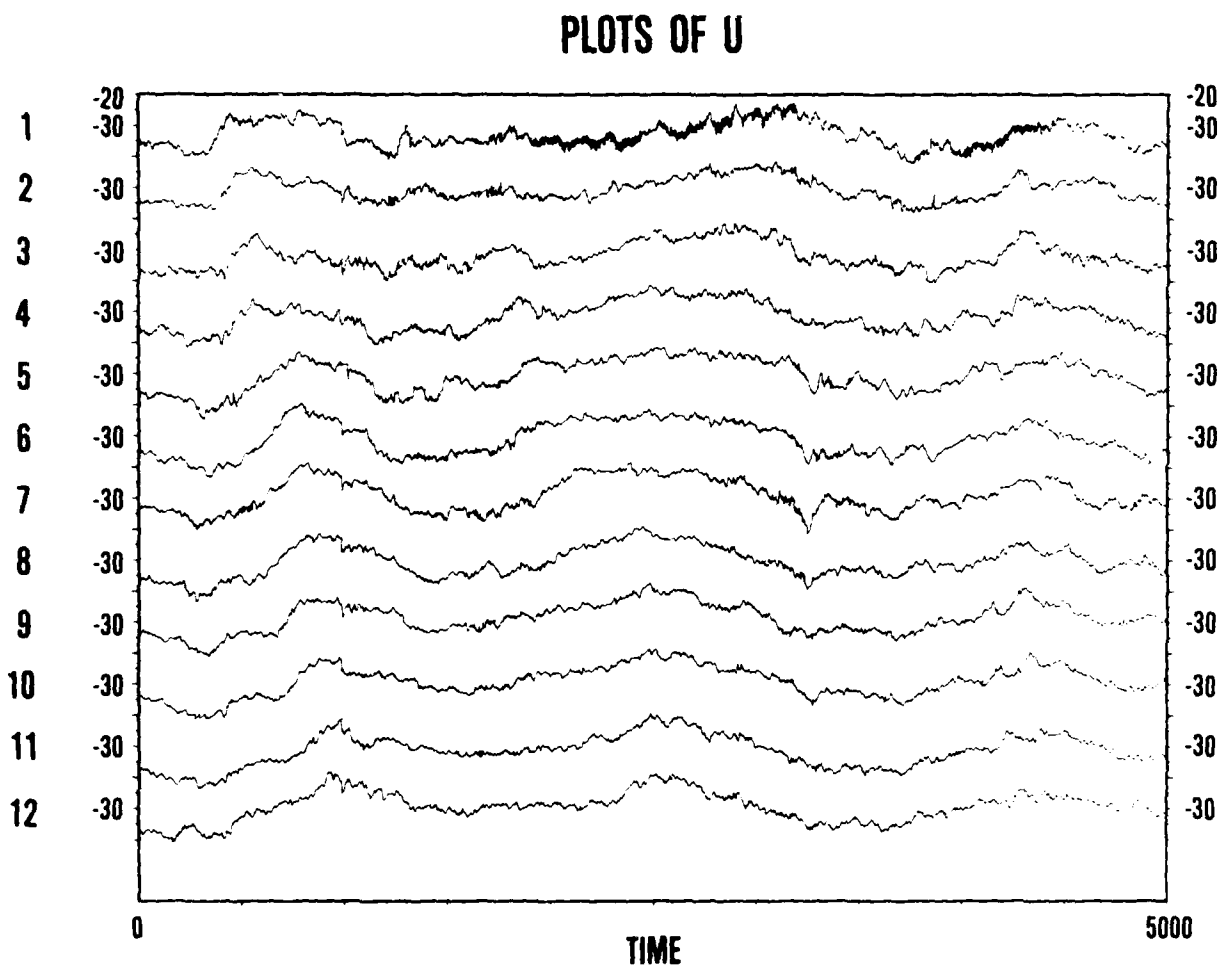

Figure 26. Eastward current components for all acoustic current meters - first 5000 minutes

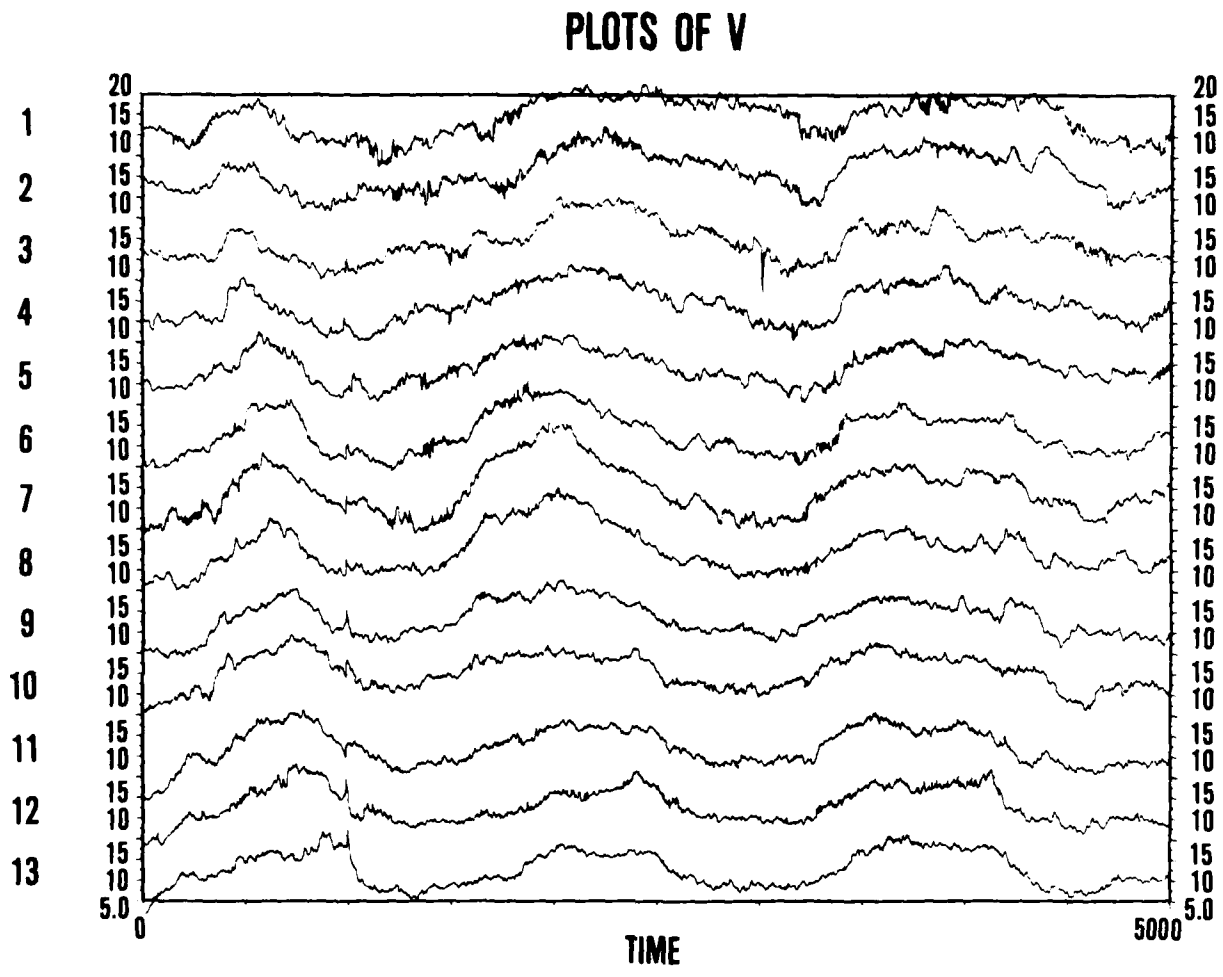

Figure 27. Northward current components for all acoustic current meters - first 5000 minutes

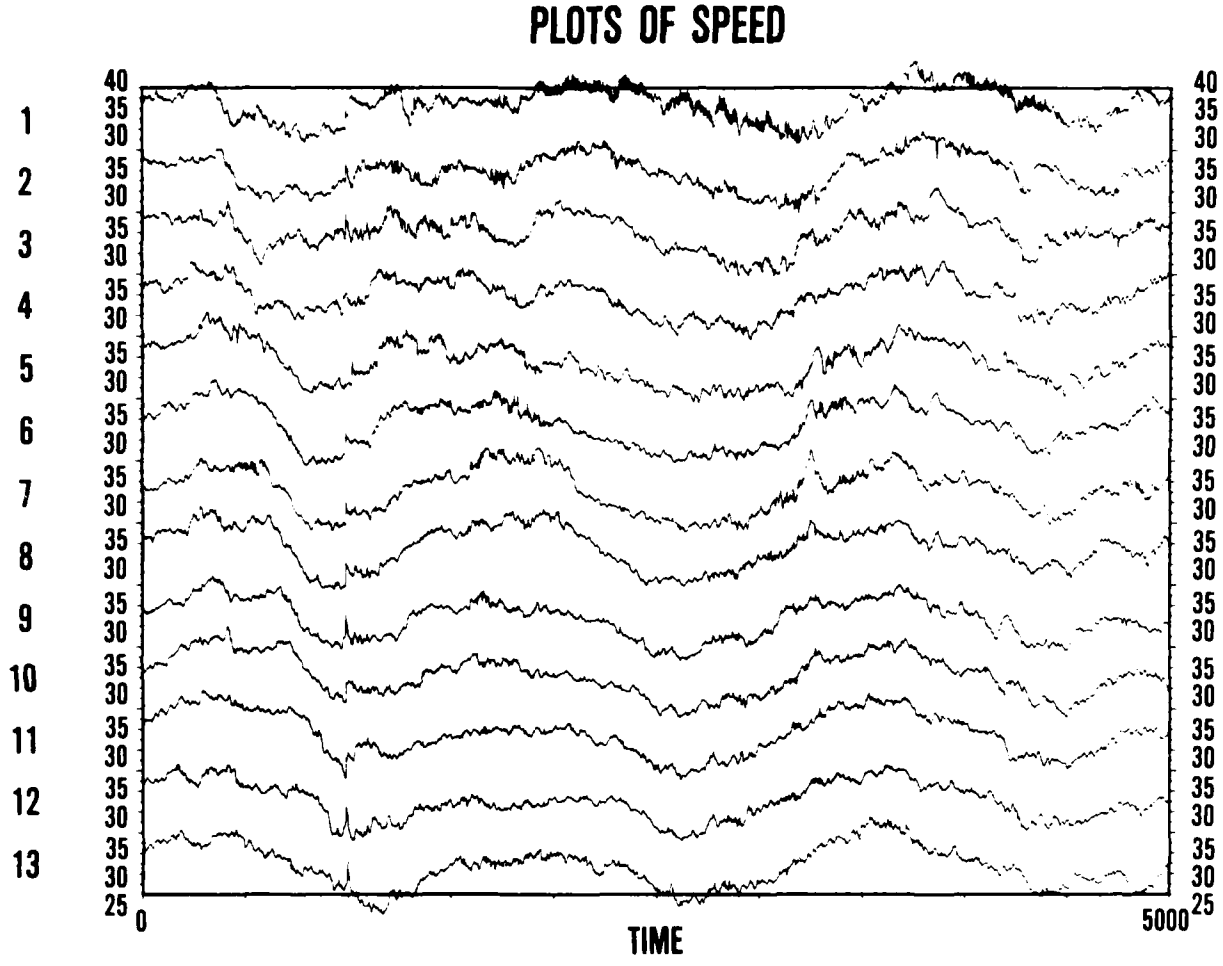

Figure 28. Speeds for all acoustic current meters - first 5000 minutes

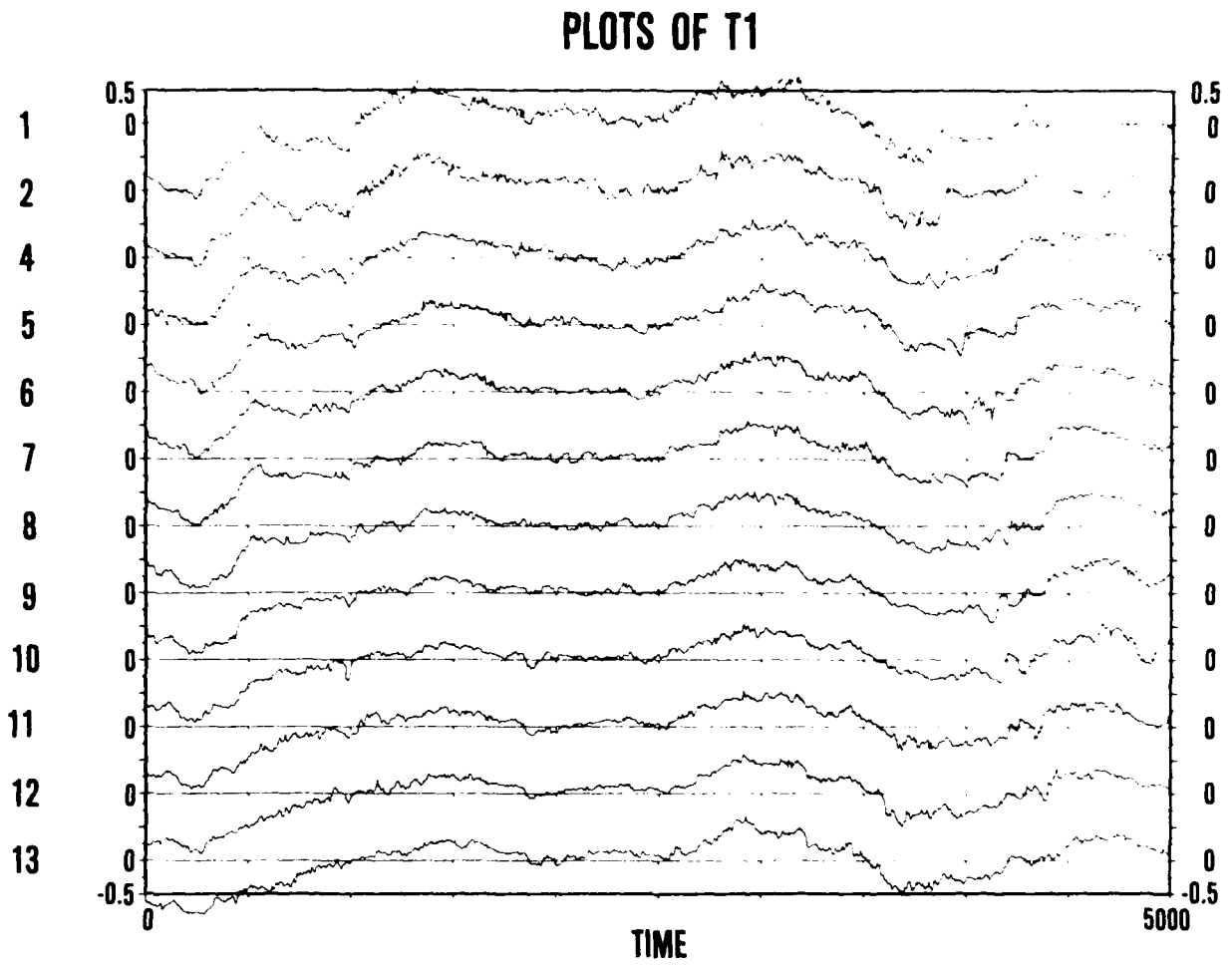

Figure 29. Temperatures for all acoustic current meters - first 5000 minutes

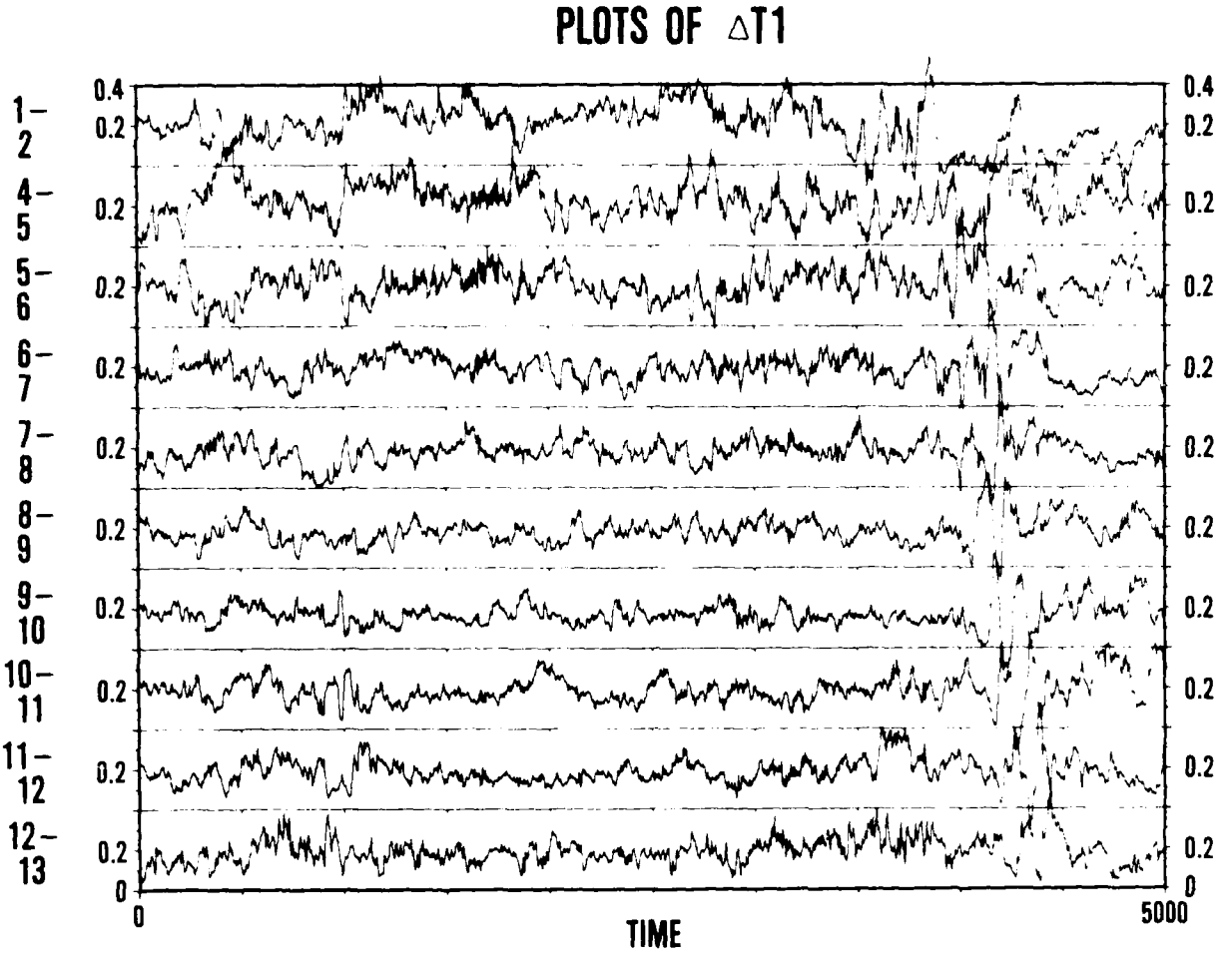

Figure 30. Temperature differences between adjacent pairs of acoustic current meters first 5000 minutes

local regions of intense shear that could lead to dynamic instability, overturning and the eventual radiation of high frequency internal waves from the overturn regions. A second mechanism which could modulate high frequency internal waves is the elastic scattering process (McComas, 1977; McComas and Bretherton, 1977; McComas and Muller, 1981). This is the process by which downward propagating high frequency waves are scattered by low frequency inertial waves with twice the vertical wavelength of the high frequency waves. The induced diffusion mechanisms denote the scattering of a high vertical wavenumber, high frequency wave into a nearby high frequency, high wavenumber wave by a low frequency, low wavenumber wave (McComas, 1975; McComas and Muller, 1981). The parametric subharmonic instability mechanism (McComas, 1975) generates low frequency, high vertical wave number waves from a low vertical wave number wave of higher frequency. The McComas and Muller (1981) theory is based on assumptions that the transfers of energy (action) are slow (occur over many wave periods) and are not influenced by steady vertical shear. In the upper ocean, particularly in the ATOM experiment, the ambient steady shear is usually intense; consequently, it is doubtful that the weak interaction theory is directly applicable. Another assumption of the McComas and Muller theory is that the spectral exchange processes are in steady equilibrium. The surface layer and the near surface pycnocline are assumed to be source areas for internal waves; thus, generation of a concentration of wave action (energy/frequency) by a near surface process momentarily may disturb the spectral equilibrium and cause an exchange from high frequency waves with high and low wave number components to lower frequency. If a process such as this occurs, we should expect to see a strong correlation between high- and low-frequency power levels, or stated as an hypothesis: the power levels of the high- and low-frequency, near inertial, internal gravity wave are correlated.

The hypothesis was tested by correlating the energy envelopes of high-passed current data with the envelopes of the energy of the same currents band-passed near the inertial frequency. Figure 31 depicts the high frequency energy (~1 cph) envelope in the inertial band and Figure 32 depicts the corresponding inertial envelopes.

Referring to Figure 31, it is clear that the level of energy in the high frequency bands changes both with time and depth. In general, the energy level changes do not appear to be correlated even between pairs of adjacent current meters. If the fluctuations of the high frequency energy are compared to those of the inertial band energy, there does not appear to be any strong correlation. This is borne out by actual correlation calculations, the results of which appear in Table 2. Thus, we can state with some confidence: in the context of the ATOM '79 oceanic environment, the high frequency activity does not appear to be strongly correlated with low frequency inertial wave activity.

METEOROLOGICAL FORCING OF INERTIAL WAVE ACTIVITY

The forcing of inertial wave activity by meteorological events (winds) is well known (Pollard, 1970; Pollard and Millard, 1970; Fu, 1981). The extent of such forcing below the mixed layer in a stong frontal region is not well known. It was a hypothesis of this study that the wind forcing at the sea surface might be the primary source of inertial wave activity variation in the pycnocline and below.

To test this hypothesis, the mooring was located near (~5 nm) a NOAA Data Buoy Office data buoy. The winds recorded at this buoy and a neighboring buoy to the west are plotted in Saunders, Green, and Bergin (1980). The buoy failed for a period during January, leaving a large data gap, thus the wind forcing must be deduced from the secondary data buoy. Where the data existed, they were filtered at the inertial band, the energy density computed, and the envelope computed. The energy envelopes

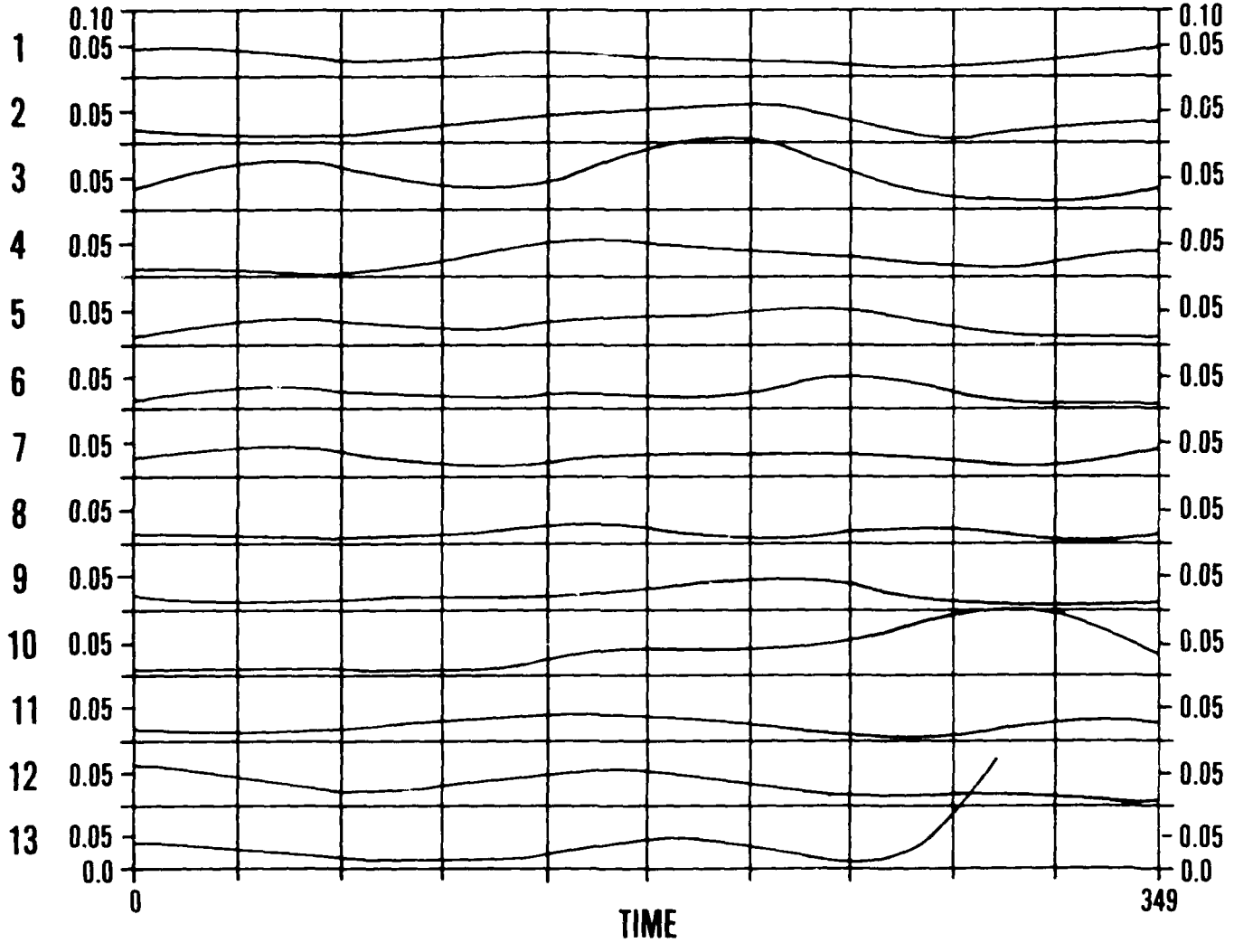

Figure 31. Envelope of variance of high frequency currents - 350 hr

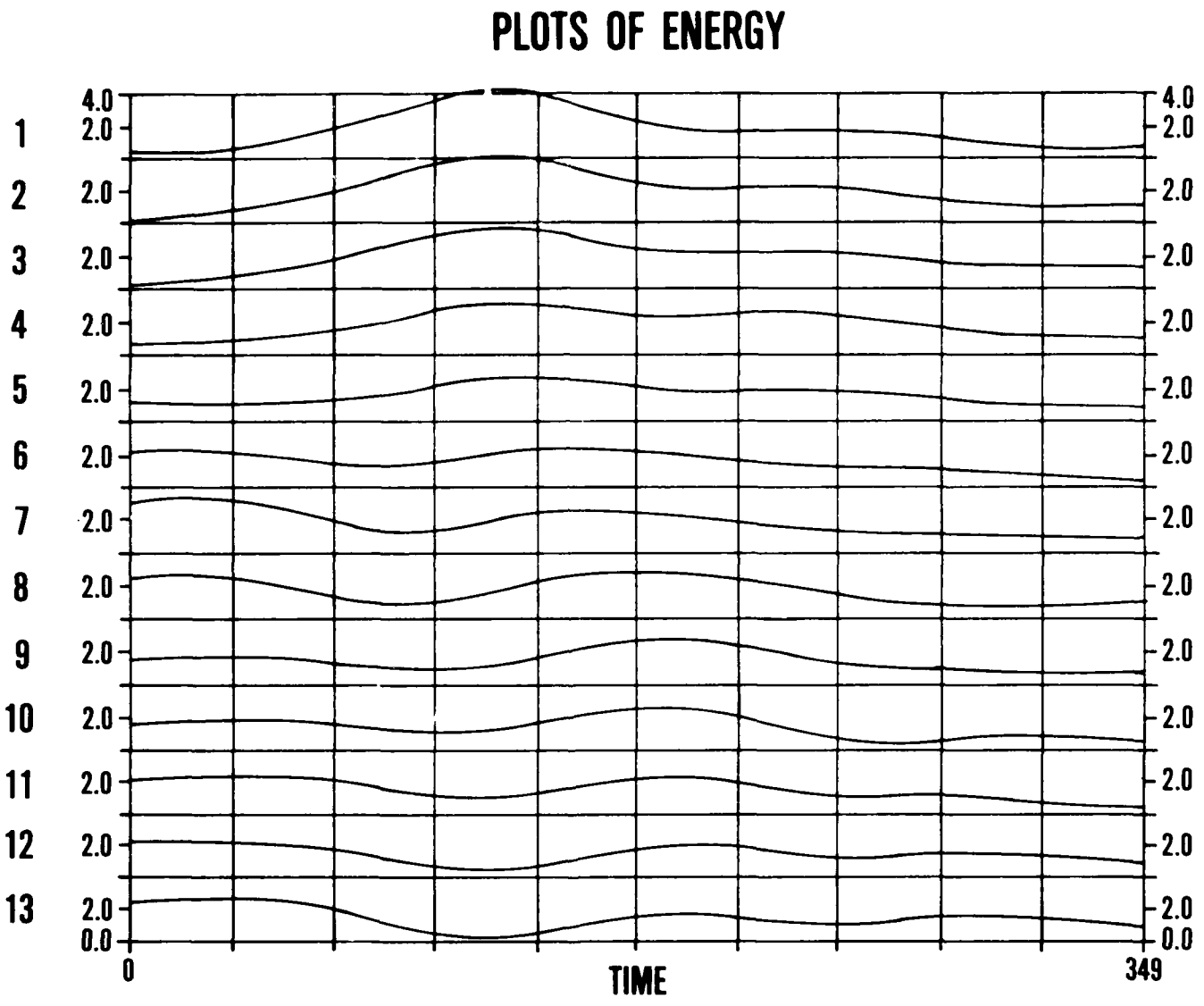

Figure 32. Envelope of variance of inertial frequency currents - 350 hr

TABLE 2

Current Meter No.	HF/INERT*	INERT/$WIND_1$**	HF/$WIND_1$**
1	.0034	.534	.0786
2	.0659	.662	.0351
3	.0428	.603	.0299
4	.0477	.608	.0469
5	.0306	.590	.0230
6	.0207	.436	.0394
7	.0313	.497	.0339
8	.0090	.417	.0515
9	.0517	.326	.0326
10	.0320	.496	.0288
11	.0458	.526	.0602
12	.0373	.421	.0684
13	-.0193	.510	.0592

Correlation coefficients between the high frequency (HF) current energy, the inertial current (INERT) energy and the wind energy.

* 0 LAG

** Maxima over $\pm$50 hr Lags.

for both data buoys are plotted in Figure 33. The upper plot is unreliable due to missing data. Comparison of the lower plot with the plots of inertial current energy envelopes show no clearly apparent correspondence. A large wind peak at about 100 hrs was followed slightly later by a significant current maximum, but the second and third wind energy peaks do not appear to be associated with clear events in the current records. However, the moderate correlations (Table 2) indicate a significant relation between the wind and the inertial motions in general.

Thus, the relation of wind forcing to inertial motion in strong baroclinic currents below the mixed layer appears significant in general, though the gaps in the wind data at the mooring site reduces the strength of this assertion.

EFFECT OF PROXIMITY OF THE BRUNT-VÄISÄLÄ FREQUENCY MAXIMUM ON HIGH FREQUENCY INTERNAL WAVE ACTIVITY

The current data were high-pass filtered with a cutoff at 1 cph. The filtered data were squared and averaged over 1000 minute intervals and over the entire 20,000 minute record at each current meter. The plot of the mean high frequency variance versus depth (Fig. 34) shows a net decrease of high frequency variance with depth. However, there is wide variation between the upper current meter (1) and the next lower meter (2) and between meters 2 and 3. Current meter 7 also appears to have high variance with respect to its upper and lower neighbors. Below current meter 10 there is a net increase in high frequency current variance with increasing depth.

The peak of the Brunt-Väisälä frequency profile occurs just below 100 m and while there are secondary peaks, these are small compared to the main peak. Although the current meter array was forced by the current field to undergo large vertical excursions: nevertheless, the upper current meters were always nearer the B-V peak than the lower meters. Thus, while on the mean it is strictly correct to assert that the data show a net decrease in high frequency activity with increasing distance from the B-V peak, the large variations in the high frequency variability tend to mask this effect.

MOORED VERTICAL COHERENCE

The complex coherence function of two random processes, x(t) and y(t), is properly defined as:

$$\gamma\ (f) = \frac{Sxy(f)}{\sqrt{Sxx(f)\ Syy(f)}}$$

where $S_{xy}(f)$ is the exact cross spectrum between x and y and $S_{xx}(f)$ and $S_{yy}(f)$ are the exact autospectra of x and y, respectively. These exact spectra cannot be obtained from natural oceanographic data. The best that can be done is to calculate an estimate of the complex coherence, $\hat{\gamma}\,(f)$, defined as:

$$\hat{\gamma}\ (f) = \frac{\langle \underline{X}(f)Y^*(f) \rangle}{\sqrt{\langle \underline{X}(f)\underline{X}^*(f) \rangle \langle \underline{Y}(f)\underline{Y}^*(f) \rangle}}$$

where X(f) and Y(f) are the Fourier transforms of x(t) and y(t).

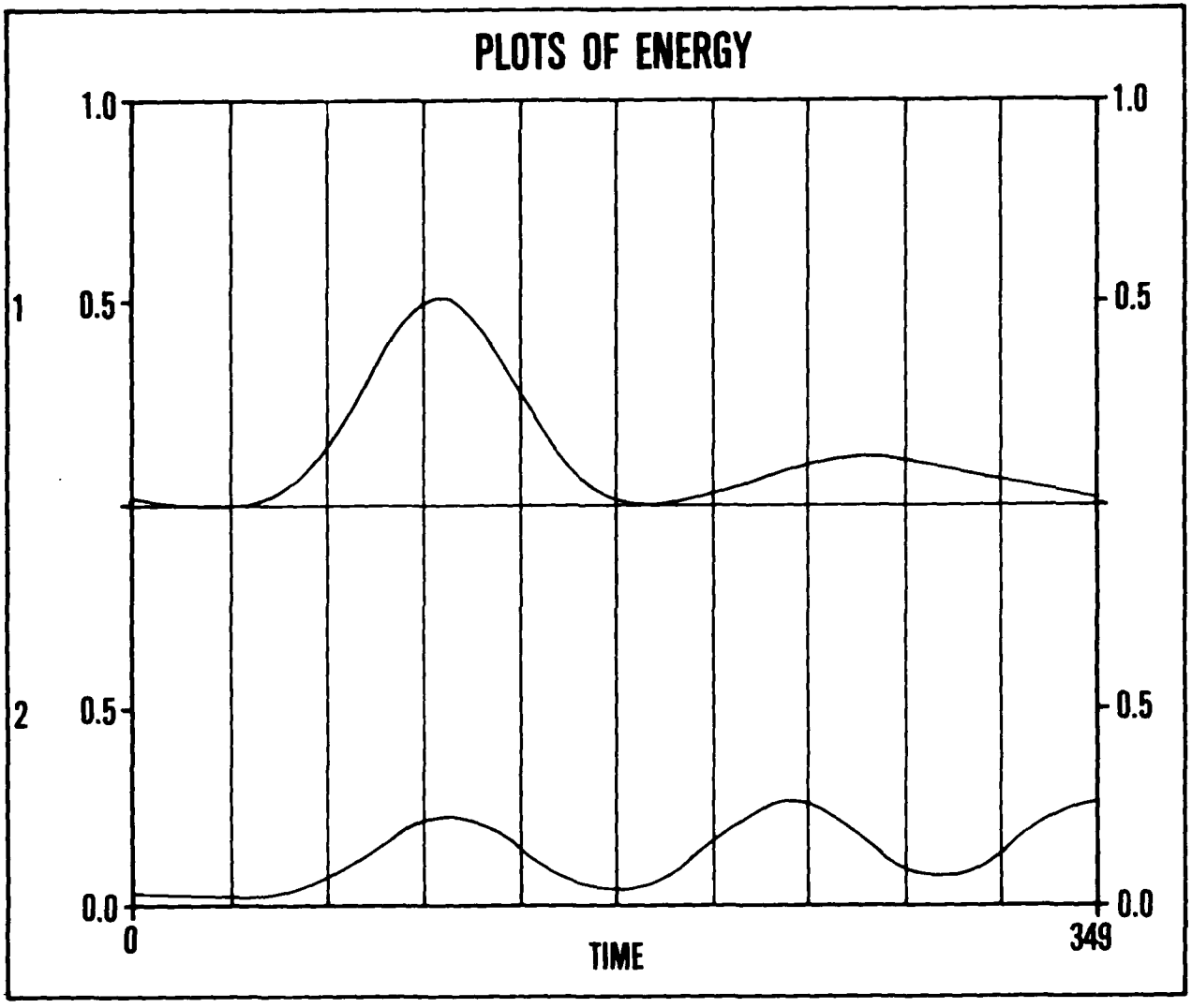

Figure 33. Envelope of variance of inertial frequency winds - 350 hr

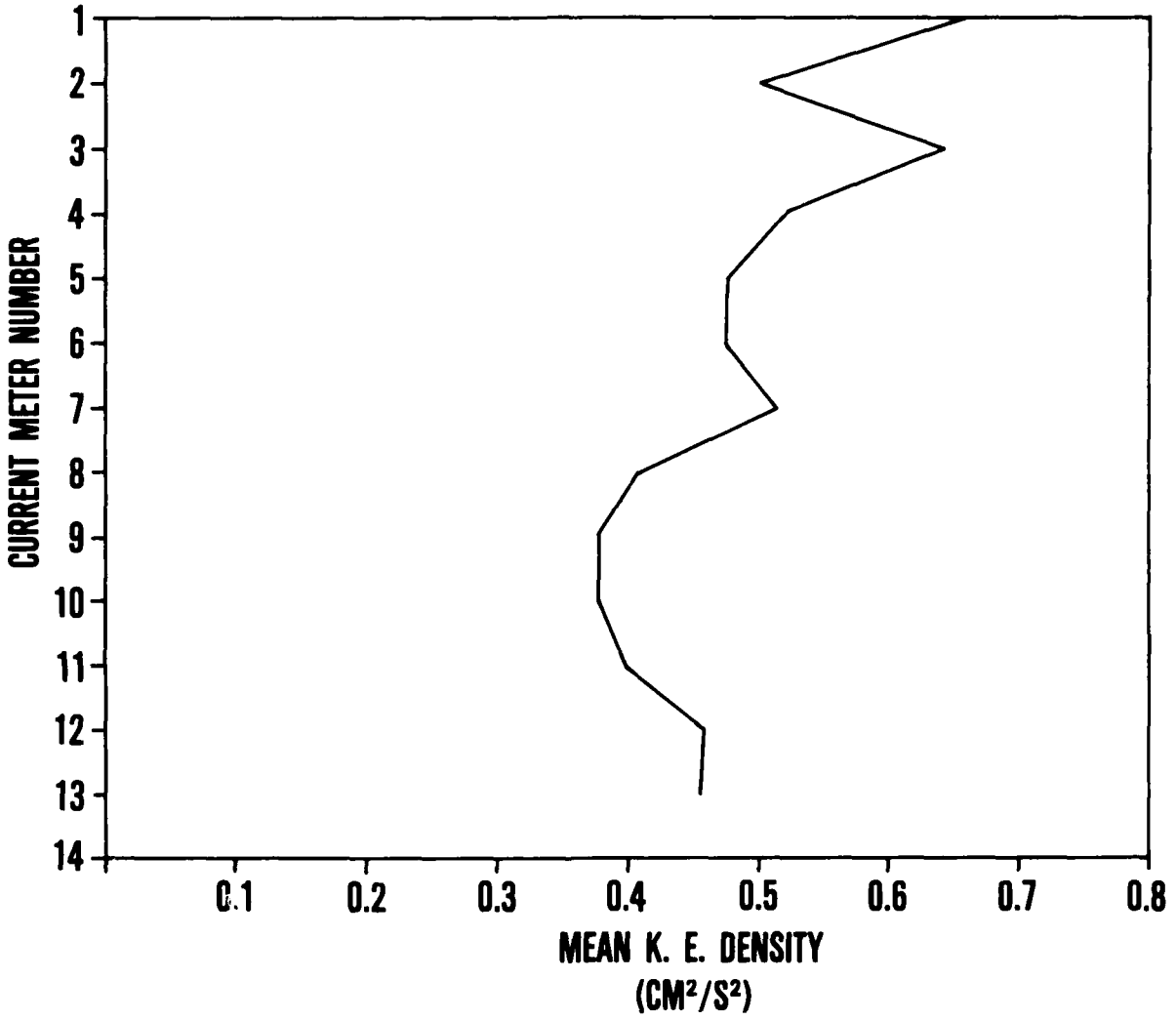

Figure 34. Average energy content in high frequency band versus depth

In actual practice the Fourier transforms are not really those of x(y) and y(t), but of w(t) x(t) and w(t) y(t), where the weighting function w(t) is known as a window and the averaging is done over a sequence of Fourier transforms computed from a number of time segments of the data:

$$\hat{X}_i(f) = FFT\{w_i(t)x(t)\}$$

$$\hat{S}_{xy}(f) = \frac{1}{N} \sum_{i=1}^{N} X_i(f)Y_i^*(f)$$

For the coherences shown in this report, a Hanning window was used (Nuttall, 1981). The estimated complex coherence is usually expressed as:

$$\hat{\gamma}(f) = |\hat{\gamma}(f)|e^{i\hat{\phi}(f)}$$

where $|\hat{\gamma}(f)|$ is the magnitude of the coherence and $\hat{\phi}$, the phase. If $|\hat{\gamma}(f)| = 1$, the signals are completely coherent; if $|\gamma(f)| = 0$, the signals are incoherent. $|\hat{\gamma}(f)$ is itself a random variable and possesses a probability distribution. The theoretical probability density functions and cumulative distribution functions for $\hat{\gamma}(f)$ are plotted in Figures 35 through 37 for $|\gamma(f)| = 0.9$, 0.5 and 0, respectively. These are based on the theory presented in Carter, Knapp, and Nuttall (1973) for N=37, the number of independent segments used in this study and computed by the algorithms of Barnard (1981), and Lee (1981).

A sample set of current and temperature coherences appears in Figures 38 through 51. From Figure 37 we see that the 80% confidence bands for zero coherence are 0.055 and 0.249. Thus, a coherence estimate must be greater than 0.249 for there to be a probability of 10% or less that the true coherence is zero. At the minimal separations (i.e., 7 m) we see that the velocity coherence is just at or below the 80% upper confidence limit for all frequencies greater than 1 cph and is definitely below this limit for the same frequency band and greater current meter separation.

The coherence functions between the temperatures at meters 1 and 6 and the pressure signal from the upper T/P recorder were computed. These are displayed in Figures 52 and 53. The data in the plots indicate that there is essentially zero coherence between the temperature and pressure fluctuations in the frequency band of 1-30 cph.

1. currents in the high frequency band (1 cph) are generally incoherent at separations of 7 m and above.
2. temperatures possess greater coherence with separation than the currents, possibly due to internal wave motions that have leaked from the band of Brunt-Väisälä frequencies where they exist as free waves.

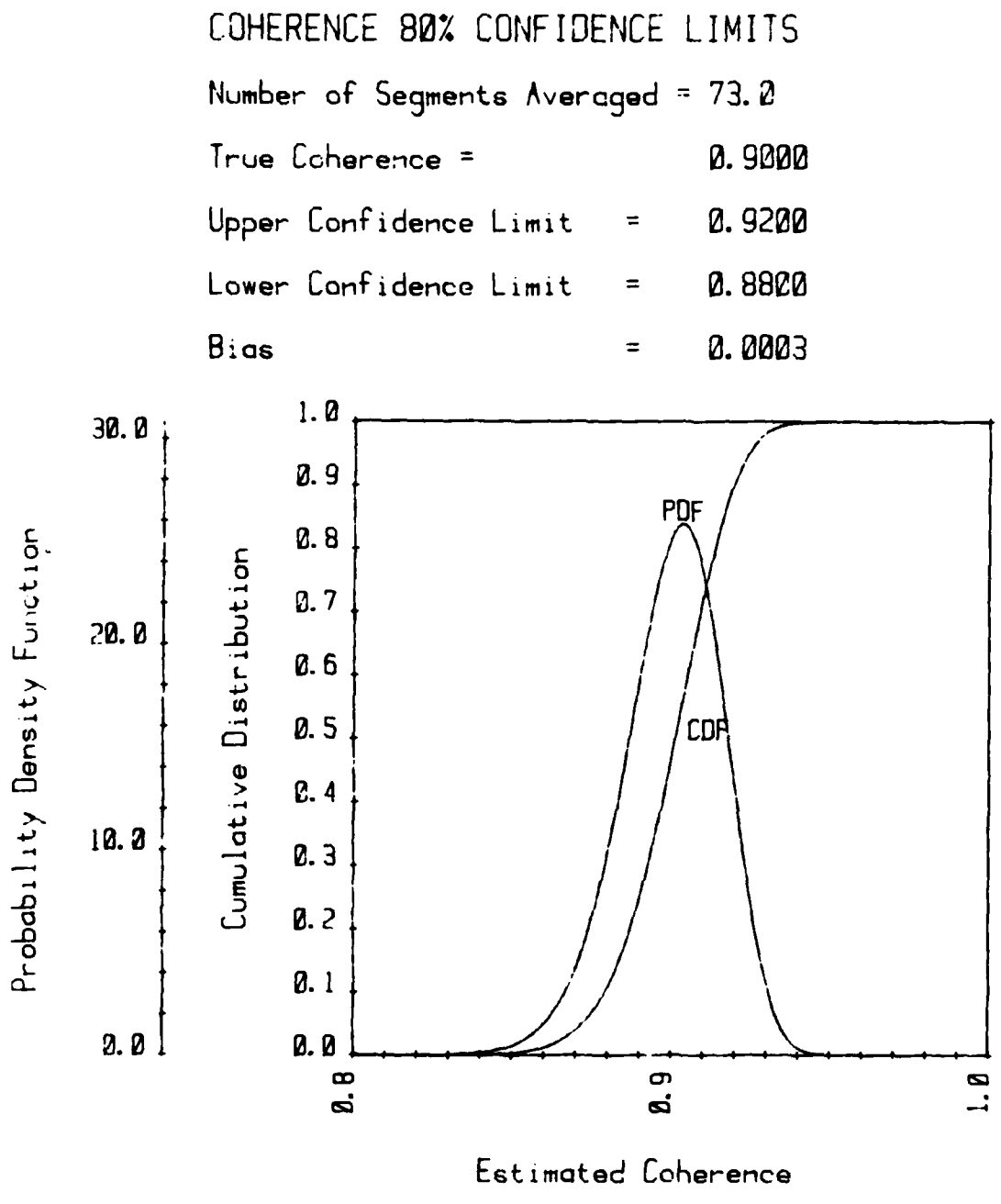

Figure 35. Probability density function and cumulative distribution for estimated coherence - 73 segments, true coherence = 0.9

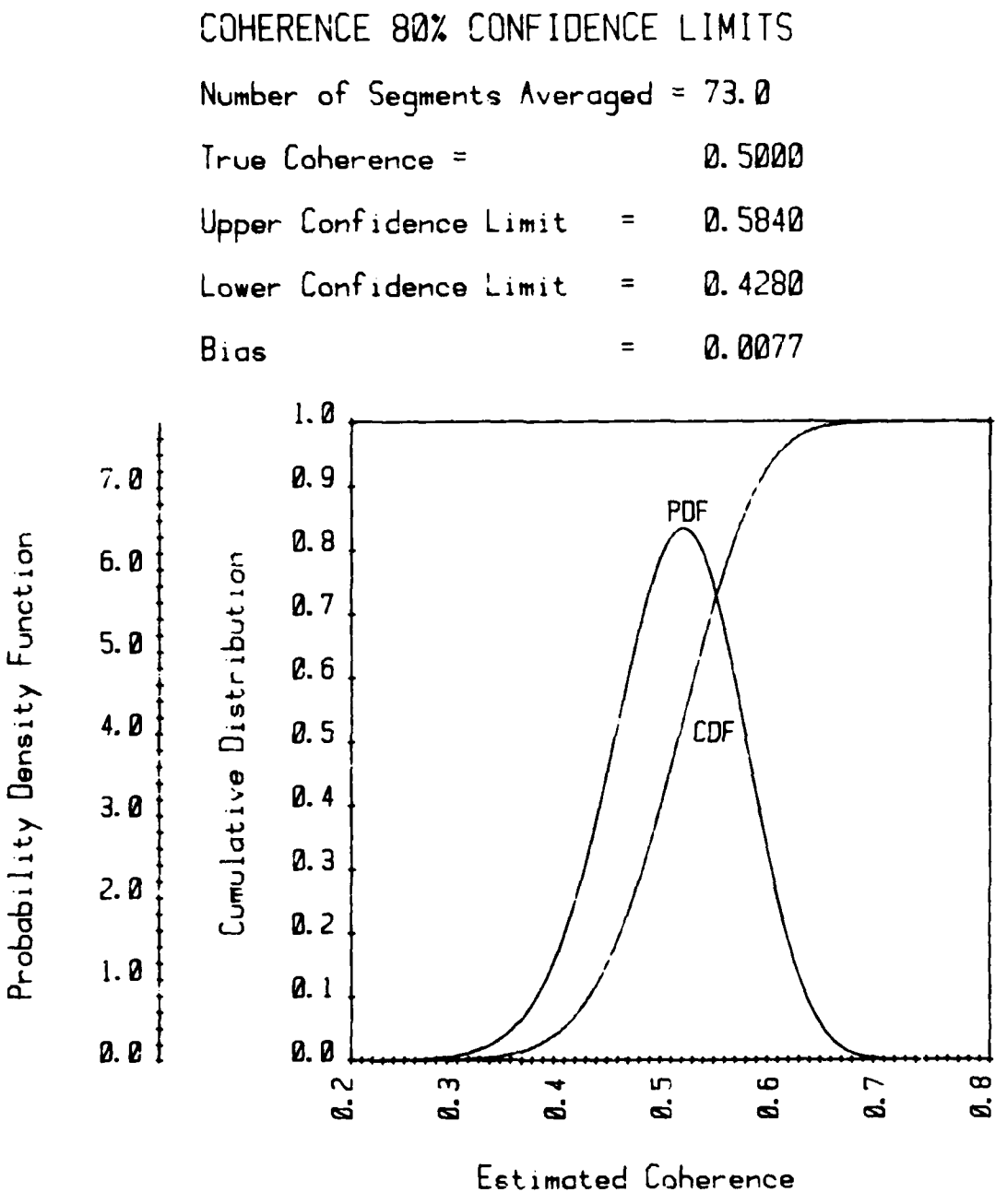

Figure 36. Estimated coherence - 73 segments, true coherence = 0.5

COHERENCE 80% CONFIDENCE LIMITS

Number of Segments Averaged = 73.0

True Coherence = 0.0000

Upper Confidence Limit = 0.1800

Lower Confidence Limit = 0.0400

Bias = 0.1170

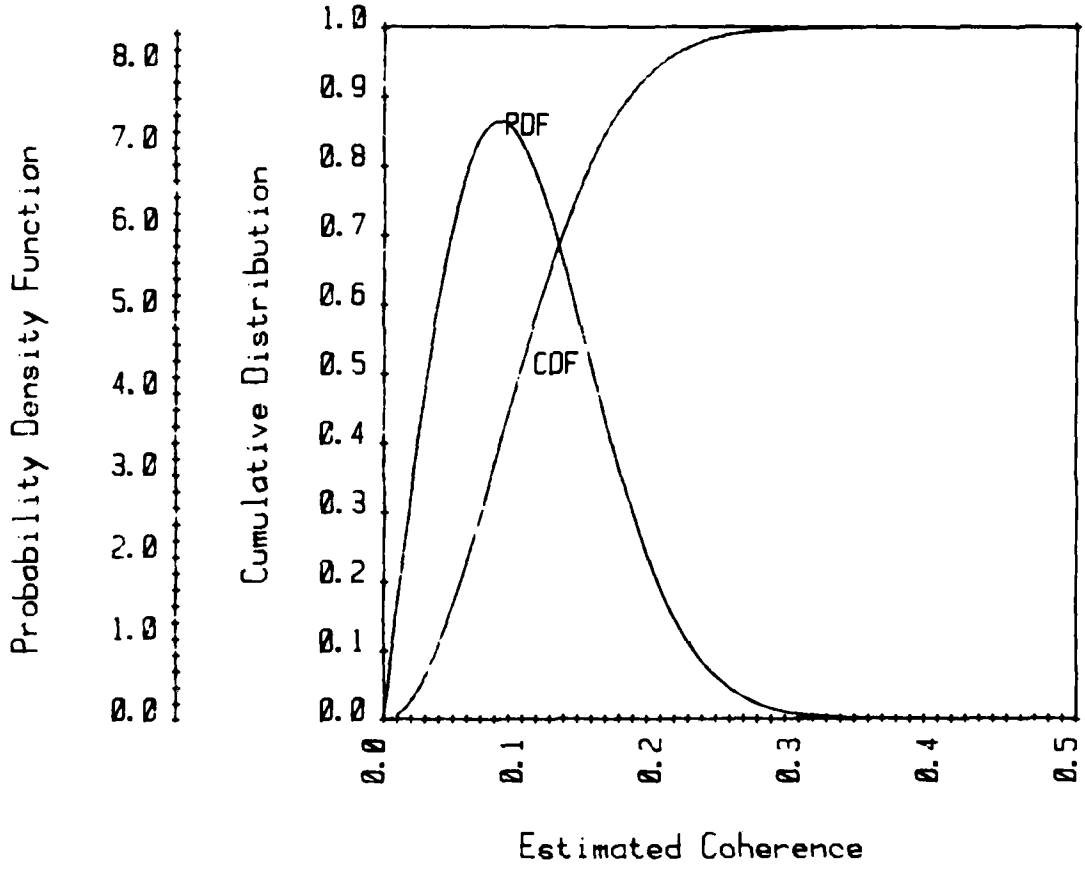

Figure 37. Estimated coherence - 73 segments, true coherence = 0.0

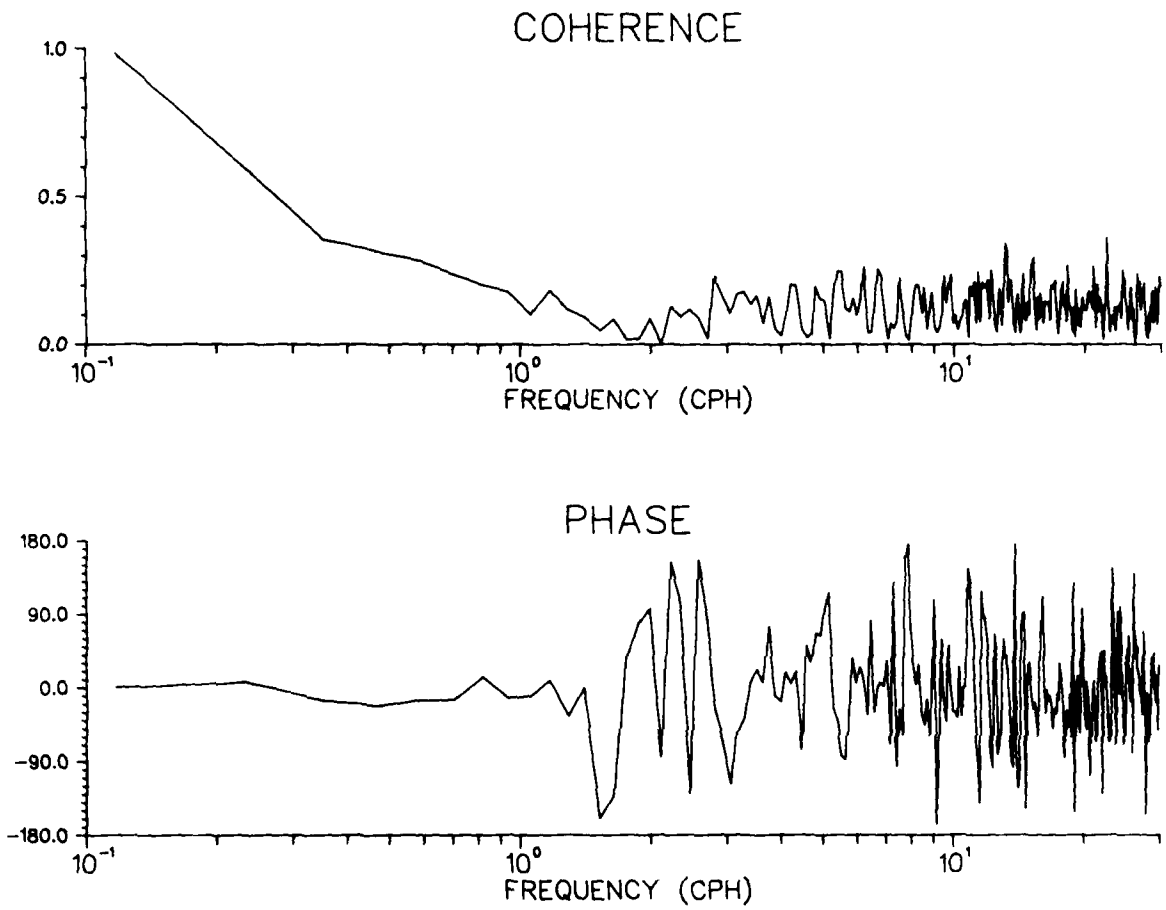

Figure 38. Coherence and phase between U velocity components: meters 1 and 2

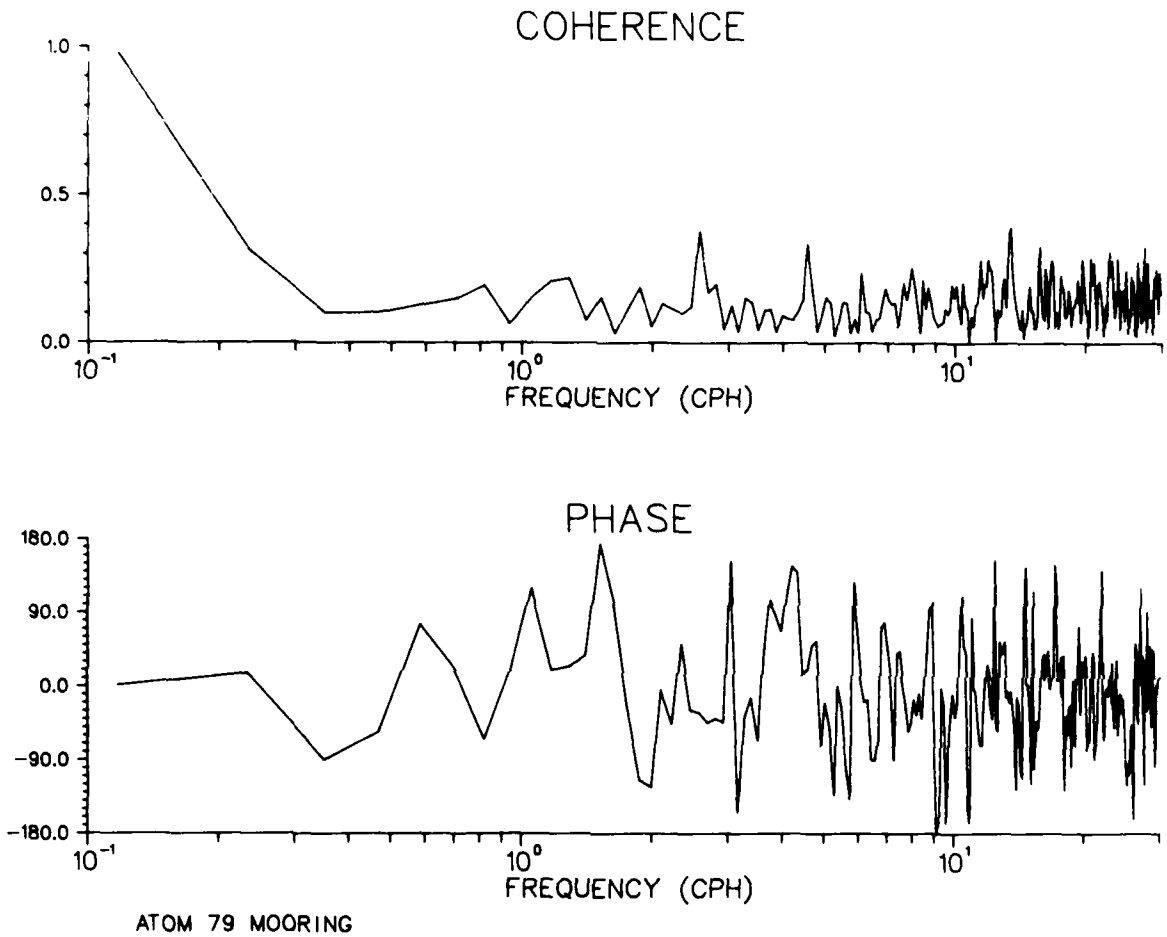

Figure 39. Coherence and phase between U velocity components: meters 1 and 3

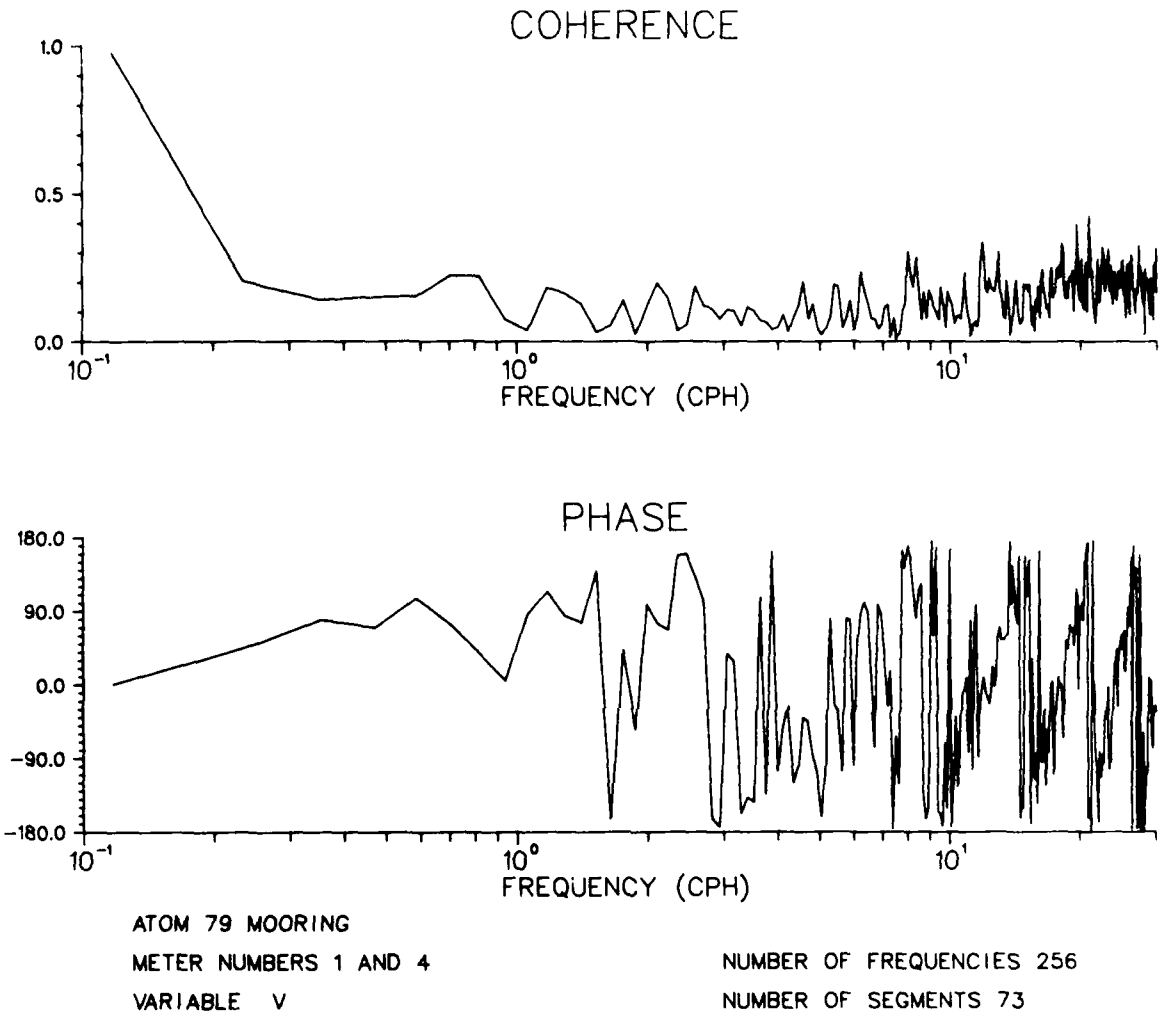

Figure 40. Coherence and phase between U velocity components: meters 1 and 4

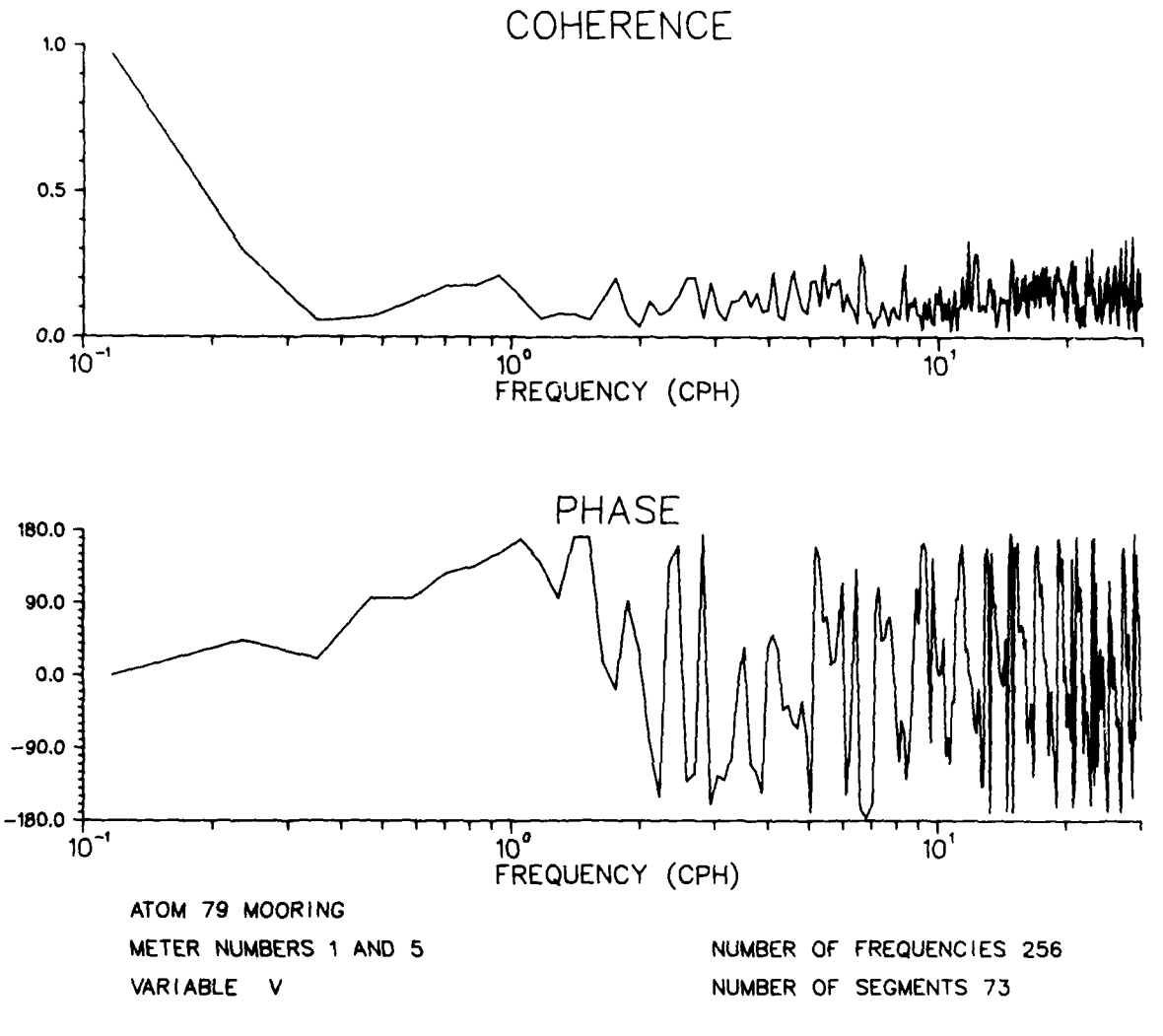

Figure 41. Coherence and phase between U velocity components: meters 1 and 5

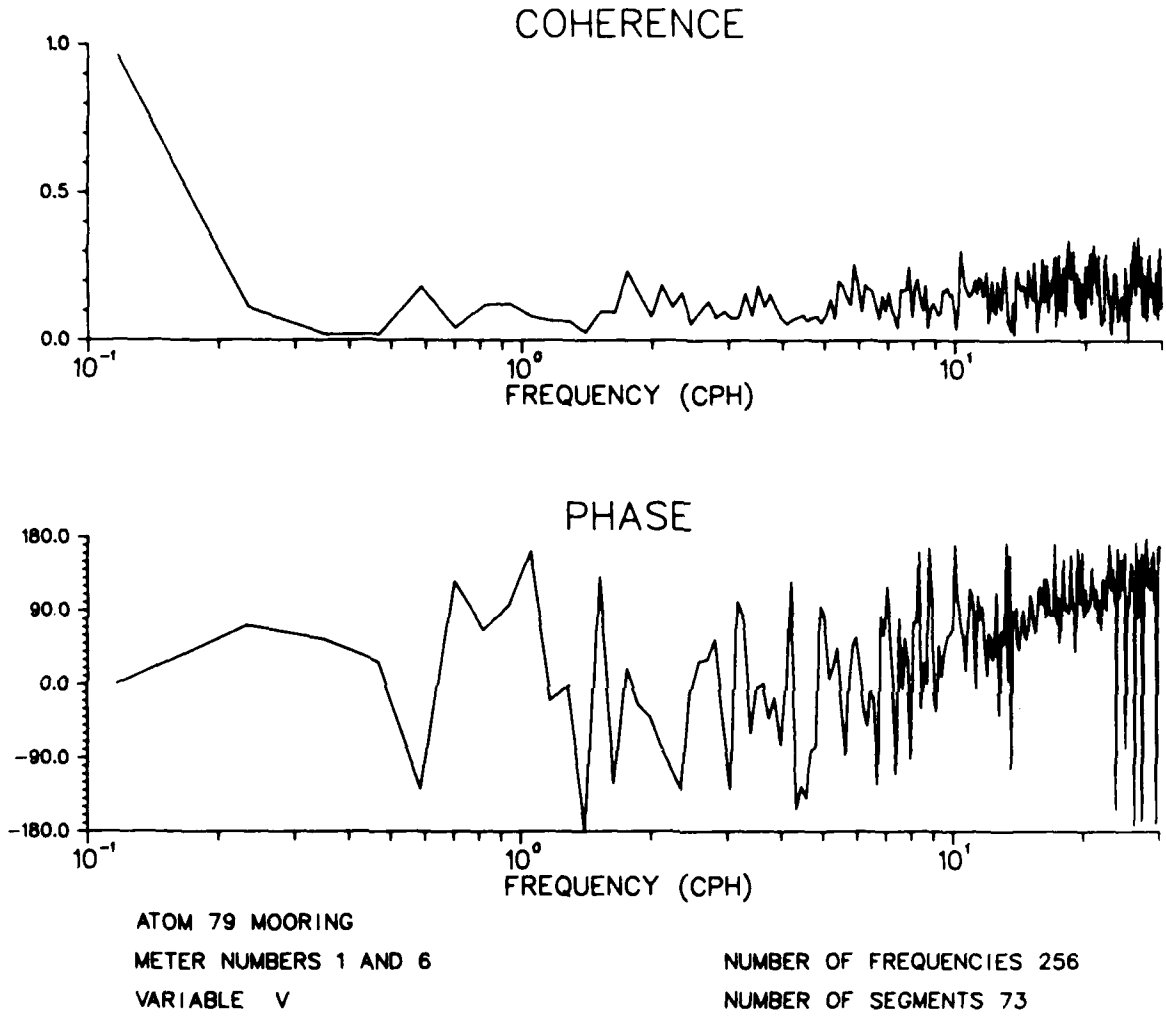

Figure 42. Coherence and phase between U velocity components: meters 1 and 6

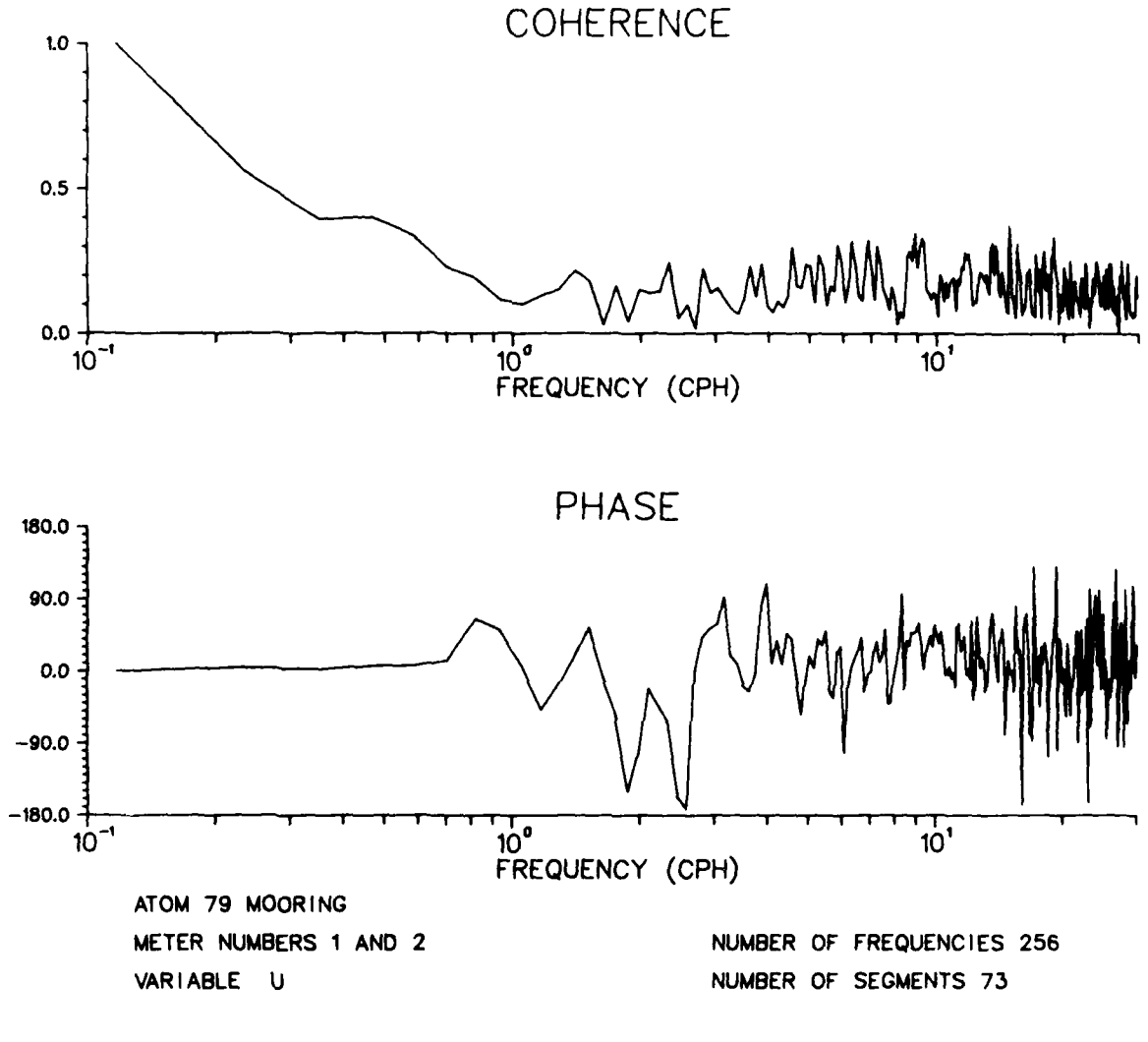

Figure 43. Coherence and phase between V velocity components: meters 1 and 2

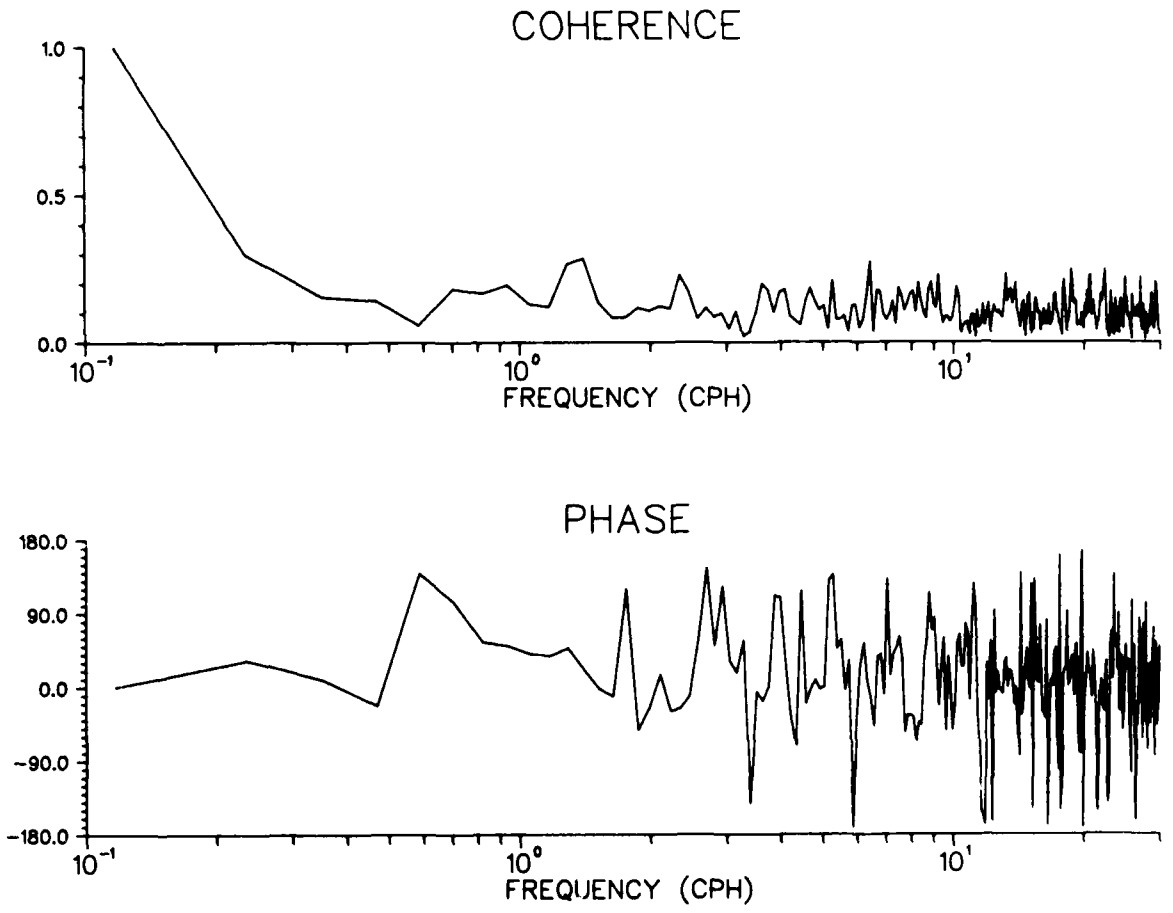

Figure 44. Coherence and phase between V velocity components: meters 1 and 3

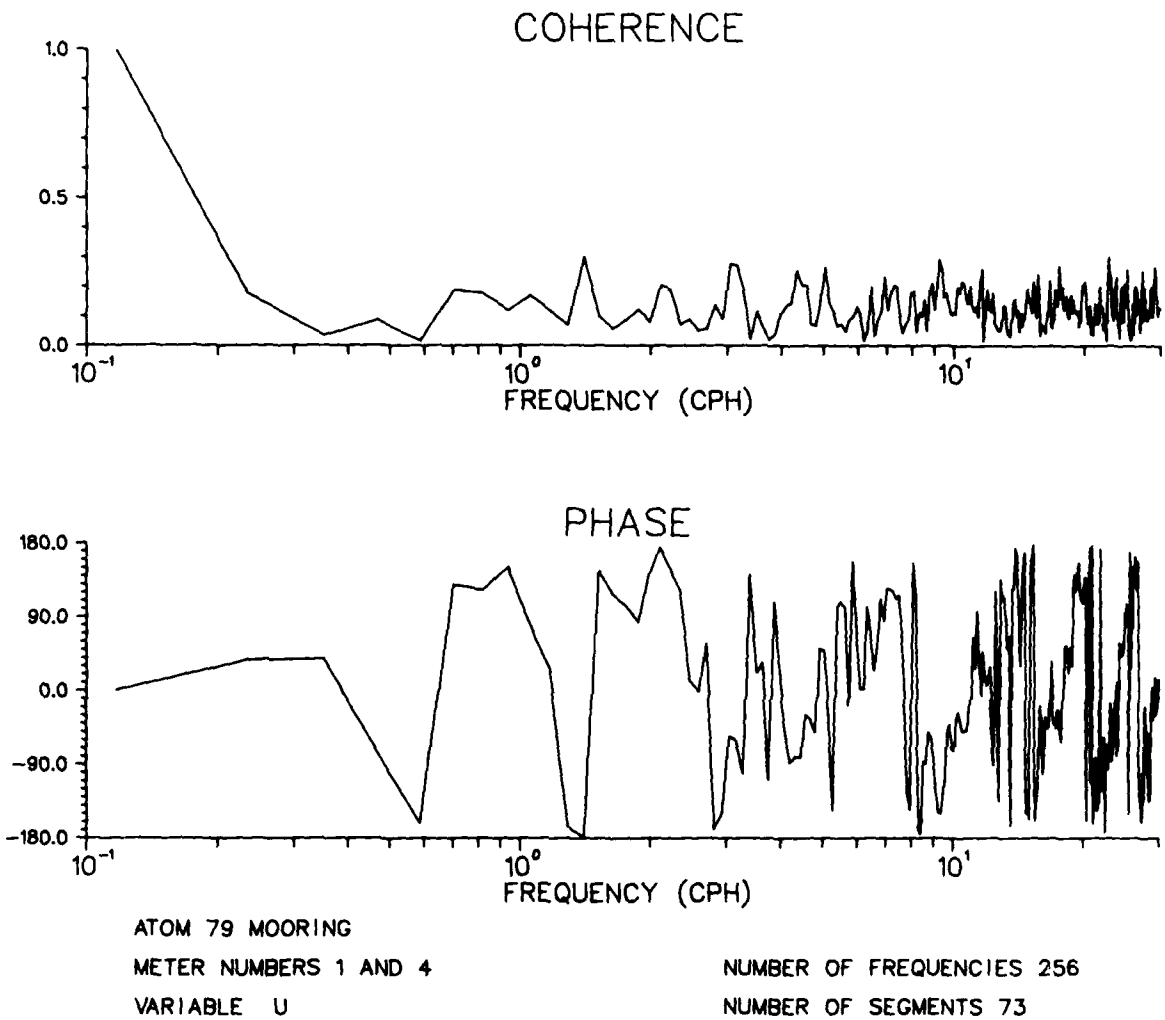

Figure 45. Coherence and phase between V velocity components: meters 1 and 4

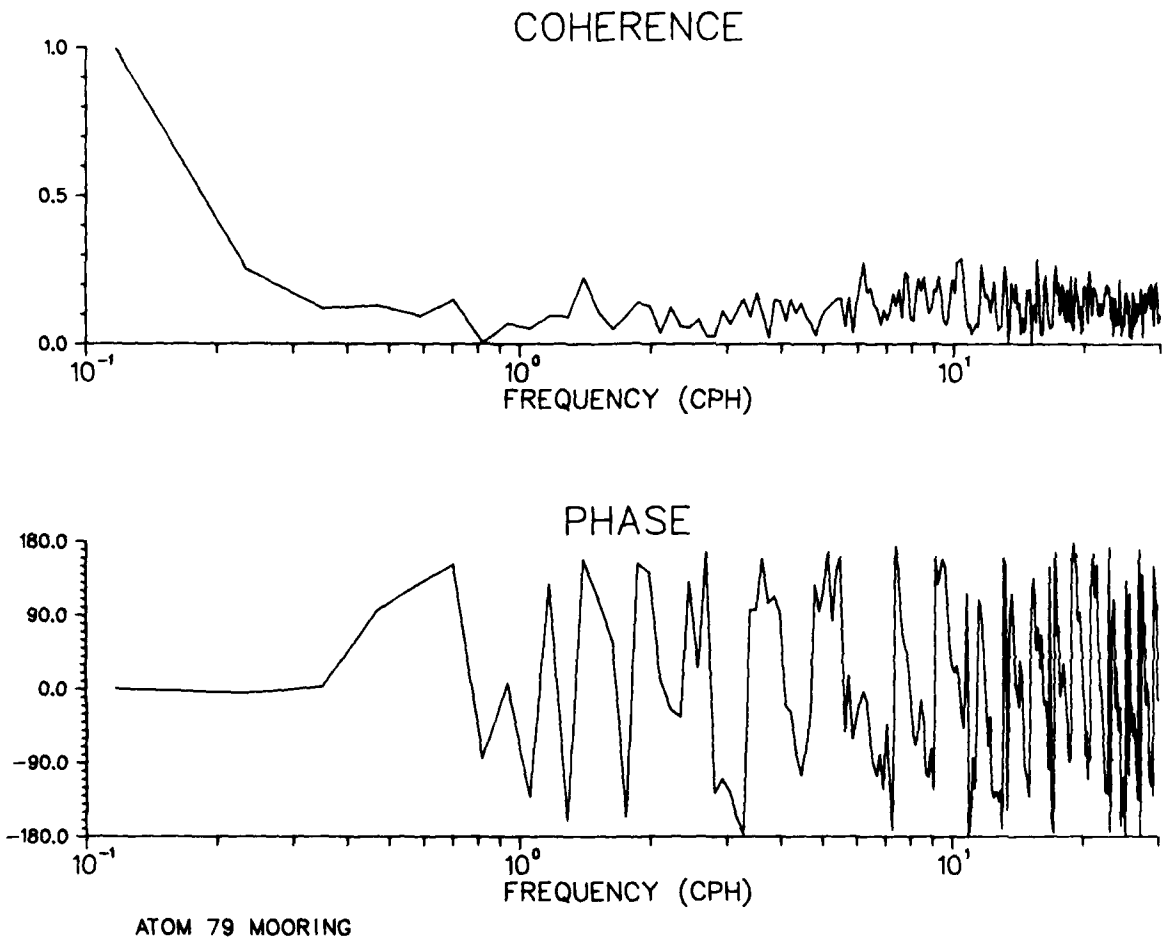

Figure 46. Coherence and phase between V velocity components: meters 1 and 5

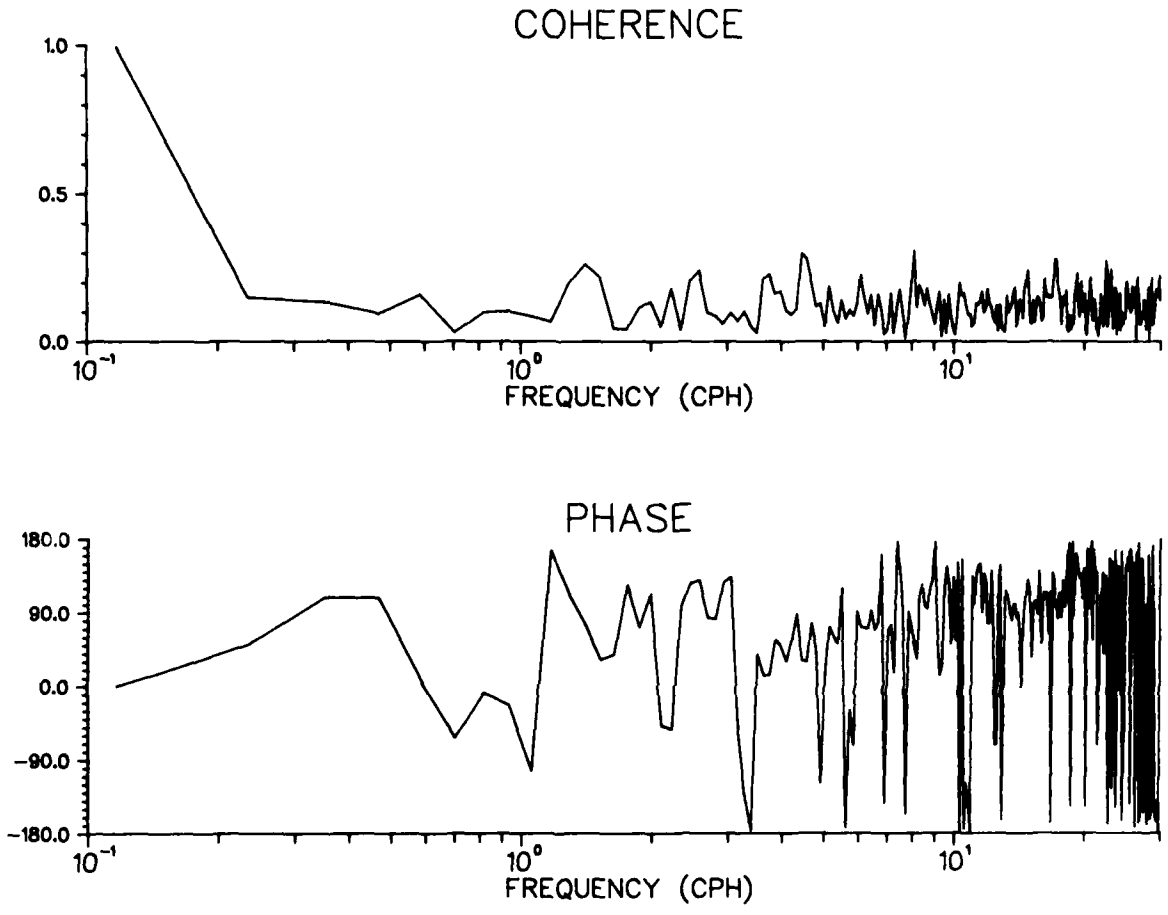

Figure 47. Coherence and phase between V velocity components: meters 1 and 6

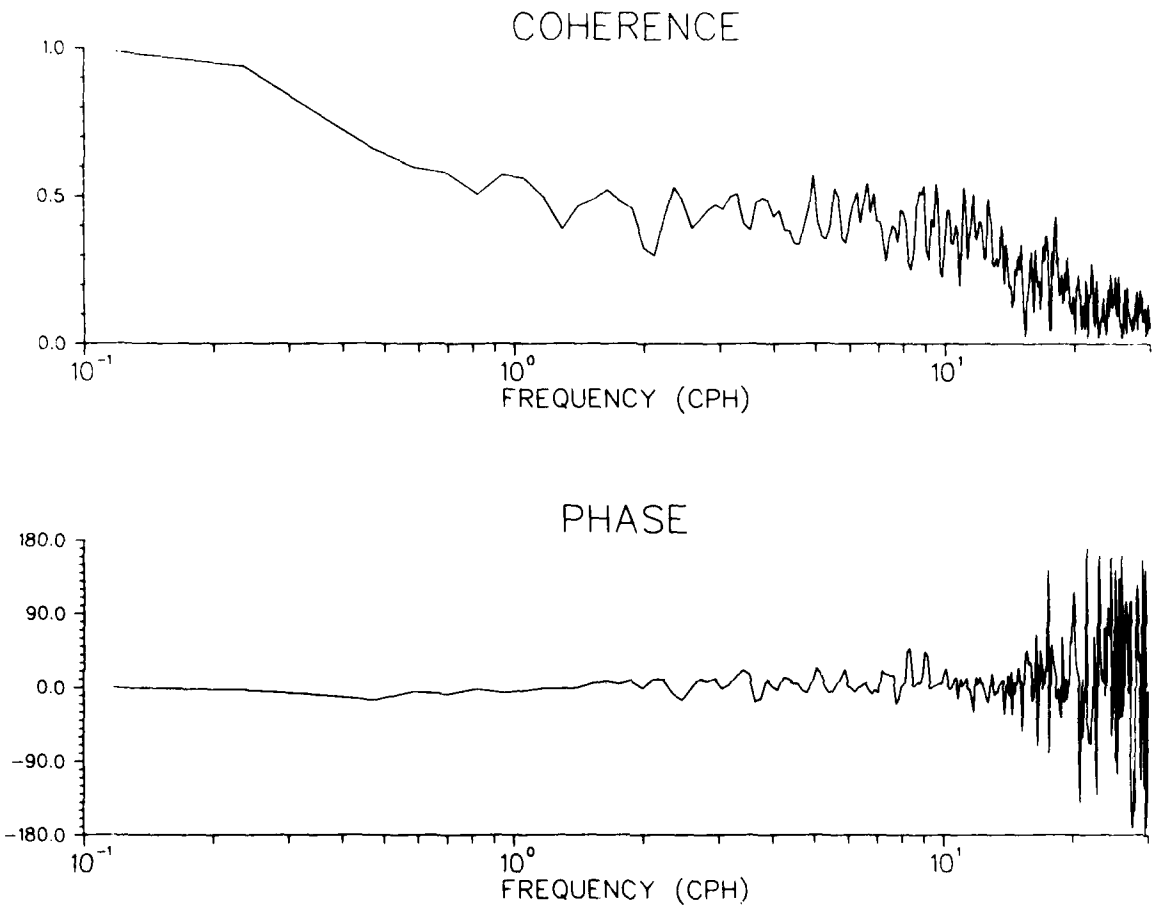

Figure 48. Coherence and phase between temperatures: meters 1 and 2

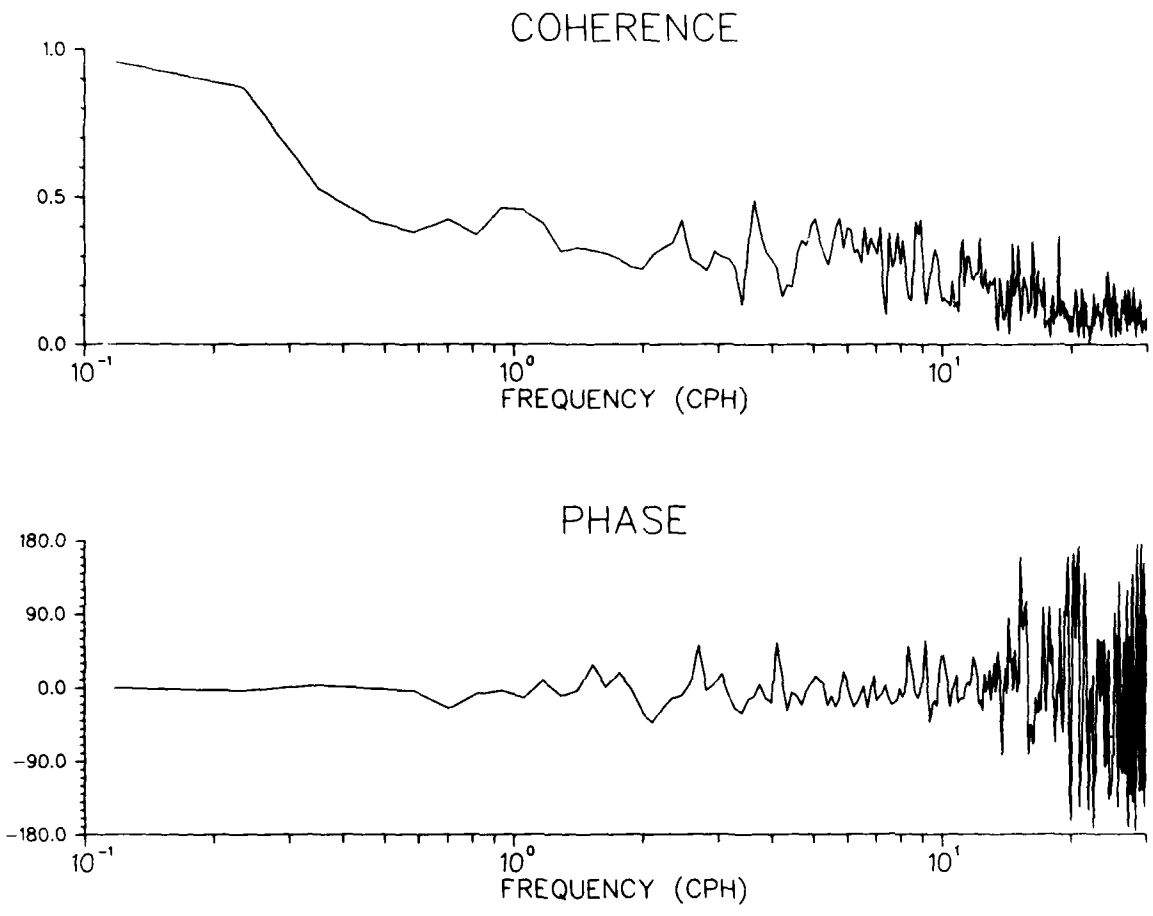

Figure 49. Coherence and phase between temperatures: meters 1 and 4

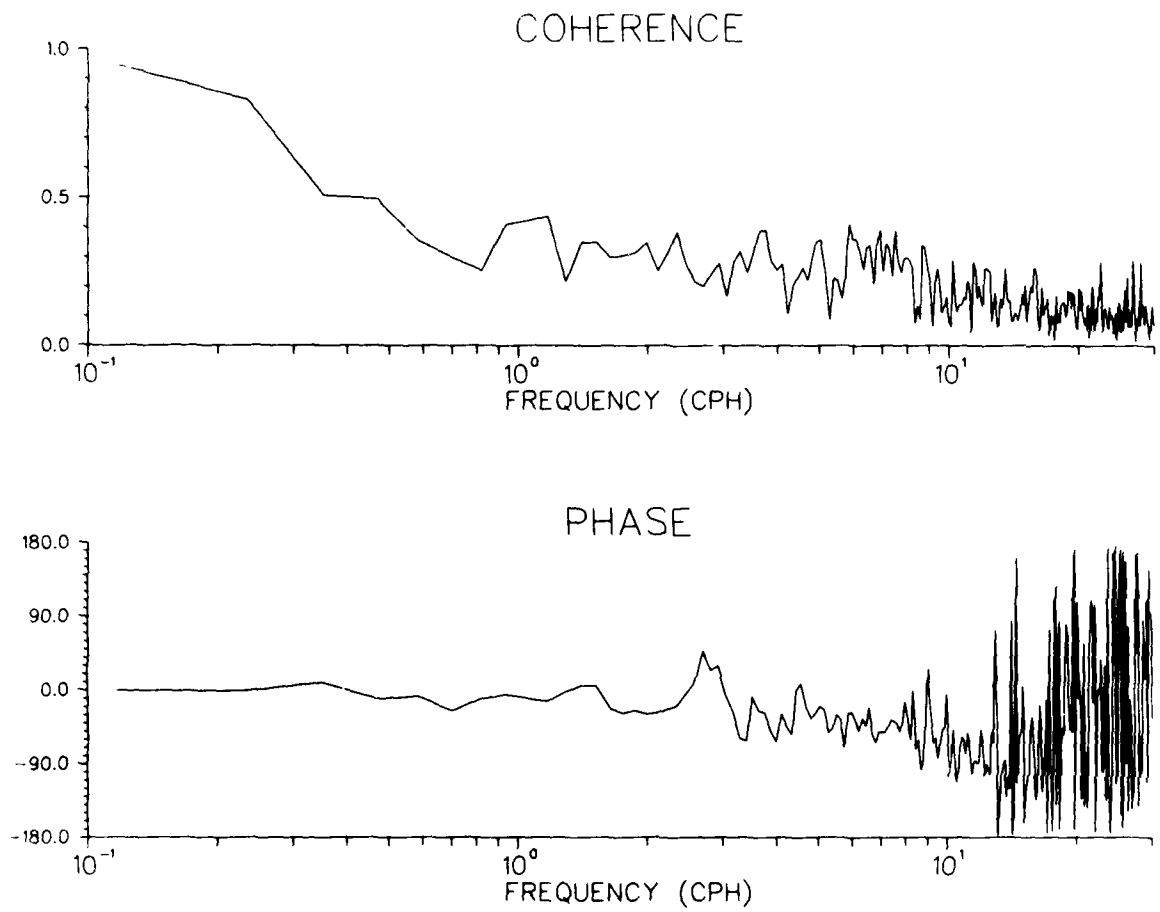

Figure 50. Coherence and phase between temperatures: meters 1 and 5

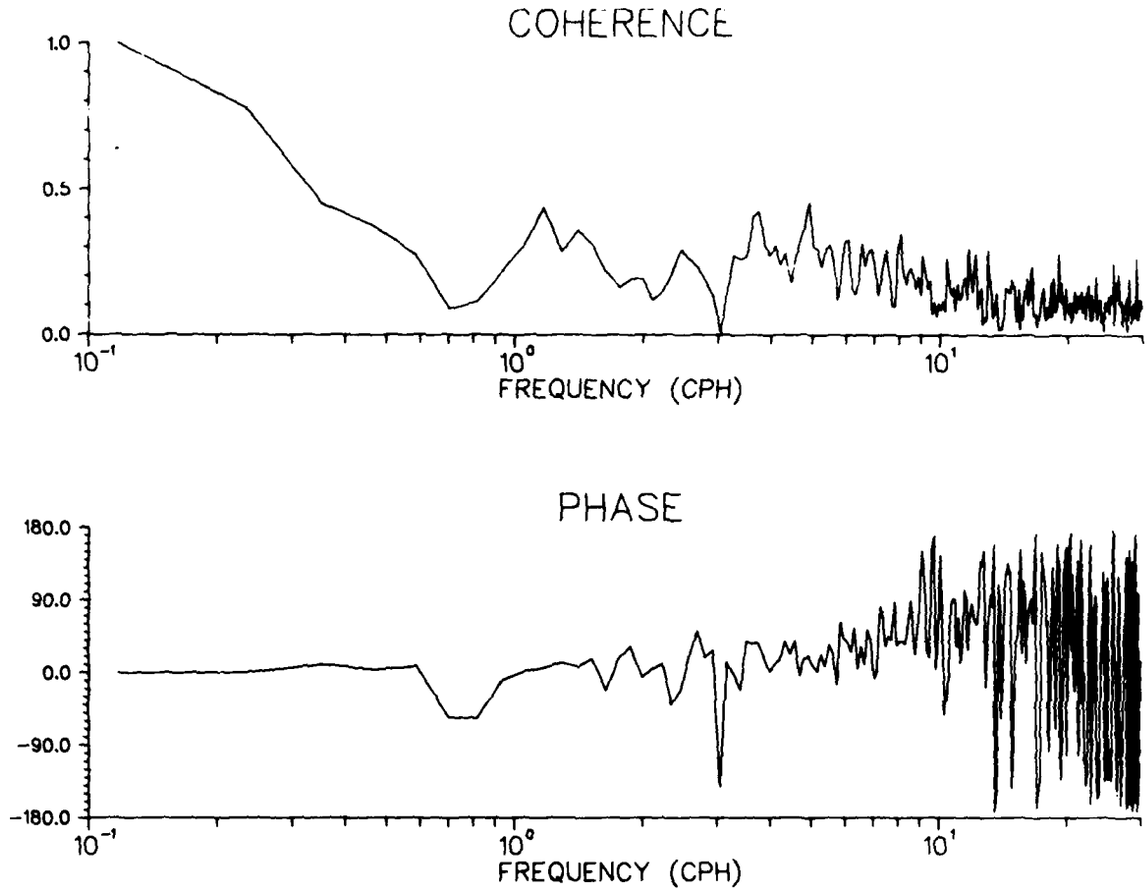

Figure 51. Coherence and phase between temperatures: meters 1 and 6

CONCLUSIONS

The scientific method is based on the sequence of hypothesis formulation, testing and reformulation, usually with respect to a simplified model of the process under study. The ATOM experiment was intended as an early step in this loop within a framework of an oceanic internal wave continuum in a shear field as the model.

We have formulated our hypotheses and tested them. In the process, we have added new hypotheses and have found that some of our original ones have not been well posed. The results of the testing process have provided input to the next stage of the formulation-testing loop and are summarized below.

THE VERTICAL DEPENDENCE OF HIGH FREQUENCY HIGH WAVE NUMBER (HFHWN) VARIABILITY

We hypothesized that: HFHWN variability is dependent on proximity to the peak of the buoyancy profile. In the mean this hypothesis is true. The data are erratic in the sense that the variations about the mean trend are very large.

MODULATION OF HFHWN VARIABILITY BY INERTIAL CURRENT SHEAR

We hypothesized that: HFHWN variability is modulated by inertial-band waves. We found no evidence that HFHWN variability is correlated with intensity of inertial-band modulation below the pycnocline.

INFLUENCE OF LOCAL METEOROLOGY ON HRHWN VARIABILITY

Hypothesis: Low frequency (inertial) variability is dependent on local meteorological conditions. This hypothesis is true; the variation of inertial band energy below the pycnocline correlate with variations in surface wind intensity. Abcve the pycnocline the variations of the surface and internal wave energies are known to be well correlated with surface wind, but there appears to be little influence on the HFHWN intensity below the pycnocline.

VERTICAL COHERENCE OF HF VARIABILITY

Hypothesis: HF variability is coherent over vertical separations greater than 5 m but less than 40 m. This hypothesis is true for current fluctuations. Coherences of current fluctuations above 1 cph are not significant for meter separations greater than 35 m.

Spectral analyses of the XCP data have shown that the shear spectrum is white down to scales of 8 m. Thus, any future experiment should be desigred to sample currents on spacings much smaller than 8 m in order to obtain good estimates of shear.

CONTAMINATION OF HF MEASUREMENTS BY MOORING MOTION

Hypothesis: HF measurements (greater than 1 cph) from a high tension, in-line mooring are significantly contaminated by mooring motions. This hypothesis can be rejected in the band from inertial to about 5 cph, since the mooring motions are more than an order of magnitude smaller than the recorded currents. Above 5 cph the estimated noise level of the Doppler acoustic tracking system becomes large enough (about one-half) to seriously impact the validity of estimates of mooring motion effects on higher frequency current fluctuations. This is a technical problem in the Doppler system.

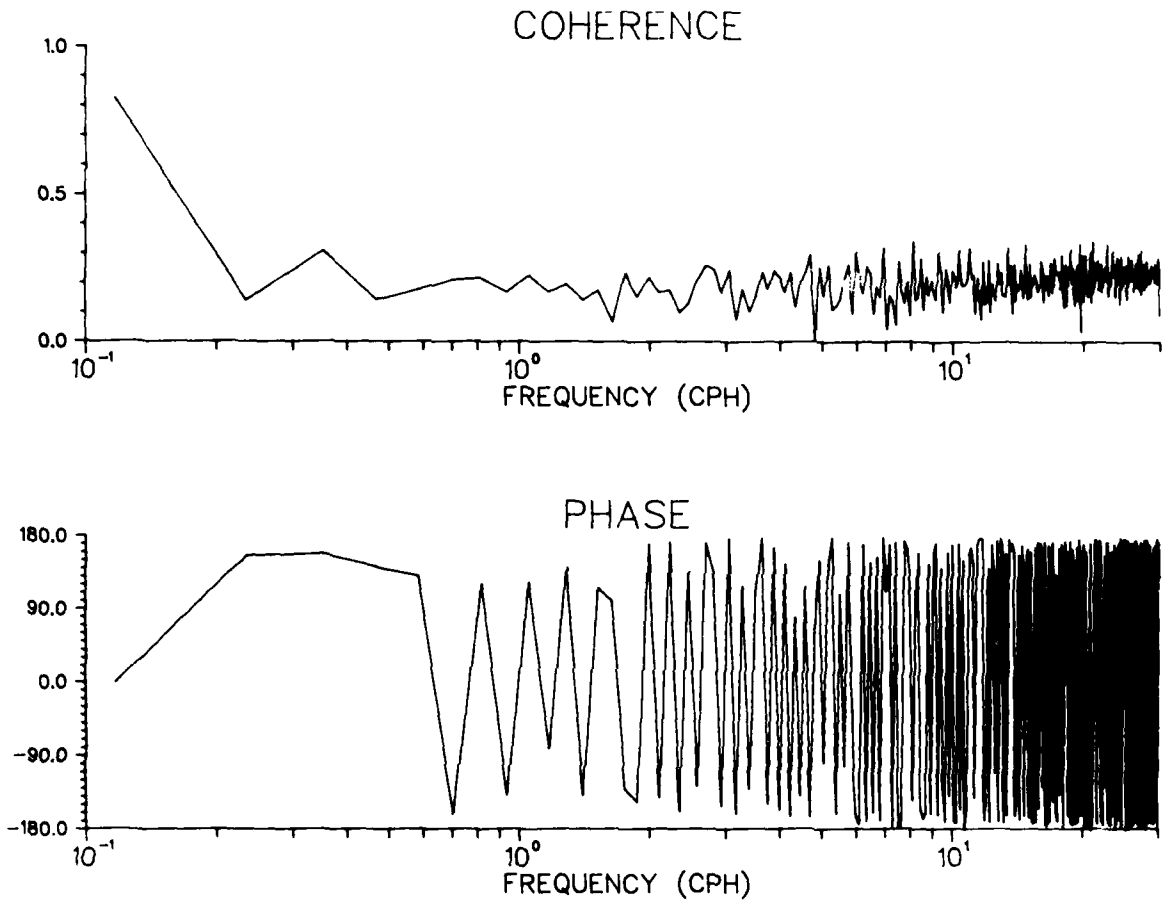

Figure 52. Coherence and phase temperature at meter 2 and pressure at the upper T/P recorder

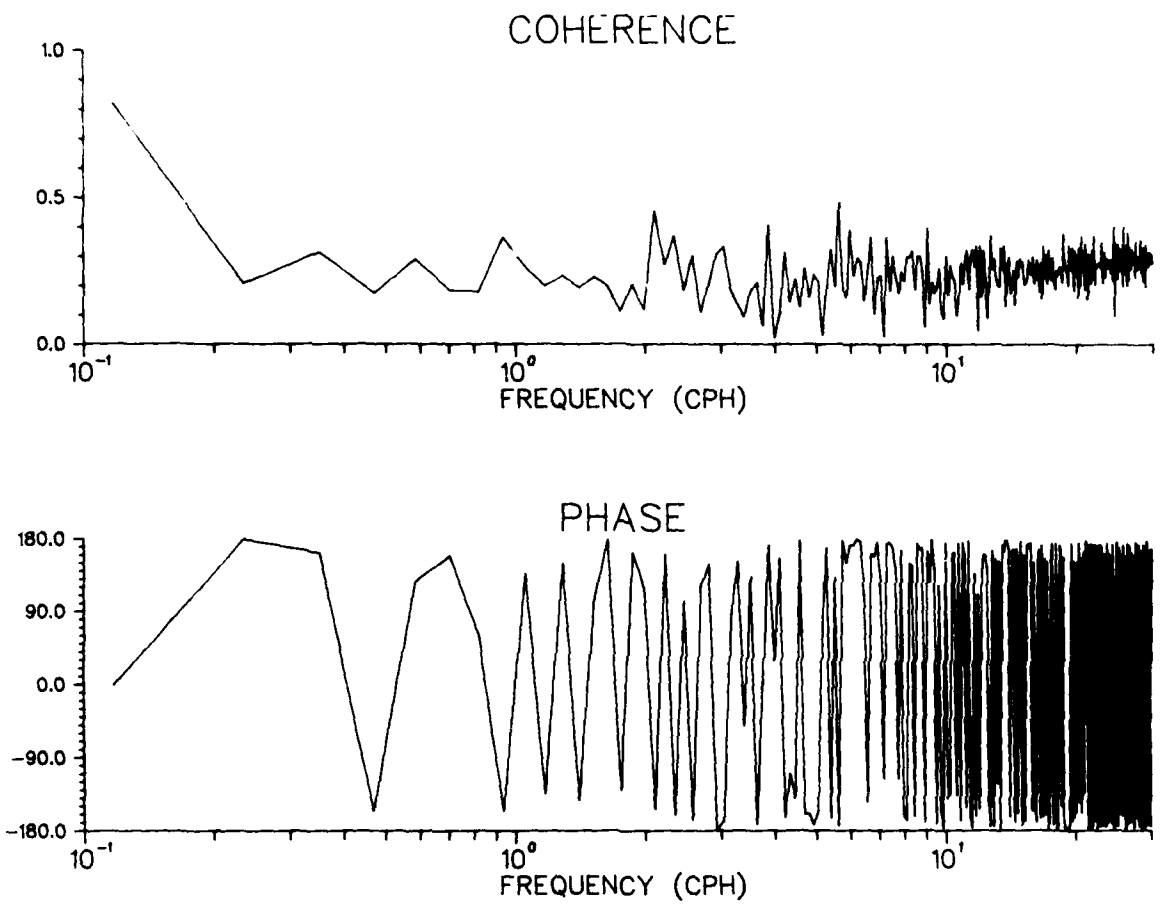

Figure 53. Coherence and phase temperature at meter 6 and pressure at the upper T/P recorder

REMOVAL OF MOORING MOTION FROM MEASUREMENTS

Hypothesis: A significant amount of recorded mooring motion contamination of HF internal wave records can be removed (using tracking records or numerical models). The test of this hypothesis had ambivalent results because: mooring motions did not significantly "contaminate" measurements up to about 5 cph. Down to the noise limit of the Doppler acoustic tracking system it is possible (but not particularly helpful) to subtract the vector time series of the mooring motions from the measured currents. Above that frequency the tracking data are not sufficient. A numerical model of the mooring response could conceivably push the correction to higher frequencies, but the model would not be validated.

In addition to evaluating these hypotheses we had to consider some problems that infringed on the analyses of the measurements.

IMPORTANT TECHNICAL PROBLEMS TO BE ADDRESSED IN FUTURE WORK

XCP

We found that the empirical fall distance formula for the XCP had significant error, and the empirical measurements of fall distance are subject to erratic scatter that cannot be fully rationalized. It is clear that introduction of a time marking fall start would decrease offset depth error. Improved ventilation of the thermistor would enhance empirical fall rate/distance estimates. We hypothesized that the XCP response was sensitive to the electric field surrounding the CTD. This hypothesis was found to be true. The range of vertical influence appears to be about $\pm$20 m. The effect is not observed every time, and it is easily identified in proximity cases.

ACM/VACM AZIMUTHAL RESPONSE

As a result of calibrations made after the original experimental design, we had hypothesized that azimuthal orientation of ACMs and VACMs with respect to the current could be a source of significant velocity measurement error. This hypothesis was found to be valid; in fact, the current measurement errors contributed by azimuthal case orientation uncertainties are greater than those attributed to mooring motions by about a factor of three. This problem can be reduced by calibrations of the azimuthal responses of the meters, incorporation of these calibrations in the conversion to current velocities and sampling of the case orientations as rapidly as the currents. Alternatively, the redesign of the cases of the ACMs and VACMs so that they have improved azimuthal response would reduce this error.

MOORING DYNAMICS IN INTENSE CURRENTS

ATOM was inadvertently deployed in an exceptionally intense current, which caused larger horizontal and vertical displacements than had been expected. If ATOM-like moorings are deployed in the future, the certainty of keeping instruments at design depths could be improved by decreasing the fluid dynamic drag on the elements of the mooring. The dynamical models were not evaluated for conditions encountered; work should proceed on validating dynamical models with observations made under a broad range of conditions--including strong currents.

REFERENCES

Appell, G.F. (1978). A Review of the Peformance of an Acoustic Current Meter. Proc. of a Working Conf. on Currurent Measurement, U. of Delaware, Tech. Rept. DEL-SG-3-78, College of Marine Studies, U. of Delaware, Newark DE 19711, 372 p.

Barnard, T.E. (1981). Legendre Polynomial Expressions for the Probability Density Function of Magnitude-Squared Coherence Estimates, IEEE Trans. Acoustics, Speech and Signal Proc., ASSP-29 (1), 107-108.

Carter, G.C., C.H. Knapp and A.H. Nuttal (1973). Estimation of the Magnitude Squared Coherence Function Via Overlapped Fast Fourier Transform Processing. IEEE Trans. Audio and Electroacoustics, AU-21 (4), 337-344.

Chhabra, N.K. (1977). Correction of Vector-Averaging Current Meter Records from the MODE-1 Central Mooring for the Effects of Low Frequency Mooring Line Motion. DSR 24, 279-287.

Chimonas, G. (1978). Packet-Scale Motions Forced by Nonlinearities in a Wave System. JAS 35, 382-396.

Erickson, C. C. (1978). Measurements and Models of Fine Structure, Internal Gravity Waves, and Wave Breaking in the Deep Ocean, J. Geophys. Res. 83, 2989-3009.

Fu, L. (1981). Observations and Models of Inertial Waves in the Deep Ocean. Rev. Geophys. and Space Phys., 19 (1), 141-170.

Gargett, A.E., P.J. Hendricks, T.B. Sanford, T.R. Osborn and A.J. Williams III (1980). A Composite Spectrum of Vertical Shear in the Upper Ocean from the Profilers EMVP.SCIMP and CAMEL. Pac. Mar. Sci. Rep. 80-11, Inst. of Ocean Sci., Sidney, B.C.

Gould, W.M., W.M. Schmitz and C. Wunsch (1974). Preliminary Field Results for a Mid-Ocean Dynamics Experiment (MODE-0). DSR 21, 911-932.

Gould, W.M. and E. Sambuco (1975). The Effect of Mooring Type on Measured Values of Ocean Current. DSR 22, 55-62.

Green, A.W. and K.D. Saunders. Theoretical and Empirical Fall Rates of XCP's and XBT's, Proc. OCEANS '81, in press.

Hallock, Z.R. (1980). The Fast and Easy Binary (FEB) File. TN 7210-12-80, NAVOCEANO, NSTL Station, MS, 29 p.

Halpern, D. (1978). Mooring Motion Influences of Current Measurements. Proc. of a Working Conference on Current Measurement Tech. Rept. DEL-SG-3-78, College of Marine Studies, U. of Delaware, 69-75.

Halpern, D., R.A. Weller, M.G. Briscoe, R.E. Davis and J.R. McCullough (1981). Intercomparison Tests of Moored Current Measurements in the Upper Ocean. JGR 86 (C1) 419-428.

Halpern, D., R.D. Pillsbury and P.L. Smith (1974). An Intercomparison of Three Current Meters Operating in Shallow Water. Deep Sea Res., 21, 489-497.

Holland, R. (1980). Operation and Maintenance Manual for the XBT Data Acquisition System, NORDA Tech. Note No. 60.

Korotayev, G.K. and N.A. Panteleyev (1977a). Hydrodynamic Instability of the Internal Waves in the Ocean for a Nonstationary Shear. Isv. At. & Oc. Phys. 13, 713-719.

Korotayev, G.K. and N.A. Panteleyev (1977b). Experimental Studies of Hydrodynamic Instability in the Ocean. Oceanology 17, 623-630.

Landahl, M. and W. Criminale (1977). Wave Breakdown in Stratified Shear Flows. JFM 79, 481-497.

Lee, D.F. (1981). An Algorithm for Computing the Cumulative Distribution Function for Magnitude Squared Coherence, IEEE Trans. AASP 29 (1), 117-119.

McComas, C.H. (1977). Equilibrium Mechanisms within the Oceanic Internal Wave Field J.P.O. 7 (6), 836-845.

McComas, C.H. and P. Bretherton (1977). Resonant Interaction of Oceanic Internal Waves, J.G.R. 82 (9), 1399-1412.

McComas, C.H. (1975). Nonlinear Interaction of Internal Gravity Waves, Ph.D. Thesis, The Johns Hopkins University and NCAR. (NTIS No. PB-252-832).

McCullough, J.R. (1978). Near Surface Ocean Current Sensors: Problems and Performance Proc. Work. Conf. Curr. Meas., U. of Delaware Tech. Rept. DEL-SG-3-78, 9-33.

McComas, C. H. and P. Muller (1981). Time Scales of Resonant Interactions Among Oceanic Internal Waves. J. Phys. Oceanog., 11, 139-147.

Nuttall, A.H. (1981). Some Windows with Very Good Sidelobe Behavior. IEEE Trans. Acoustics Speech & Signal Proc., ASSP-29 (1), 84-91.

Pinkel, R. (1975). Upper Ocean Internal Wave Observations from FLIP. J. Geophys. Res. 80, 3892-3910.

Pollard, R.T (1974). The Joint Air-Sea Interaction Trial, JASIN, 1972. Memoires de la Societe Royale des Sciences de Liege, Tome VI, 17-34.

Pollard, R.T. (1970). On the Generation by Winds of Inertial Waves in the Ocean. DSR 17, 795-812.

Pollard, R.T. and R.C. Millard (1970). Comparison Between Observed and Simulated Wind-Generated Inertial Oscillations. DSR 17, 813-821.

Porter, R.P., R.C. Spindel and R.J. Jaffee (1973). CW Beacon System for Hydrophone Motion Determination. J.A.S.A. 53, 1691-1679.

Sanford, T.B., R.G. Drever and J.H. Dunlap (1974). The Design and Performance of a Free Fall Electro-magnetic Velocity Profiler. Woods Hole Oceanographic Institution Ref. No. 74-76, 123 p. (Unpublished manuscript)

Sanford, T. B., R. G. Driver and J. H. Dunlap (1978). A Velocity Profiler Based on the Principles of Geomagnetic Induction. Deep Sea Res., 25, 183-210.

Saunders, K.D. (1980). Direction Response of the NBIS Acoustic Current Meter. Proc. OCEANS '80, (IEEE Pub. No. 80CH1572-7), 220-225.

Saunders, K.D. and A.W. Green (1980). Preliminary Results of the ATOM Mooring Motion Experiment. (Unpublished manuscript)

Saunders, K.D., A.W. Green and M.T. Bergin (1980). A Comprehensive Graphical Representation of Data Obtained in the Acoustically Tracked Oceanographic Mooring (ATOM) Experiment. NORDA Technical Note 85.

Saunders, P. M. (1976). Near Surface Current Measurements. Deep Sea Research, 23, 249-258.

SCOR Working Group 21 (1975). An Intercomparison of Some Current Meters, III. UNESCO Technical Papers in Marine Science No. 23, UNESCO, Paris, 42 p.

Spindel, R.C., R.P. Porter and J.A. Schwoerer (1978). Acoustic Phase Tracking of Ocean Moorings. IEEE J. Oceanic Eng., OE-3 (1), 27-30.

Spindel, R.C., R.P. Porter, W.M. Marguet and J.L. Durham (1976). A High-Resolution Pulse-Doppler Underwater Acoustic Navigation System. IEEE J. Oceanic Eng., OE-1, 6-13.

Thorpe, S. (1978). On the Shape and Breaking of Finite Amplitude Internal Gravity Waves in a Shear Flow. JFM 85, 7-31.

Webster, F. (1967). A Scheme for Sampling Deep Sea Currents from Moored Buoys. Proc. 2nd Int. Buoy Tech. Symp., MTS, Washington, D.C., 419-431.

Zenk, W., D. Halpern and R. Kase (1978). Influence of Mooring Configuration and Surface Waves upon Deep-Sea Near-Surface Current Measurements. GATE Symposium on Oceanography and Surface Layer Meteorology, 16-20 May, 1978, Kiel.

APPENDIX A

1. Derivation of the method for obtaining vertical velocity from the temperature and pressure records.

The basic equation for temperature at a point in the fluid is

$$\frac{\partial T}{\partial t} + \vec{u}\cdot\nabla T = N\nabla^2 T$$

or

$$\frac{\partial T}{\partial t} + u\frac{\partial T}{\partial x} + v\frac{\partial T}{\partial t} + w\frac{\partial T}{\partial z} = N\nabla^2 T$$

if we <u>assume</u> $u\frac{\partial T}{\partial x}$, $v\frac{\partial T}{\partial y}$, $N\nabla^2 T \ll \frac{\partial T}{\partial t}$, $w\frac{\partial T}{\partial z}$;

Then we have

$$\frac{\partial T}{\partial t} = -w\frac{\partial T}{\partial z}$$

or

$$w = -\frac{\left(\frac{\partial T}{\partial t}\right)}{\left(\frac{\partial T}{\partial z}\right)}$$

If we consider a point on the mooring, the observed velocity is given by

W_{OBS} = W (due to mooring motion) + W (due to water)

$= W_I + W_w$

Now $W_w = W_{OBS} + W_I$

and $W_I = -\frac{1}{\bar{\rho}g}\frac{dp}{dt}$

$$W_{OBS} = -\frac{\partial T}{\partial t} \Big/ \frac{\partial T}{\partial z}$$

So the true water velocity is given by

$$w = -\frac{\partial T}{\partial t} \Big/ \frac{\partial T}{\partial z} - \frac{1}{\bar{\rho}g}\frac{dp}{dt}$$

APPENDIX B: THE DERIVATION OF VERTICAL EDDY VISCOSITIES

1. Consider the horizontal momentum equations; say for u.

$$\frac{\partial u}{\partial t} + \hat{u}\cdot\nabla u - fv = -\frac{1}{\rho_o} Px + \nu\nabla^2 u$$

If we denote an average by an overbar and define

$$u = \bar{u} + u',$$

The averaged equation is the same except for an extra term of the form

$$\overline{\hat{u}'\cdot\nabla u'} = \overline{u'\frac{\partial u'}{\partial x}} + \overline{v'\frac{\partial u'}{\partial x}} + \overline{w'\frac{\partial u'}{\partial z}}$$

If we assume that

$$\overline{u'\frac{\partial u'}{\partial x}},\ \overline{v'\frac{\partial u'}{\partial y}} \ll \overline{w'\frac{\partial u'}{\partial z}}$$

and that

$$\overline{w'\frac{\partial u'}{\partial z}} \simeq \frac{\partial}{\partial z}\overline{w'u'} \qquad \left(\text{i.e. } \overline{u'\frac{\partial w'}{\partial z}} \ll \frac{\partial}{\partial z}\overline{u'w'}\right)$$

then we can define an eddy viscosity such that

$$\frac{\partial}{\partial z}\left(\overline{w'u'}\right) = \nu_{Eu}\frac{\partial^2 \bar{u}}{\partial z^2}$$

or

$$\frac{\partial}{\partial z}\left[\overline{w'u'} - \nu_{Eu}\frac{\partial \bar{u}}{\partial z}\right] = 0$$

which will hold whenever

$$\overline{w'u'} - \nu_{E}\frac{\partial \bar{u}}{\partial z} = \text{constant}$$

The simplest choice is to assume V_{Eu} is defined when the constant = 0 or

$$\nu_{Eu} = \frac{\overline{w'u'}}{\left(\frac{\partial \bar{u}}{\partial z}\right)}$$

UNCLASSIFIED

SECURITY CLASSIFICATION OF THIS PAGE (When Data Entered)

REPORT DOCUMENTATION PAGE		READ INSTRUCTIONS BEFORE COMPLETING FORM
1. REPORT NUMBER NORDA Technical Note 129	2. GOVT ACCESSION NO. AD-A124 007	3. RECIPIENT'S CATALOG NUMBER
4. TITLE (and Subtitle) Measurements of High Frequency, High Wavenumber Processes in the Upper Ocean: The Acoustically Tracked Oceanographic Mooring Experiment (ATOM '79) Final Report, Part I		5. TYPE OF REPORT & PERIOD COVERED Final 6. PERFORMING ORG. REPORT NUMBER
7. AUTHOR(s) K. D. Saunders A. W. Green		8. CONTRACT OR GRANT NUMBER(s)
9. PERFORMING ORGANIZATION NAME AND ADDRESS Naval Ocean Research and Development Activity NSTL Station, Mississippi 39529		10. PROGRAM ELEMENT, PROJECT, TASK AREA & WORK UNIT NUMBERS
11. CONTROLLING OFFICE NAME AND ADDRESS Naval Ocean Research and Development Activity NSTL Station, Mississippi 39529		12. REPORT DATE August 1982 13. NUMBER OF PAGES 86
14. MONITORING AGENCY NAME & ADDRESS(if different from Controlling Office)		15. SECURITY CLASS. (of this report) UNCLASSIFIED 15a. DECLASSIFICATION/DOWNGRADING SCHEDULE

16. DISTRIBUTION STATEMENT (of this Report)

Distribution Unlimited

17. DISTRIBUTION STATEMENT (of the abstract entered in Block 20, if different from Report)

18. SUPPLEMENTARY NOTES

19. KEY WORDS (Continue on reverse side if necessary and identify by block number)

oceanography	variability
physical oceanography	high frequency processes
mooring technology	high vertical wavenumber processes
acoustic tracking	inertial forcing
upper ocean	internal waves

20. ABSTRACT (Continue on reverse side if necessary and identify by block number)

The ATOM '79 (Acoustically Tracked Ocean Mooring) experiment was designed to study the natural background of high frequency, high wavenumber processes in the upper ocean and to determine the magnitude and effects of mooring motion on the measurements of velocity and temperature. The mooring was deployed for about one month in the central Gulf of Mexico from December 1979 through January 1980.

It was determined that translational mooring motion is not a significant source

DD FORM 1 JAN 73 1473 EDITION OF 1 NOV 65 IS OBSOLETE
S/N 0102-LF-014-6601

UNCLASSIFIED

SECURITY CLASSIFICATION OF THIS PAGE (When Data Entered)

of error. Observations of the background currents showed no strong correlation between low frequency inertial period activity and high frequency activity, little, if any, effect of proximity of the peak in the Brunt-Vaisala frequency profile on the high frequency activity and some significant relation of wind forcing to sub-mixed layer inertial currents.


DATE
ILME